รายงานวิจัยฉบับสมบูรณ์

การจัดโครงสร้างโมเลกุลและวิศวกรรมโปรตีนของ *Bacillus thuringiensis* Cyt Toxin

Molecular Folding and Protein Engineering of the *Bacillus thuringiensis* Cyt Toxin

โดย ชาติชาย กฤตนัย

มกราคม 2552

สัญญาเลขที่ RSA4780025

รายงานวิจัยฉบับสมบูรณ์

การจัดโครงสร้างโมเลกุลและวิศวกรรมโปรตีนของ *Bacillus thuringiensis* Cyt Toxin

Molecular Folding and Protein Engineering of the *Bacillus thuringiensis* Cyt Toxin

ผู้วิจัย

นายชาติชาย กฤตนัย

สถาบันอณูชีววิทยาและพันธุศาสตร์ มหาวิทยาลัยมหิดล

สนับสนุนโดยสำนักงานกองทุนสนับสนุนการวิจัย

(ความเห็นในรายงานนี้เป็นของผู้วิจัย สกว.ไม่จำเป็นต้องเห็นด้วยเสมอไป)

สารบัญ

Acknowledgement

โครงการวิจัยนี้ได้รับทุนสนับสนุนจากสำนักงานกองทุนสนับสนุนการวิจัย (สกว.) ตามโครงการทุนพัฒนานักวิจัย สัญญาเลขที่ RSA4780025 และได้รับการสนับสนุนด้านเครื่องมือและห้องปฏิบัติการจากสถาบันอณูชีววิทยาและพันธุศาสตร์ มหาวิทยาลัยมหิดล

Abstract

Project Code: RSA4780025

Project Title: Molecular Folding and Protein Engineering of the *Bacillus thuringiensis* Cyt Toxin

Investigators: Chartchai Krittanai

Institute of Molecular Biology and Genetics, Mahidol University

Email Address: stckt@mahidol.ac.th

Project Period: August 2005 – August 2008

Cyt2Aa2 is a 29-kDa cytolytic toxin produced by *Bacillus thuringiensis* subsp.*darmstadiensis*. It has a larvicidal activity against *Dipteran* larvae. The toxin has a single domain of α/β architecture comprising two outer layers of α-helix hairpins wrapped around β-sheet, and require proteolytic processing to become an active toxin. This research project aims to characterize the process of protein unfolding and refolding of Cyt2Aa2 using a guanidinium hydrochloride induced environment. We have successfully identified three conformational states of Cyt2Aa2 as native (N), intermediate (I) and unfolded (U) states. Unfolding and refolding of toxin in 0-6 M GuHCl were observed as the reversal process. The determined conformational free energies of native and intermediate states are approximately 5.8 and 14.8 kcal/mol, respectively. The transitional kinetics of the two states revealed activation energy around 20-25 kcal/mol. Further characterization of the intermediate state has identified a molten-globule like conformation. The stabilizing role of amino acid residues in various positions of toxin structure relating to toxin conformation and function was also explored. Site-directed mutagenesis was employed to generate various mutant toxins with amino acid substitutions and deletions. These mutant toxins were investigated by unfolding experiment and assayed for their biological activity. Our results has shown that the amino acid residues located on the N and C termini of Cyt2Aa2 play a critical role in the production of expressed mutant toxins. Φ analysis of amino acid mutation on various secondary structure elements of Cyt2Aa2 suggested that the helical element of toxin may have a contributing role in the transition between the unfolded and native conformation. From these results, the conformational intermediate was proposed to be partially maintained as the native conformation with a rearrangement on helical structural elements. This revealed intermediate may involve in the detailed mechanism of cytolytic toxin function.

Keywords: protein unfolding, conformational change, free energy, *B. thuringiensis*, Cyt2Aa2

บทคัดย่อ

รหัสโครงการ: RSA4780025

โครงการ: การจัดโครงสร้างโมเลกุลและวิศวกรรมโปรตีนของ *Bacillus thuringiensis* Cyt Toxin

ผู้วิจัย: รองศาสตราจารย์ชาติชาย กฤตนัย

สถาบันอณูชีววิทยาและพันธุศาสตร์ มหาวิทยาลัยมหิดล

E-mail Address: stckt@mahidol.ac.th

ระยะเวลาโครงการ: 31 สิงหาคม 2547 – 30 สิงหาคม 2551

โปรตีน Cyt2Aa2 เป็นโปรตีนที่สร้างขึ้นจากเชื้อจุลินทรีย์ *Bacillus thuringie*nsis spp. *darmstadiensis* โปรตีนชนิดนี้มีโครงสร้างเป็นโดเมนเดี่ยวประกอบด้วยชั้นของเกลียวอัลฟาจำนวนสองชั้นแทรกตรงกลางด้วยชั้นของแผ่นเบต้า เมื่อโครงสร้างโมเลกุลผ่านการตัดย่อยอย่างจำเพาะด้วนเอ็นไซม์โปรติเอสแล้ว สามารถออกฤทธิ์ในการฆ่าลูกน้ำของยุงลายและยุงรำคาญได้ดี โครงการวิจัยนี้มีวัตถุประสงค์เพื่อศึกษาเกี่ยวกับความรู้พื้นของขบวนการจัดตัวและคลายตัวของโครงสร้างโปรตีน Cyt2Aa2 ในสภาวะที่ถูกเหนี่ยวนำด้วยสารเคมี รวมทั้งวิเคราะห์ถึงบทบาทของกรดอะมิโนในตำแหน่งต่างๆของโครงสร้างโมเลกุลว่ามีความสำคัญและสัมพันธ์อย่างไรกับกลไกการรักษาเสถียรภาพและการทำงานในระดับโมเลกุล ผลจากการศึกษาวิจัยในโครงการนี้ พบว่าขบวนการม้วนจัดตัวและขบวนการคลายตัวเป็นขบวนการย้อนกลับซึ่งกันและกัน มีการเปลี่ยนแปลงสถานะของโครงสร้างระหว่างสภาวะโครงสร้างปกติ (Native) โครงสร้างที่คลายตัวบางส่วน (Intermediate) และโครงสร้างที่คลายตัวสมบูรณ์ (Unfolded) สอดคล้องกับ Three-state model เมื่อวิเคราะห์Unfolding/ Refolding curve ที่ได้ พบว่าค่าพลังงานFree Energy ของการเปลี่ยนแปลงระหว่าง Native (N) และ Intermediate (I) มีค่าประมาณ 5-6 kcal/ mol และ ค่าพลังงานของการเปลี่ยนแปลงสถานะระหว่าง Intermediate (I) และ Unfolded (U) มีค่าประมาณ 12-16 kcal/ mol ตามลำดับ และต้องการพลังงานกระตุ้น 20-25 กิโลแคลอรี่ต่อโมล ซึ่งในการก้าวข้ามจุดเปลี่ยนแปลงโครงสร้าง เกิดขึ้นผ่านโครงสร้างที่มีลักษณะจำเพาะ (intermediate) ที่มีการจัดตัวของโครงสร้างตติยภูมิ (Tertiary structure) ต่างจากโครงสร้างNative แต่ยังคงอนุรักษ์ลักษณะโครงสร้างทุติยภูมิ (Secondary structure)ไว้ สามารถระบุได้ว่าโครงสร้างดังกล่าวมีลักษณะเป็น Molten globule state ในการตรวจสอบถึงบทบาทของกรดอะมิโนที่ตำแหน่งต่างๆที่เกี่ยวข้องกับขบวนการจัดตัวของและการทำงานของของโครงสร้างโมเลกุล ได้ทำการออกแบบและสร้างโปรตีนฆ่าลูกน้ำยุงชนิดกลายพันธุ์ (mutant toxins) ขึ้นจำนวนหนึ่ง โดยมีการแทนที่หรือตัดกรดอะมิโนที่อยู่ในตำแหน่งต่างๆของโครงสร้างโมเลกุลออก พบว่าโปรตีนกลายพันธุ์ส่วนหนึ่งมีพฤติกรรมเปลี่ยนแปลงไปจากโปรตีนต้นแบบทั้งในส่วนของขบวนการคลายตัวในและค่าของพลังงานที่เกี่ยวข้อง โดยกรดอะมิโนที่อยู่ที่ปลายด้าน N- และ C-terminal มีบทบาทสำคัญต่อการผลิตและจัดโครงสร้างโปรตีน และในการวิเคราะห์ ค่าΦ ของโปรตีนกลายพันธุ์ต่างๆ ชี้แนะว่ากรดอะมิโนในหลายตำแหน่ง โดยเฉพาะอย่างยิ่งในตำแหน่งที่อยู่บนเกลียวαHelix มีความเกี่ยวข้องกับกลไกของการคลายตัว ความรู้ความเข้าใจจากงานวิจัยนี้ จะช่วยให้นักวิจัยได้ทราบถึงรายละเอียดและการปรับเปลี่ยนโครงสร้างสามมิติของโปรตีน ซึ่งจะเป็นแนวทางในการเข้าใจกลไกในการทำงานของโปรตีนฆ่าลูกน้ำยุงกลุ่ม Cyt2 ได้ต่อไป

คำหลัก: โครงสร้างโมเลกุล พลังงาน โปรตีนฆ่าลูกน้ำยุง

สรุปเนื้อหาของงานวิจัย

INTRODUCTION

Delta-endotoxins are crystalline parasporal inclusion proteins, synthesized by a gram-positive bacterium, Bacillus thuringiensis (Bt). These toxins are considerable applied as environmentally-safe insecticides [1]. The toxins can be categorized into 2 groups of Crystal (Cry) and Cytolytic (Cyt) proteins [2, 3]. Currently, there are many distinct Bt-toxins characterized by structural similarities and insecticidal spectra for Lepidoptera-specific (I), Lepidoptera- and Diptera-specific (II), Coleoptera-specific (III) and Diptera-specific (IV) activity.

Crystal (Cry) toxins

The three dimensional structures of six different Cry proteins, Cry1Aa, Cry2Aa, Cry3Aa, Cry3Bb, Cry4Aa and Cry4Ba have been determined by X-ray crystallography. All of these structures display a high degree of conservation with three-domain organization, suggesting a similar mode of action among the Cry protein family. The N-terminal domain (domain I) is a bundle of seven α-helices in which the central helix-α5 is hydrophobic and is encircled by six other amphipathic helices; and this helical domain is responsible for membrane insertion and pore-formation. Domain II consists of three antiparallel β-sheets with exposed loop regions, and domain III is a β-sandwich [4-9]. The exposed regions in domains II and III are also proposed to be involved in receptor binding [10-12].

Cytolytic (Cyt) toxins

There are 2 groups of cytolytic (Cyt) toxin: Cyt1 (CytA) and Cyt2 (CytB). The amino acid sequence contain 249 amino acids for Cyt1 (ca.27.3 kDa) and 259 amino acids for Cyt2 (ca. 29.2 kDa). The protein sequence alignment of these Cyt toxins showed 39% identity and 70% similarity [13-15]. In 1996, the X-ray crystal structure of Cyt2A has been resolved by Li J, et.al. Its structure contains a single domain of alpha-beta architecture comprising of six alpha-helices and seven beta-sheets. There are two outer layers of alpha-helix hairpins wrapped around mixed beta-sheets in the middle. The alpha-helix A, B, C and D show an amphipatic character that the hydrophobic site interacts to the beta-sheets and turn the hydrophilic site to the environment. There is an N-terminal arm consisting of a beta-strand and its extensions, which are involved in dimerisation [16].

The secondary structure of six alpha-helices in the Cyt2 monomer involved a total of 55 residues or 24% of the polypeptide. The beta-sheet involves 75 residues or 33% if the polypeptide. The helices αA, αB, αC, and αD all have an amphiphilic characteristics, with

hydrophobic residues packed against the b-sheet, and polar and charged residues on the molecular surface. The amphiphilicity of the region in the Cyt1 sequence corresponding to αC was previously noted [17]. Since the helices are short and only cover the sheet over part of its length, the long strands in the β-sheet also show an amphiphilic feature. On the long strands β5, β6 and β7, the residues on the ‘‘helix A-B face’’ are predominantly hydrophilic, while those on the ‘‘helix C-D face’’ are predominantly hydrophobic. Cyt toxin is structurally related to volvatoxin A2, a PFT cardiotoxin produced by a straw mushroom Volvariella volvacea [18].

It has been reported that protease K-processed Cyt1 and Cyt2 are both haemolytic, whereas unprocessed Cyt1 is less haemolytic and unprocessed Cyt2 is non haemolytic. For Cyt2, the initial product is a 23 kDa fragment extending from Thr34 to Phe237, while further digestion yields the 20 kDa fragment from Ser38 to Ser228. Both products are cytolytically active [30]. The processing cleaves the intertwined N-terminal arm, including β1 responsible for dimerization, thereby releasing the active toxin as a monomeric form. It also removes the C-terminal tail and αF, to uncover the three-layered core [16]. However, when Cyt1 and Cyt2 were first incubated with phospholipid liposomes, new protease-sensitive sites were created for most of the proteases used, resulting in smaller fragments of about 10}12.5 kDa. This suggests that a major conformational change was induced by membrane binding [19].

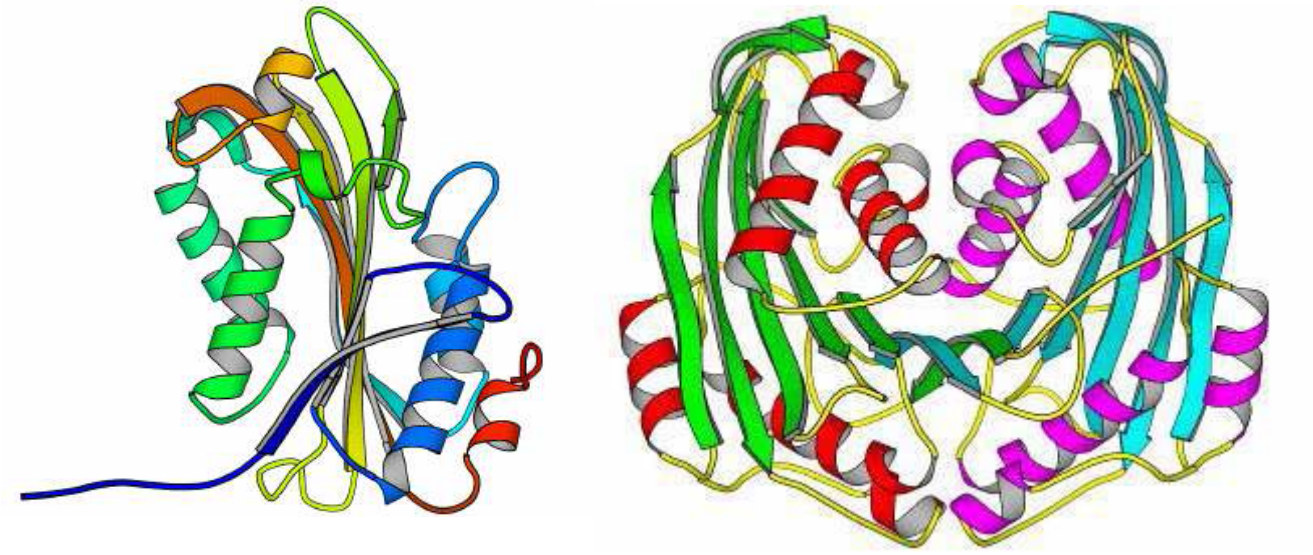

Figure 1: Three-dimensional structure of Cytolytic Cyt2 toxin and toxin dimerization (http://www.bioc.cam.ac.uk/~dje1/)

Mode of action

The delta-endotoxins are ingested by insect larvar and dissolved under the alkaline pH and reducing conditions in the midgut of larvae. They are then processed to an active toxin by the gut proteases. The active form of Cry toxins can bind to specific proteins on the membrane of microvilli of midgut epithelial cell. These membrane-bound toxins can undergo a conformational change, leading to an oligomerization and ion pore formation. The osmotic imbalance and cell swelling can consequently cause cell lysis [20].

In contrast, Cyt toxins do not require specific binding or docking on membrane proteins. They interact directly with membrane and cause the cell lysis. The mechanism of their action has been proposed either by a membrane pore-formation [21-23] or by a membrane disruption via detergent-like interaction [25]. However Cyt toxin has been shown to be specifically lethal to the dipteran larvae *in vivo* and also cytolytic activity to a broad range of cells including erythrocytes *in vitro* [25]. The toxicity of Cyt1Aa to mosquito larvae is found, on average, one order of magnitude lower than that of Cry4 or Cry11Aa toxins [26]. Interestingly, several studies have found that the Cry toxins also showed a synergistic toxicity when combined with Cyt toxins. The synergistic effect has been found very useful and applied to overcome insect resistance to Bt-toxins [27-29].

Currently the mechanism of the Cyt toxin is still unclear. The two models have been proposed to be a pore-forming model and the detergent-like model. In the pore-forming model, the toxin undergoes oligomerization, insertion into the lipid membrane, and formation of the lytic pores. For the detergent-like model, the toxin aggregates onto the lipid membrane and disrupt the cell membrane stabilization [30]. Li et al. has proposed that Cyt toxins can form a membrane pore based on a β-barrel structure. It is noteworthy that the helical elements of Cyt toxin are not long enough to span the 30A° width of the hydrophobic layer of biological membrane. While, the lengths of beta strands, $\beta 5$, $\beta 6$, and $\beta 7$, estimated on the basis of an average rise of 3.3A° per residue in twisted parallel and antiparallel sheet, are sufficient to span membrane width [16]. In addition, it has been found that the segment containing $\beta 4$, $\beta 5$, $\beta 6$, αE and $\beta 7$ remains tightly associated with the membrane after proteolysis of membrane bound Cyt2Aa toxin. The pore is suggested to be oligomeric, with each monomer contributing $\beta 5$, $\beta 6$ and $\beta 7$ to form the barrel [23].

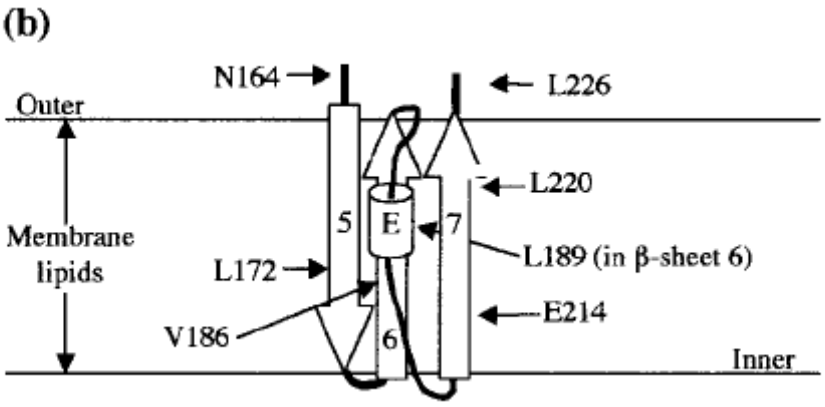

Figure 2: Proposed insertion model of Cyt toxins [23]

Protein stability

The amino acids sequence in the polypeptides is crucial to create the conformational structure of protein. These amino acids are happened to interact either to each other or the environment and develop the arrangement. There are several stabilized interactions within the polypeptide which can be categorized into covalent and non-covalent bonds. The examples of the covalent bonds are the peptide bonds and disulfide bonds. The non-covalent bonds are addressed in hydrogen bonds, van der Waals interactions, electrostatic interactions and hydrophobic interactions [31]. These interactions are essential for protein stability and folding. Under physiological conditions, the native and denatured states of a protein are in equilibrium. The free energy change of these two states, ΔG, represents the conformational stability of a protein.

$$\text{Unfolded (U)} \underset{k_{-1}}{\overset{k_1}{\rightleftharpoons}} \text{Native (N)}$$

This reaction is reversible, where the equilibrium lies to the right (Keq > 1 = [N]/[U]) for the native state (N) to be defined as more stable than the unfolded state (U). The k1 and k-1 represent the rate constants of the forward and reverse reactions, respectively.

There are many factors agitated the stability of protein especially structure perturbation such as heat, temperature, pH, pressure and some chemical denaturants. The chemical denaturants such as urea and guanidine hydrochloride are widely used for the protein unfolding experiments because they are convenient for estimating the conformational stability of a protein [32]. It was found that the ionic strength is a potentially confounding variable and linear extrapolation is generally less applicable to guanidinium salt so that

Maxwell et. al. [33] recommended urea as a denaturant for protein unfolding investigation. However, some proteins do not unfold in saturated urea solution, so the guanidinium chloride or guanidinium thiocyanate may be required. There are some advantages of GuHCl over urea. Since the solutions of urea slowly decompose to form cyanate and ammonium ions, the cyanate ions are capable of chemically modifying the amino groups of the protein so the urea stock solutions should be prepared and used within the same day. By contrast, solutions of GuHCl are stable for months. Because the GuHCl is hygroscopic compound, its molarity is determined by refractive index measurement after the solution has been prepared [32]. The free energy change can be calculated from the unfolding curve from native (N) to the unfolded (U) states.

Phi (Φ) Analysis of Amino Acid Substitution

The degree of formation of structure at individual positions in a particular state, I, on the folding pathway can be estimated by phi value from the changes of its free energy on mutation ($\Delta\Delta G\#\text{-}U$) relative to the change in the overall free energy of folding ($\Delta\Delta G_{F\text{-}U}$). When the quantity $\Phi_F(\#) = \Delta\Delta G\#\text{-}U / \Delta\Delta G_{F\text{-}U}$ is = 1, then the transition state is destabilized by mutation in the same amount of energy as is the fully folded state, F. When $\Phi_F(\#) = 0$ means transition state is as unaffected by mutation as is the unfolded state, U. Intermediate values of Φ indicate either partial formation of structure or a mixture of states of different degrees of formation of structure [34].

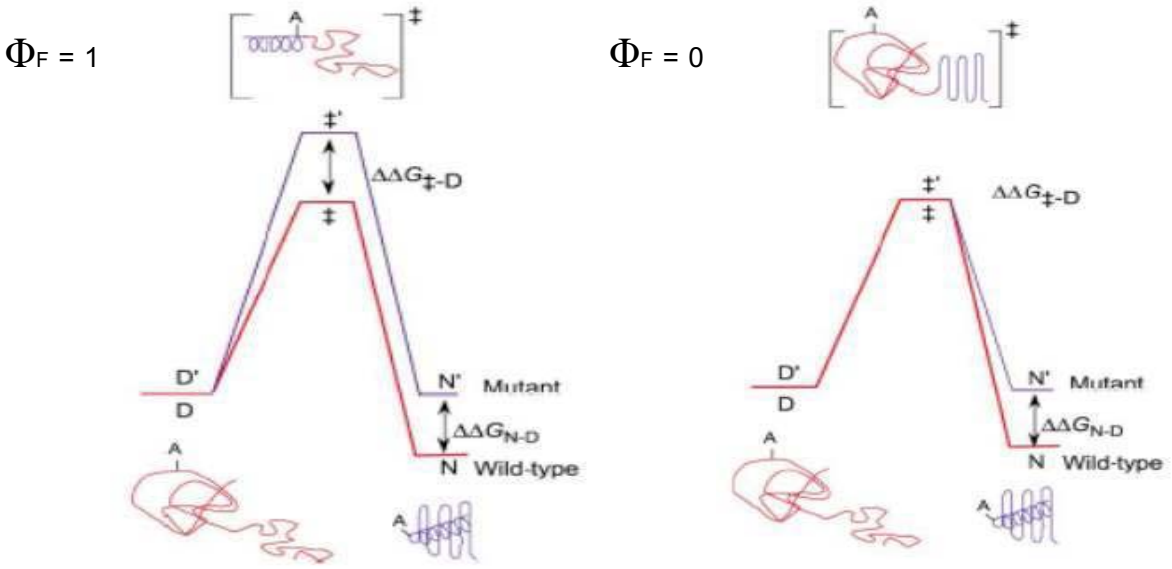

Figure 3: Transition state of mutant similar to folded ($\Phi F = 1$), and unfolded state ($\Phi F = 0$)

The Φ-value analysis requires the availability of a set of non-disruptive mutants, mutants in which the structure is not significantly altered outside the position of the mutation. In hydrophobic cores of the protein molecule, preferentially the mutations delete only one or two methyl-groups, for example Val Ala, Leu Ala, Ile Ala, Ala Gly. In helices mutations may be used which delete interaction of neighboring amino acid residues, for example Gln Ala, Gln Gly, Ala Gly and Ser Ala [35].

This research project aim to investigate structural folding pathway and molecular stability of Cyt2Aa2 toxin by using a chemical induced unfolding/refolding experiment. Based on guanidine hydrochloride induced unfolding/refolding of the protoxin, we have identified three states of toxin in native (N), intermediate (I) and unfolded (U) conformations. The transitional free energy for each transition was determined and reported. The Φ (phi)-value analysis was then employed for further study of the unfolding pathway to reveal the degree of the conformational states and energetic quantities, related to changes in the protein's stability and folding rate between wild type and single-site mutant toxins. Fifteen mutants were constructed with point mutation on each secondary structure elements of the toxins. These mutant are V32A (β-1), V46A (β-2), A57G (α-A), A80C (α-B), V109A, L114A (α-C), F131A, V135A, G141A (α-D), H158A (β-5), Y168T (β-6), V186A, A190G, V193A (β-6), and V223A (β-7). The results revealed the unfolding/folding states affected by the point mutation. The experiment also included structural characterization on the intermediate state that might be involved in the mechanism of action of toxin

MATERIALS AND METHODS

Protein Expression

E. coli colony was inoculated in 3 ml LB broth containing 100 mg/ml ampicillin and incubated at 37°C 250 rpm for overnight. The overnight culture was transferred into a new flask of LB-ampicillin broth to make up 1% of final concentration. The culture was incubated at 37°C 250 rpm for 2-3 hours until OD600 reached 0.3-0.5. An expression was induced by adding isopropyl-B-D-thiogalactopyranoside (IPTG) with a final concentration 0.1 mM and incubated for 4 hours. OD600 of the culture was measured and 1 OD was collected by centrifugation 5,000 rpm for 5 minutes. The cell pellet was re-suspended with 50 ml of distilled water and 20 ml of 4X sample buffer. The 0.1 OD of cell suspension was loaded and analyzed on 10% SDS-PAGE.

Protein Purification by Size-Exclusion Chromatography

The activated toxin was purified by FPLC system (GE Healthcare, USA) using Superdex 200 HR 10/30 column to separate the proteins by their sizes. The column was equilibrated with 50 mM $NaHCO_3/Na_2CO_3$, pH 9.8 at the flow rate 0.4 ml/minute. The purification profile was observed under the UV absorbance of 280 nm. Both buffer and protein sample were filtered through 0.2 mm membrane before applied to the column. The corresponded peaks were collected and then analyzed on 13% SDS-PAGE.

Protein Solubilization and Quantification

Inclusion protein was dissolved in 50 mM of carbonate buffer pH 9.8 ($NaHCO_3/Na_2CO_3$), incubated at 37°C for 1 hour and the supernatant was collected by centrifugation at 10,000 rpm for 10 minutes. Protein concentration was determined by using Bio-Rad protein assay reagent based on method described by Bradford (36). The Bovine Serum Albumin (BSA) was used as protein standard for calibration curve. The concentrations of BSA were prepared with distilled water from 0.1, 0.2, 0.4, 0.6, and 0.8 mg/ml. A 10 ml of either standard BSA or partial-purified inclusion was mixed with 300 ml of Bradford dye reagent and the mixture was further incubated at room temperature for 10 minutes. The absorption at 595 nm was measured by using Hitachi U-2000 spectrophotometer. The protein concentration was calculated from the standard curve. For spectroscopic analysis, the protein concentration was also determined based on the absorbance at 215 and 225 nm (37). The protein spectrum was measured from 190 to 350 nm and subtracted with baseline spectrum. Protein

concentration was calculated by the formula: Protein concentration (mg/ml) = 0.144 x (OD_{215} - OD_{225}), when pathlength of cuvette = 1 cm.

Circular Dichroism Spectroscopy

CD spectra were obtained by a Jasco J-715 spectropolarimeter, purged with oxygen-free nitrogen (Jasco, Japan). The instrument was calibrated daily with 1.0 mg/ml (+)-10-camphorsulphonic acid (CSA), yielding an intensity ratio between 192 and 290 nm greater than 2.0. A sample of 0.4-0.6 mg/ml was loaded into a cylindrical quartz cuvette of 0.02-cm path length (Hellma, USA) and analyzed from 190 to 260 nm. Scanning was set at a rate of 20 nm/min, with 1.0-second response time, 50-millidegree sensitivity and four accumulations. All spectra were subtracted by baseline spectra of buffers containing an appropriate concentration of GuHCl.

Intrinsic Fluorescence Spectroscopy

Emission spectra were monitored from 300 to 500 nm on Jasco FP-6300 and Perkin Elmer LS-50B spectrofluorometers, based on an excitation of intrinsic fluorescence from aromatic side chains at 280 nm. Samples containing 20-40 μg/ml of protein were analyzed in a rectangular quartz cuvette of 0.5-cm path length. Scanning rate was set at 50 nm/min. At least three repetitive scans were obtained and averaged.

Steady-State Unfolding

A series of GuHCl stock from 0-6.0 M was freshly prepared and used to unfold the protein at 4 ^{o}C. The purified toxin was incubated overnight in various concentrations of GuHCl, and then monitored for conformational state by fluorescence spectroscopy. An accurate concentration of GuHCl in each individual condition was confirmed by a refractive index, as described by Nozaki [38]. An unfolding curve of the toxin was constructed from a fluorescence intensity ratio between 330 and 350 nm ($F_{330/350}$). The apparent fraction of unfolding (f_{app}) was determined based on the equation:

$$f_{app} = \frac{I_{obs} - (\alpha_N + \beta_N [C])}{(\alpha_U + \beta_U [C]) - (\alpha_N + \beta_N [C])}$$

where I_{obs} is the observed intensity; α_N and α_U are Y-intercepts for the native and unfolded states; β_N and β_U are slopes at low and high GuHCl concentrations; and [C] is the GuHCl concentration. The transitional midpoint $[C]^{50\%}$ and unfolding free energy of the protein in the absence of denaturant $\Delta G^{o}_{w} = m[C]^{50\%}$ at 25 ^{o}C were obtained by curve fitting using the model equation [39].

$$f_{app} = \frac{(\alpha_N + \beta_N [C]) + (\alpha_U + \beta_U [C])\, exp^{[\,m\,([C] - [C]^{50\%})\,]/RT}}{1 + exp^{[\,m\,([C] - [C]^{50\%})\,]/RT}}$$

Kinetic Unfolding

The toxin (20-40 μg/ml) was mixed with various concentrations of GuHCl. The fluorescence spectra decay was recorded at 340 nm over a time course from 2000 to 5000 sec, using an excitation wavelength of 280 nm. The bandwidths of excitation and emission were 5 nm. The fluorescence decay spectra were subtracted by baseline spectra obtained in the first 50 seconds. Each curve was then fitted to the first order single exponential equation:

$$I_t = I_\alpha + \Delta I_o \exp^{(-k_{obs})t}$$

where I_t is the signal intensity at a given time, I_α is the signal intensity at the plateau, I_o is the initial intensity, ΔI is the difference of I_α and I_o, k_{obs} is the kinetic rate constant (which is denaturant dependent), and t is time. The ln k_{obs} was plotted against the GuHCl concentration and fitted with the linear equation

$$\ln k_{obs} = m[GuHCl] + \ln k_w$$

where $\ln k_w$ is the natural log of the kinetic rate constant in water, m is the slope, and [GuHCl] is the concentration of GuHCl. The k_w value was used for the activation energy calculation

$$k_w = (k_B T/h)\exp^{(-E_{ac,w})/RT}$$

where k_B is Boltzmann's constant (1.3807×10^{-23} J/K), h is Planck's constant (6.6261×10^{-34}), T is absolute temperature (^{o}K), R is the gas constant (1.987 cal/mol K) and $E_{ac,w}$ is the activation energy.

ANS Binding Assay

1-anilino-8-naphthalene-sulfonate (ANS; Sigma) was applied to determine the conformational state of an unfolding intermediate. Cyt2Aa2 protoxin (30 μg/ml) was incubated in various concentrations of GuHCl for 16-18 hrs. ANS was then added to a final concentration of 100 μM, mixed and incubated for 5 minutes in the dark. The samples were scanned for emission spectra from 420-600 nm at an excitation wavelength of 350 nm. Slit width for excitation and emission spectra was 5 nm. The spectra of blank solution (without protein) were recorded for subtraction. Intensity changes at a particular wavelength (465 nm) versus GuHCl concentrations were documented.

DNA Extraction and Analysis

An extraction of plasmid DNA from *E. coli* cell culture is based on the method using cationic detergent cetyl-trimethylammonium bromide (CTAB) for DNA precipitation [40]. In general, the E.coli cell was cultured in LB-broth for overnight. Cells are collected by centrifugation and re-suspended in STET buffer. The reaction included digestion with lysozyme, ribonuclease A and recovered in 5% CTAB. Extraction was employed by chloroform and precipitated in absolute ethanol at –20°C. DNA pellet was obtained by centrifugation, washed with 70% ethanol and then dried in room temperature. The agarose gel was prepared in TBE buffer (0.09 M Tris-HCl, 0.09 M Boric acid, 2 mM EDTA pH 8.0), and melted until reaching homogeneity in microwave oven. The gel solution was poured into an electrophoretic tray and allowed to solidify. The TBE buffer was used as an electrophoretic buffer. DNA sample was mixed with gel-loading dye (15% (w/v) Ficoll 400, 0.01% (w/v) Bromophenol blue) and then loaded into the well. After running with appropriate voltage, the gel was stained in ethidium bromide solution and destained in distilled water. The DNA patterns were visualized under UV light and photographed.

Site-Directed Mutagenesis

Site-directed mutagenesis based on the method of Stratagene's QuikChange^{TM} was employed. The recombinant plasmid containing the targeted gene, was mutated using complementary oligonucleotide primers containing the desired mutation in the polymerase chain reaction (PCR). The high fidelity polymerase, *Pfu* DNA polymerase, was used in temperature cycling. The mutagenic primers were designed and synthesized based on the

selected amino acid. The sample reaction (50 μl) was comprised of 100 ng DNA template, 50 μM for each dNTP, 10 pmole for each forward and reverse primers, 5 μl 10X *pfu* buffer, 2.5 U *Pfu* polymerase, and distilled water to make it to 50 μl. The PCR cycling was set to 95°C 1 min 1 cycle, 95°C 1 min, 44-50°C 1.30 min, 68°C 13 min 18 cycle, and 68°C 7 min 1 cycle. Following temperature cycling, the reaction was added with *Dpn* I, and incubated at 37oC for 3 hours to digest the template DNA.

Transformation of Plasmid DNA into Competent Cells

The *Dpn*I-treated PCR product approximately 20-40 ng was added into 200 μl competent cells and gently mixed. The transformation reaction was chilled on ice for 30 minutes, then placed in 42°C for exactly 90 seconds and immediately chilled on ice 2-5 minutes. The reaction was added with LB broth 800 μl and incubated at 37°C for 1 hour with shaking. The transformed cells were collected by centrifugation at 5,000 rpm for 2 minutes and re-suspended in 200 μl of media. The transformation culture was plated on LB agar plate containing 100 μg/ml of ampicillin and incubated at 37°C for 16-20 hours.

Restriction Endonuclease Analysis

The analysis was used to screen for the mutant plasmids based on their recognition sites which were introduced by the mutagenic primers. The 20 μl of reaction solution contained 100-200 ng of DNA plasmid, 1X restriction enzyme digestion buffer, 1-2 units of restriction enzyme and sterile distilled water to achieve the final volume 20 μl. The reaction solution was incubated at optimum temperature for each enzyme for 2-3 hours. The DNA product was analyzed in 0.8-1% agarose gel electrophoresis.

Mosquito Larvicidal Assay

The 2 day-old *Aedes aegypti* mosquito larvae were obtained from the mosquito-rearing facility of the Institute of Molecular Biology and Genetics, Mahidol University. The cell culture of 10 OD was collected by centrifugation 5,000 rpm for 10 minutes. The cell pellet was re-suspended with 2 ml of distilled water. The larvae were counted on 48-well titration plate (11.3 mm well diameter, Costar, MA, USA). 10 wells were performed for either wild type or mutant. Each well contained 10 larvae and was added with 200 ul (1 OD) of cell suspension. The larvae were counted after 24 hours incubation at room temperature.

Proteolytic Processing of Protoxins

The soluble protoxin was activated with Proteinase K (US Biologicals) at the ratio of protein:proteinase K 100:1 w/w. The mixture was incubated at 37oC for 1 hour and the reaction stopped was by 4 mM PMSF (Sigma) in final concentration. The mixture was centrifuged to remove the pellet and then the digestion product was analyzed on 12.5% SDS-PAGE.

Haemolytic Activity Assay

Sheep red blood cells were collected by centrifugation at 3,000 rpm, 4 °C for 5 min and then washed twice with PBS buffer pH 7.4 for 2% diluted preparation. Toxin samples (500 μg/ml) were diluted in two-fold serial dilutions with PBS buffer (100 μl/well). 2% sheep red blood cells were mixed with the diluted toxin and left at room temperature. The end-point of haemolysis was monitored after 24 hours.

Determination of Φ-value [41]

To determine the Φ-value for each mutant toxin, the difference of Gibb's free energy that is obtained from thermodynamic experiment and the rate constant of kinetic experiment were employed to calculate the phi value. For each step in the folding reaction the molecule transitions from the state i to the state j = i+1, the increase of the Φ-value is

$$\Delta\Phi_{j\text{-}i} = \frac{\Delta\Delta G_{j\text{-}I}}{\Delta\Delta G_{F\text{-}U}}$$

$\Delta\Delta G_{j\text{-}i}$ is the difference in the Gibbs energy changes for this reaction between mutant and the wild type. $\Delta\Delta G_{j\text{-}i}$ is calculated from the folding rate constants, *ki,mt* and *ki,wt* or unfolding rate constant k-*i*,mt and k-*i*,wt.

For multi-state transition:

$$\Delta\Delta G_{j\text{-}i} = -RT \times \ln\left(\frac{ki,mt}{ki,wt}\right)$$

or

$$\Delta\Delta G_{j\text{-}i} = -RT \times \ln\left(\frac{k\text{-}i,mt}{k\text{-}i,wt}\right)$$

The Φ-value of the state n is given by summing the increments of the Φ-values,

$$\Phi_n = \sum_{J=2}^{n} \Delta\Phi_{j-i}$$

For example, Φ_I of the intermediate I, of a three-state folding reaction is

$$\Phi_I = \frac{\Delta\Delta G_{\#1-U} + \Delta\Delta G_{I-\#1}}{\Delta\Delta G_{F-U}} = \frac{\Delta\Delta G_{I-U}}{\Delta\Delta G_{F-U}}$$

$$\Delta\Delta G_{\#1-U} = -RT \times \ln\left[\frac{k1,mt}{k1,wt}\right] \qquad \Delta\Delta G_{I-\#1} = -RT \times \ln\left[\frac{k-1,mt}{k-1,wt}\right]$$

For #2,

$$\Phi_{\#2} = \frac{\Delta\Delta G_{\#1-U} + \Delta\Delta G_{I-\#1} + \Delta\Delta G_{\#2-I}}{\Delta\Delta G_{F-U}} = \frac{\Delta\Delta G_{\#2-U}}{\Delta\Delta G_{F-U}} = 1 - \frac{\Delta\Delta G_{F-\#2}}{\Delta\Delta G_{F-U}}$$

$$\Delta\Delta G_{\#2-I} = -RT \times \ln\left[\frac{k2,mt}{k2,wt}\right] \qquad \Delta\Delta G_{F-\#2} = -RT \times \ln\left[\frac{k-2,mt}{k-2,wt}\right]$$

RESULTS AND DISCUSSIONS

Expression of Cyt2Aa2 toxin

Cyt2Aa2 protoxin can be produced from an *E. coli* culture. The expressed product was obtained as an inclusion protein. The protoxin was well solubilized when incubated with carbonate buffer pH 10-11. The product can be visualized by 10% SDS-PAGE analysis giving a single band around 29 kDa.

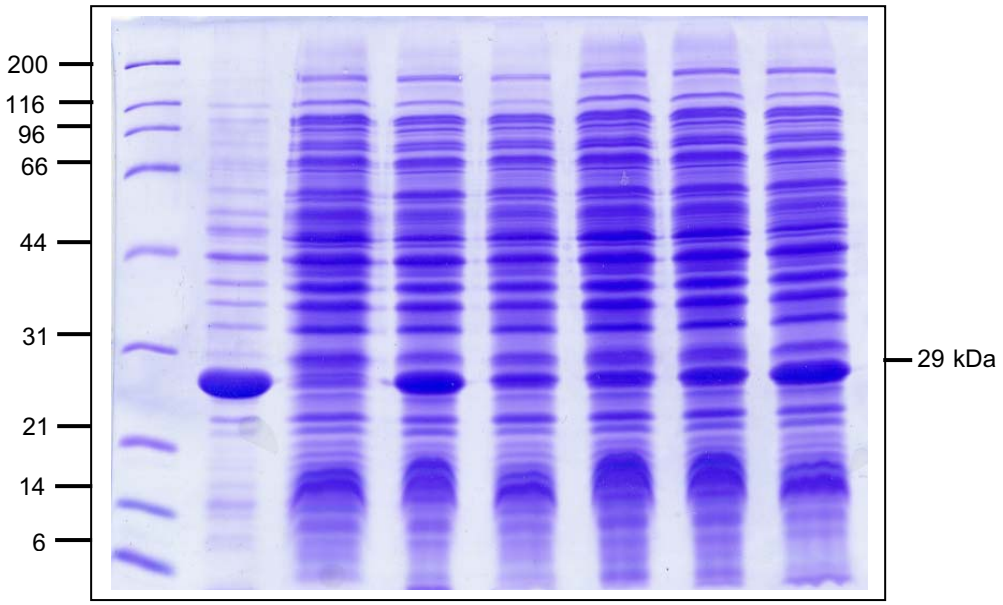

Figure 1: Expressed product of Cyt2Aa2 Toxin detected by SDS-PAGE

Purification of Toxin by Size-Exclusion Chromatography

The purification of toxin can be achieved by two steps. The first step is to obtain a partially purified of the expressed inclusion toxin by centrifugation. We normally get the partially purified product containing Cyt2Aa2 as a major component. The second step is applied to polish the purity of toxin based on size-exclusion separation. The final product can be collected as a single peak around 13-14 ml on chromatogram and observed as a single band on SDS-PAGE.

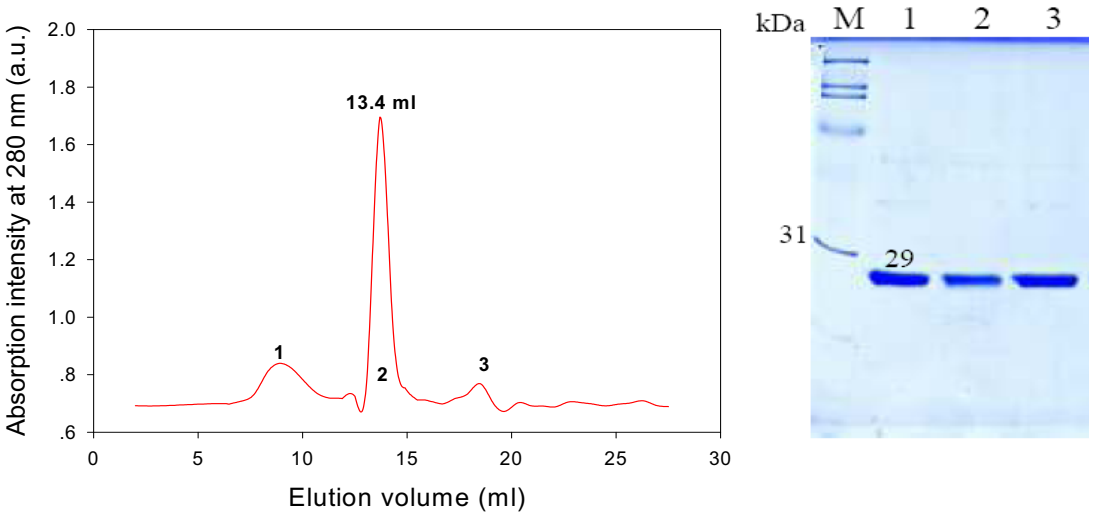

Figure 2: Chromatographic Purification of Cyt2Aa2 gives single protein on SDS-PAGE

Structural characterization by intrinsic fluorescence spectroscopy

After purification, wild type and all mutant toxins (excluding the insoluble product for V46A, F131A and V193A) were characterized for their native structures using intrinsic tryptophan as a probe. Excitation energy at 280 nm has yielded the emission spectra of the toxin molecule in the 300 to 550 nm region. The maximum wavelength (λmax) of wild type Cyt2Aa2 in carbonate buffer was found at 327 nm, representing the native conformation. This intrinsic λmax is found gradually red shifted toward 347 nm for the unfolded state obtained in 6 M GuHCl. Most of the mutants, V32A, A80G, V135A, Y168T, V186A and A190G, demonstrated the λmax of their native states similar to those of wild type. However some of the mutants, A57G, V109A, L114A, H158A and V223A showed a small shift of their λmax towards the 330-335 nm.

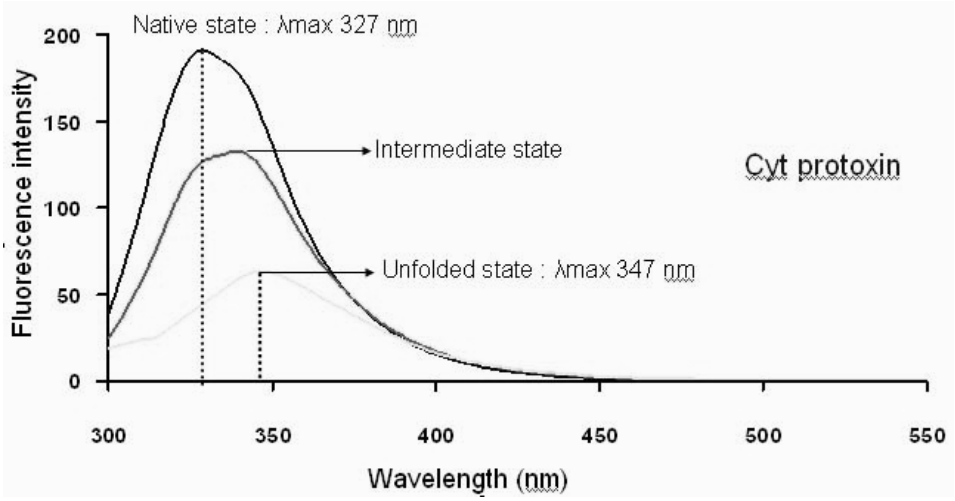

Figure 3: Intrinsic fluorescence spectra of Cyt2Aa2 in various conformational states

Steady-state unfolding/refolding and analysis of conformational free energy

We applied intrinsic fluorescence spectra of the toxin as a tool to monitor a conformational state of Cyt2Aa2 in various GuHCl concentrations. The toxin in an initial condition of carbonate buffer gives emission spectrum with λ_{max} around 330 nm. When the denaturant was gradually increased in the unfolding condition, the spectra progressively changed, with a reduction of emission intensity and a redshift of λ_{max} toward 350 nm. The shifting of λ_{max} to a longer wavelength was similar to other reported unfolding proteins such as concanavalin A, methanol dehydrogenase, and glycyl-tRNA synthetase – indicating a conformational change of tryptophan residues from an apolar to a polar environment [42-44]. With a series of intensity ratio between 330 and 350 nm representing native and unfolded conformations, an unfolding curve was then established as a function of the denaturant. The resulting curve demonstrated a well-defined feature corresponding to a three-state transitional model. These three revealed conformational states could be assumed to represent the native (N), intermediate (I) and unfolded states (U). This suggests that GuHCl could bind and help stabilize intermediate and unfolded conformations of the toxin. The steady-state conformations for N, I and U can be obtained at approximately 0-2, 3-4 and 6-7 M of GuHCl, respectively. Based on the three-state model equation, a curve fitting was performed which yielded values for denaturant concentration at a half unfolding ($[GuHCl]^{50\%}$) and transitional slope (m). These data were then used to determine the conformational free energy of protein in a denaturant-free condition (ΔG_w). After a number of independent repeats, we could report a conformational free energy of the native state at 5-6 kcal/mol, while the free energy of the intermediate against the fully unfolded state was 12-16 kcal/mol. The reverse process of these conformational changes was also analyzed by a refolding experiment. Interestingly, the derived refolding curve and free energy values were found to be very similar to those obtained from the unfolding study. These results confirmed that the two investigated pathways are simply a reversal process of the same route and existing conformations. When considering the completed transition, starting from native to unfolded state, the summation of conformational free energy found for Cyt2Aa2 toxin was 17-22 kcal/mol. This total unfolding free energy was comparable to the stabilizing energy of other native proteins with a similar molecular weight, as reported in the database [45], such as 25-kDa glutathione s-transferase, 21-kDa γD crystallin, and 28-kDa β-lactamase [46-48]. These proteins undergo a three-state unfolding involving 12 to 27 kcal/mol of free energy. Moreover, the total unfolding free energy for Cyt2Aa2 toxin was also found to be similar to the

previously reported data from the two-state unfolding of *Bacillus thuringiensis* Cry4Ba toxin [49].

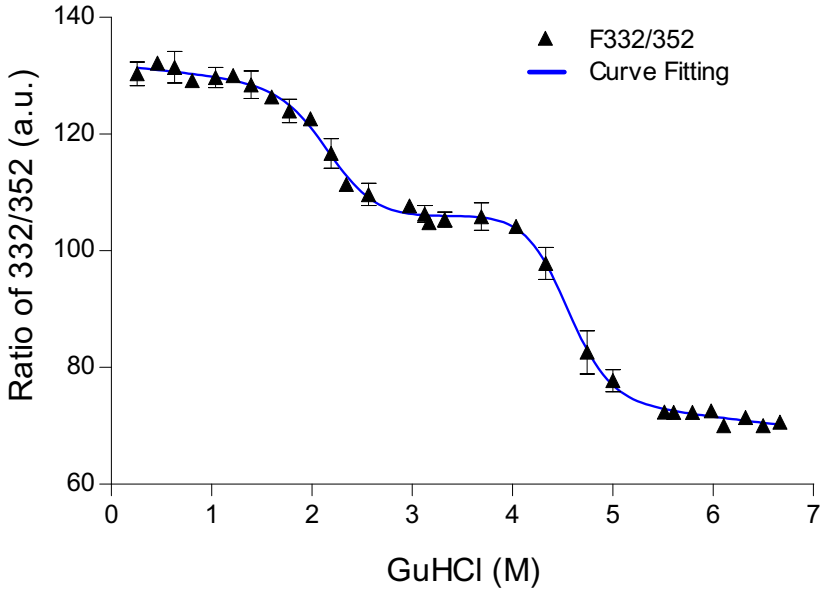

Figure 4: A typical unfolding curve of the purified toxins

Parameters	Unfolding	Refolding
m_1 (kcal/mol/M)	2.93 ± 0.22	2.55 ± 0.17
m_2 (kcal/mol/M)	3.18 ± 0.19	2.52 ± 0.14
$[GuHCl]^{50\%}_{1}$ (M)	2.14 ± 0.15	2.10 ± 0.10
$[GuHCl]^{50\%}_{2}$ (M)	4.97 ± 0.14	4.63 ± 0.09
ΔG_{w1} (kcal/mol)	6.25 ± 0.32	5.32 ± 0.20
ΔG_{w2} (kcal/mol)	15.81 ± 0.47	11.64 ± 0.28

Table 1: Conformation free energy for unfolding and refolding of wild type toxin

Kinetics of unfolding and activation energy analysis

In order to investigate the kinetics among these identified conformational states, a rapid mixing of purified toxin in carbonate buffer with various GuHCl concentrations was performed. During the mixing, intensity changes of fluorescence emission spectra were monitored over a period of time. The emission intensity corresponding to the native state at 330 nm was found to decrease obviously and rapidly after the addition of a denaturant. In addition, a more significant change of 330-nm intensity was repeatedly obtained when using a higher concentration of GuHCl. Based on the first order of single exponential equation, we were able to obtain an apparent rate constant (k_{obs}) for each denaturant condition. A linear plot between $\ln k_{obs}$ and GuHCl concentrations provided rate constants in a denaturant-free condition (k_w) of 3.60×10^{-2} and $1.94 \pm 0.55 \times 10^{-6}$ sec^{-1} for the first and second transitions. Then the activation energy ($E_{ac,w}$) for these two transitions was finally obtained around 20 and 25 kcal/mol, respectively. Despite the activation energy for both transitions being very similar, the rate constant of the second transition was much slower than that of the first one. Thus this transition from an intermediate to an unfolded state could be identified as a rate-limiting step of the unfolding pathway.

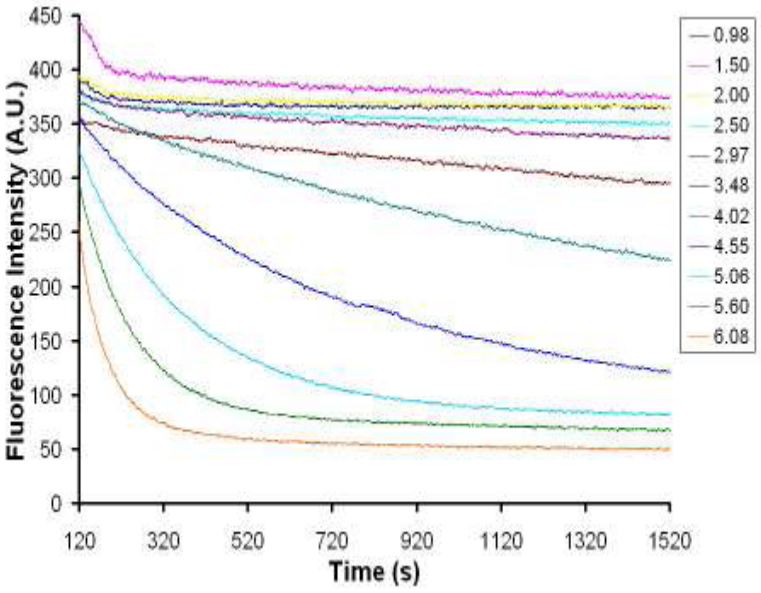

Figure 5: Kinetic of unfolding observed from fluorescence intensity at 327 nm as a function of time and various GuHCl concentrations

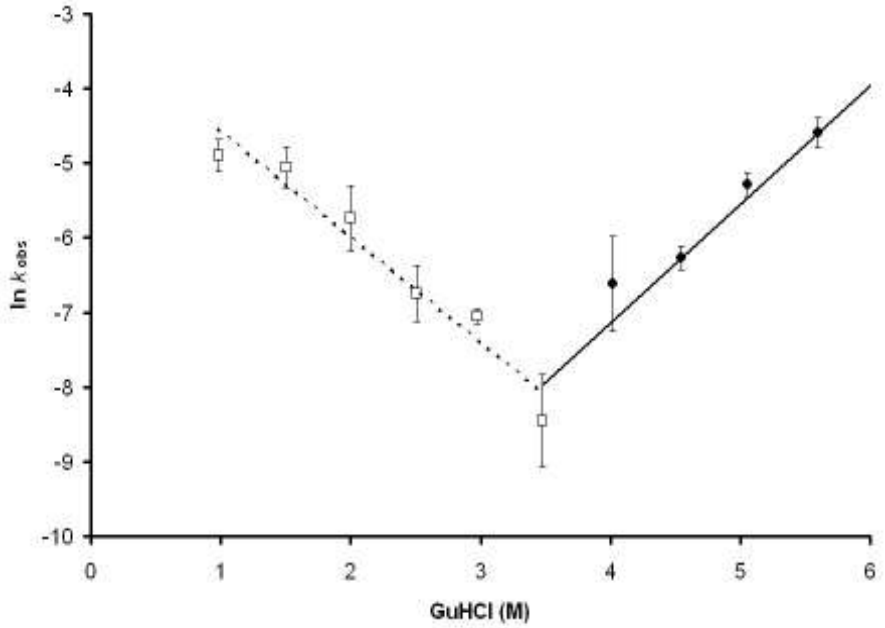

Figure 6: Chevron plots of rate constants against GuHCl concentrations for Cyt2Aa2 Blank squares represent the rate constants in the first transition from native (N) to intermediate (I) and filled circles represents the rate constants in the second transition from intermediate (I) to unfolded (U) states. Dash line and solid line are extrapolated to Y axis to obtain the ln*kw* of the first and second transitions, respectively.

Toxin	**1st transition (N -- I)**		**2nd transition (I -- U)**	
	*k*w1 (s-1)	E*ac1* (kcal/mol)	*k*w2(s-1)	E*ac2* (kcal/mol)
Cyt2Aa2	(3.60±1.03)x10-2	19.46±0.19	(1.94±0.55)x10-6	25.33±0.19

Table 2: Kinetic parameters illustrated the rate constants at 0 M GuHCl (kw) and activation energy (*Eac,w*) of the first and second transitions of Cyt2Aa2

Construction of an energy map

The combined data from steady-state and kinetic analyses can provide necessary information for the construction of a conformational energy map of the unfolding toxin. Conformational free energy (ΔG_w) of the three conformational states together with the activation energy ($E_{ac,w}$) of both transitions were mapped along the pathway progression. This energy map displays an unfolding pathway starting from a lower-energy native state, and proceeding to higher-energy intermediate and unfolded states, respectively. The transition between each conformational state involves thermodynamic free energy around 5 and 16 kcal/mol, and activation energy around 20-24 kcal/mol. This energy map for the Cyt toxin family was experimentally established for the first time in this study. It could provide relative energy characteristics for the study of protein structure and stability, and could be used as a reference for structural engineering of the mutant toxins.

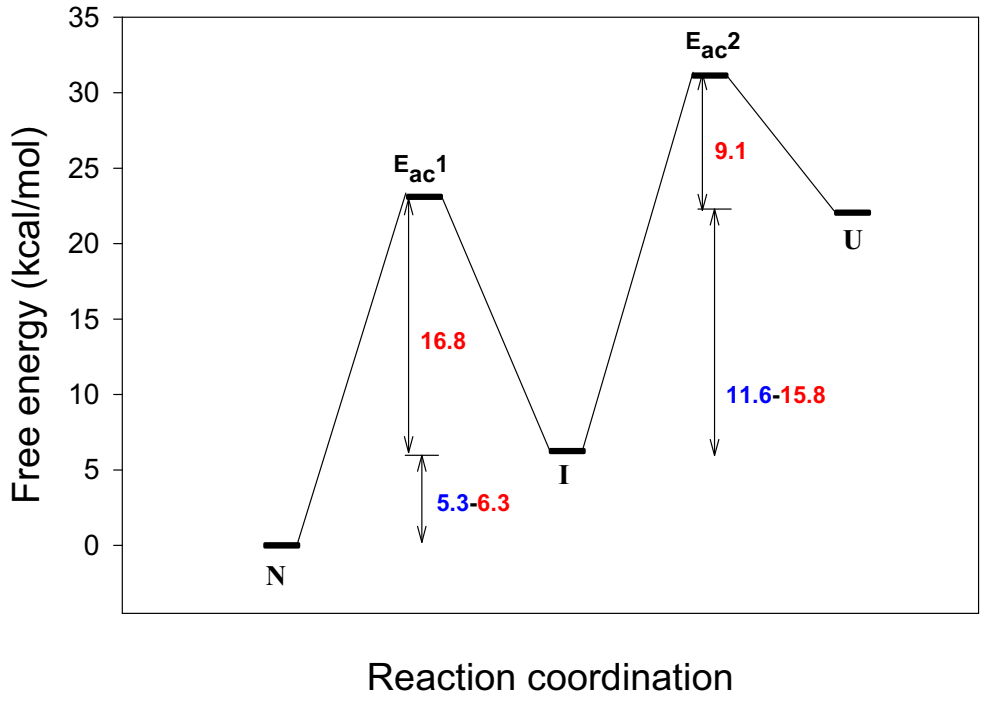

Figure 7: Energy map of protein unfolding for Cyt2Aa2 Wild Type

Characterization of intermediate state

ANS binding assay was applied to probe for an exposure of the protein hydrophobic core upon a conformational change. When fluorescent dye binds to the toxin, its emission spectrum is experimentally established with a λ_{max} of 465 nm. When this assay was performed for each denaturing condition, the results showed the maximal intensity of binding when the toxin was in 3.0-3.5 M GuHCl. It is apparent that the adopted intermediate state in this denaturing condition has a relaxed structure, and extensively exposes its hydrophobic core to the environment. We also analyzed the secondary structure of the toxin using circular dichroism spectroscopy. The CD spectra obtained for the native, intermediate and unfolded states. Interestingly, while the CD spectrum for the unfolded state indicated a significant loss of protein secondary structure, the spectra for the intermediate and native states were found to be very similar. This result suggested that the same secondary structure element is maintained in both native and intermediate states. In addition, our intrinsic fluorescence data for the intermediate state showed a red shift of λ_{max} toward 340 nm, indicating a detectable loss of the toxin's tertiary structure. Taking these data together, we were able to demonstrate that the intermediate state was present as a loose folding of the native-like secondary structure and the exposed hydrophobic core. Thus, this stable intermediate can be characterized as a defined molten globule conformation.

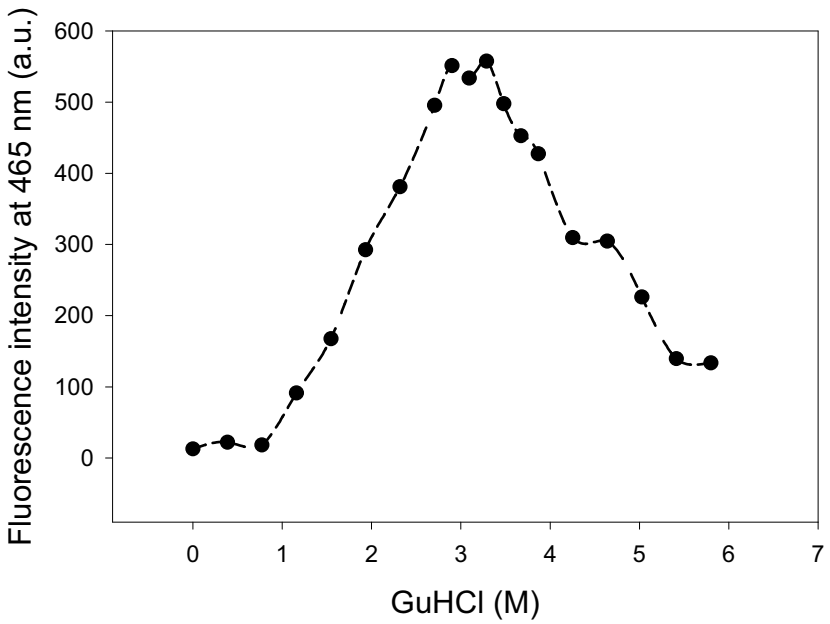

Figure 8: ANS binding assay for hydrophobic exposure of intermediate state

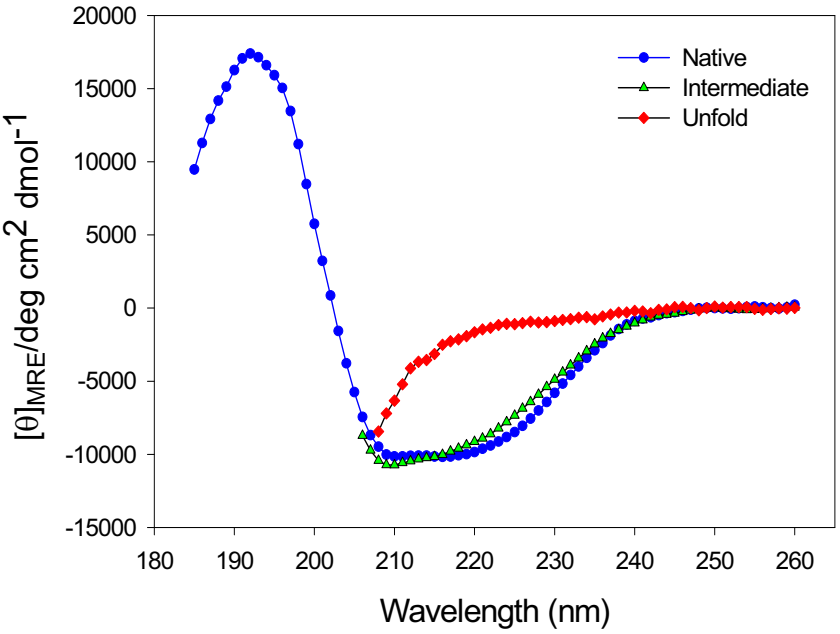

Figure 9: CD Spectra of Cyt2Aa2 Toxin at Native, Intermediate and Unfolded States

Several reports on the protein folding pathway [50-52] involve a molten globule state formation. Moreover, the molten globule states for diphtheria toxin [53], anthrax protective antigen [54] and colicins [55] had been shown to be responsible for their functions in protein-lipid membrane interactions. For *B. thuringiensis* toxin, a molten globule has been proposed for Cyt1A toxin in the presence of liposome vesicles, using differential scanning calorimetry and CD spectroscopy [56]. The toxin binds and releases the dye from lipid membrane vesicles at low pH [56-57]. It has been proposed that the molten globule structure binds to the lipid membrane independent from the net charge of the membrane. The importance of a molten globule for biological functions could also be inferred for Cyt2Aa2. Our data directly suggest a presence of molten globule in its unfolding and refolding pathway. When the native and intermediate states of the toxin are related in terms of mechanism of action, it is clear that the native conformation is required for the production of toxin, providing a stable form of protease resistance. However when the toxin undergoes a proteolytic activation and conformational change, a formation of molten globule could then be required for an active role in toxin and membrane interaction. Future investigation of the functional role and

interacting mechanism of the intermediate revealed in this work could help provide a basic understanding of the toxin structure as well as a better mechanism model to be used for the application of Cyt2A toxin.

Construction of mutant toxins

Mutant plasmids were constructed using pGEM-Cyt2Aa2 plasmid as a template. The approach was based on Stratagene's QuikChange™ site-directed mutagenesis. Agarose gel electrophoresis of the PCR products showed the expected size of plasmid of approximately 3.8 kb. After DpnI treatment and transformation to *E.coli* JM109, The mutant colonies was selected verified for their sequences. Since all the mutagenic oligonucleotide primers were designed introducing specific endonuclease restriction sites, various enzymes were used for restriction analysis and mutant screening. The results from restriction analysis showed that all the constructed mutants had the expected digestion patterns based on the introduced restriction sites. The selected clones were then subjected to be analyzed by automated DNA sequencing. The sequencing data had confirmed the designed mutation point and indicated the wild type sequence on the rest of the gene sequences. All mutant toxins were found to be expressed at a comparable level to that of wild type.

Structural unfolding of mutant toxins

All of the mutants were characterized by GuHCl induced unfolding experiment. The analyses were performed both in steady state and kinetic studies to reveal conformational free energy and activation energy respectively. Most of the mutants had demonstrated unfolding behavior similar to that of wild type showing three-state transition. Some exception was found for the mutants, A57G, L114A and V223A indicating two-state transition.

Their unfolding curves of toxins were fitted with three-state transition model to obtain the free energy values, the mid points (the point that the 50% of initial state turns to the next state) of each transition and the slopes of transition.

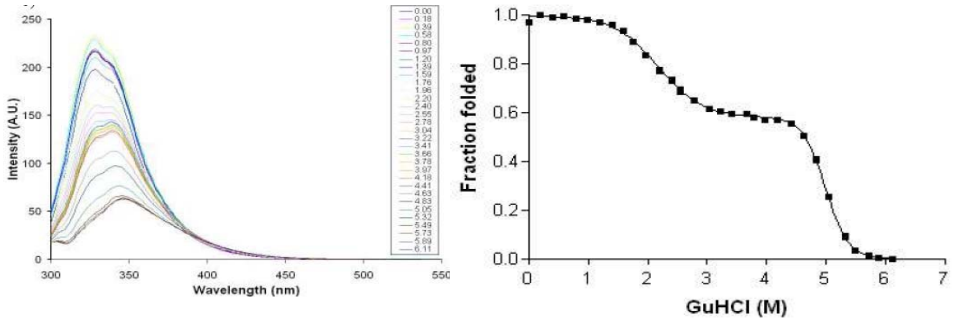

Figure 10: Steady state unfolding experiment and the typical unfolding curve obtained from mutant toxins. (This presented data come from V32A mutant)

	1st transition (N⟶I)			2nd transition (I⟶U)			
Toxin	$m_{N\rightarrow I}$ kcal/mol/M	$[D]^{50\%}$ M	ΔGw^{1st} kcal/mol	$m_{I\rightarrow U}$ kcal/mol/M	$[D]^{50\%}$ M	ΔGw^{2nd} kcal/mol	sumΔG kcal/mol
Cyt	2.70±0.53	2.19±0.02	5.89±1.08	3.79±0.13	4.72±0.72	17.89±0.89	23.78±1.16
V32A	1.68±0.28	2.04±0.04	3.41±0.54	3.42±0.09	5.01±0.03	17.13±0.05	20.54±0.10
A57G	0.84±0.06	1.66±0.22	1.39±0.17	ND	ND	ND	ND
A80G	2.78±0.55	1.26±0.28	3.50±0.79	1.99±0.20	4.74±0.04	9.45±0.97	11.87±1.47
V109A	4.55±0.08	0.77±0.01	3.51±0.10	2.61±0.01	4.79±0.21	12.48±0.48	16.06±0.48
L114A	0.46±0.09	1.38±0.35	0.62±0.07	ND	ND	ND	ND
V135A	1.74±0.06	2.75±0.14	4.81±0.41	3.60±0.31	3.63±0.09	13.05±0.80	17.86±0.39
G141A	2.06±0.44	2.17±0.11	4.39±0.74	1.72±0.33	4.92±0.26	8.55±0.19	12.94±2.60
H158A	1.45±0.17	1.10±0.24	1.65±0.55	1.71±0.27	4.58±0.02	7.81±1.24	9.45±0.72
Y168T	2.80±0.37	1.74±0.04	4.84±0.54	3.04±0.11	4.48±0.04	13.64±0.58	18.49±0.04
V186A	1.56±0.16	2.26±0.37	3.47±0.47	2.22±0.39	4.84±0.02	10.73±1.90	14.20±2.30
A190G	2.35±0.11	2.17±0.04	5.09±0.18	2.02±0.19	4.08±0.13	8.29±1.05	13.38±1.23
V223A	0.46±0.15	2.45±0.18	1.16±0.45	ND	ND	ND	ND

Table 3: Unfolding free energy of Cyt2Aa2 and its mutants in the 1st transition (N -- I) and 2nd transition (I -- U)

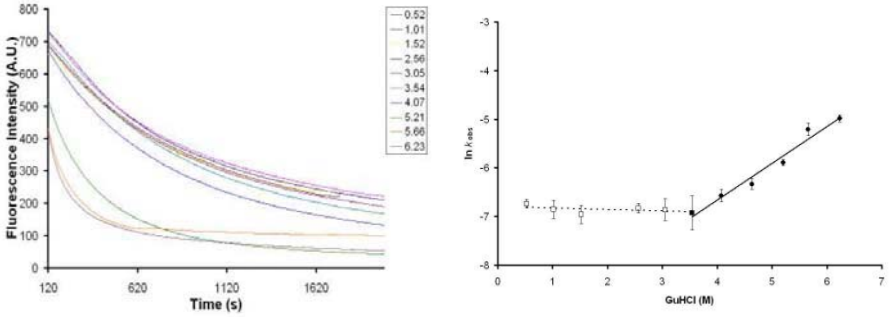

Figure 11: Kinetic unfolding experiment and the typical chevron curve obtained from mutant toxins. (This presented data come from V32A mutant)

Toxin	1st transition (N⟶I)		2nd transition (I⟶U)	
	k_{w1} (s^{-1})	$E_{ac,w1}$ (kcal/mol)	k_{w2} (s^{-1})	$E_{ac,w2}$ (kcal/mol)
Cyt	$(3.60\pm1.03)\times10^{-2}$	19.46 ± 0.19	$(1.94\pm0.55)\times10^{-6}$	25.33 ± 0.19
V32A	$(0.14\pm0.03)\times10^{-2}$	21.37 ± 0.13	$(7.26\pm2.90)\times10^{-5}$	23.18 ± 0.30
A57G	ND	ND	$(4.75\pm2.71)\times10^{-4}$	22.28 ± 0.63
A80G	$(6.26\pm2.42)\times10^{-2}$	19.12 ± 0.24	$(2.17\pm1.19)\times10^{-5}$	23.86 ± 0.34
V109A	$(15.81\pm6.39)\times10^{-2}$	18.62 ± 0.27	$(1.78\pm1.26)\times10^{-4}$	23.39 ± 1.27
L114A	ND	ND	$(3.60\pm1.14)\times10^{-4}$	22.20 ± 0.23
V135A	$(2.75\pm0.01)\times10^{-2}$	19.70 ± 0.33	$(7.07\pm3.08)\times10^{-6}$	24.55 ± 0.26
G141A	$(5.91\pm0.26)\times10^{-2}$	19.45 ± 0.40	$(3.49\pm1.41)\times10^{-6}$	25.08 ± 0.27
H158A	$(0.14\pm0.04)\times10^{-2}$	21.39 ± 0.18	$(1.16\pm0.20)\times10^{-4}$	22.83 ± 0.11
Y168T	$(0.16\pm0.00)\times10^{-2}$	21.27 ± 0.02	$(5.91\pm1.38)\times10^{-5}$	23.24 ± 0.14
V186A	$(1.51\pm0.67)\times10^{-2}$	20.02 ± 0.29	$(2.05\pm0.98)\times10^{-5}$	23.98 ± 0.38
A190G	$(0.06\pm0.00)\times10^{-2}$	21.85 ± 0.01	$(2.96\pm1.29)\times10^{-5}$	23.70 ± 0.23
V223A	ND	ND	$(1.67\pm0.23)\times10^{-4}$	22.62 ± 0.11

Table 4: Kinetic rate constant and calculated activation energy of Cyt2Aa2 and its mutants in the 1st transition (N -- I) and 2nd transition (I -- U)

Φ-value analysis of unfolding pathway

Based on Gibb's free energy values and the rate constants of wild type and its mutants were obtained from thermodynamics and kinetics unfolding, the Φ-values of each mutant were calculated to elucidate the unfolding pathway of this protein. For a multi-state transition, there are five Φ-values states of protein molecule: native (N), transition state I (TS I), intermediate (I), transition state II (TS II) and unfolded (U). The Φ-values that represent native and unfolded states were designated as 1 and 0, respectively. The Φ-values of other three states were then calculated. Beginning with native to transition state I (TS I), V32A mutant demonstrated the lowest Φ-value following by Y168T, A190G, H158A, V109A, V135A, V186A, G141A, and A80G. Most of the mutants displayed lower Φ- values in the intermediate state when compared to the transition state I except for the mutants Y168T and A190G. Compared with the intermediate state, and transition state II, most of the mutants exhibited gradually decrease of Φ-values, except V32A and V135A that presented higher Φ-values. All the mutants were set their Φ-values of unfolded state equal 0. Three mutants A57G, L114A and V223A illustrated no observed intermediate state. Their Φ-values were then calculated only in the transition state.

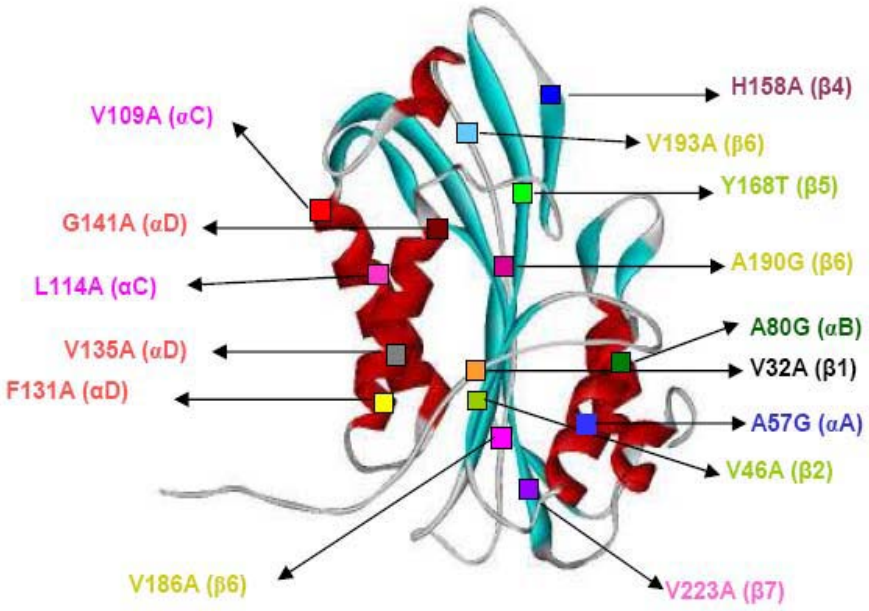

Figure 12: Structure of Cyt2Aa2, indicated the mutated residues in this study: V32A (β-1), V46A (β-2), A57G (α-A), A80C (α-B), V109A, L114A (α-C), F131A, V135A, G141A (α-D), H158A (β-4), Y168T (β-5), V186A, A190G, V193A (β-6), and V223A (β-7).

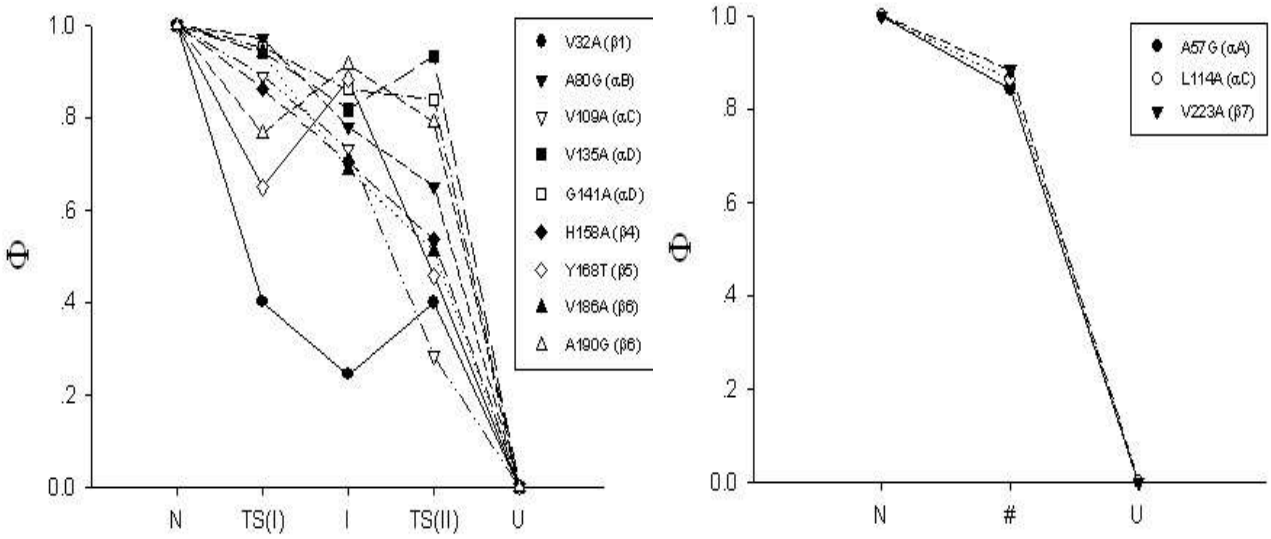

Figure 13: Φ-values of Cyt2Aa2 mutants in 3-state model transitions from native (N), transition state I (TS I), intermediate (I), transition state II (TS II) and unfolded (U) states.

Mosquito larvicidal assay

After the 2-day-old *Aedes aegypti* mosquito larvae were fed with the inclusion proteins and left for overnight, we were able to monitor the mortality rate and calculate the LC50 values for each mutant. The determined toxicity of wild type toxin was reported as LC50 = 0.48±0.03 μg/ml. While the mutants, V32A, A80G, G141A, V186A, A190G and V223A were found to toxicity comparable to that of wild type, the other mutants, V46A and H158A give a lower activity than wild type. Their LC50 are approximately 122.66±31.60 μg/ml and 69.77±2.96 μg/ml, respectively. While the mutants, A57G, V109A, L114A, F131A, V135A, Y168T and V193A showed no toxicity even when the tested concentration of the inclusion proteins were raised up to 250 μg/ml.

Hemolytic activity assay

In vitro, hemolytic activity assay was performed using 2% sheep red blood cells. The two-fold serial dilution of toxins were mixed with sheep red blood cells and left overnight. The end-point of haemolysis was observed at the lowest concentration of toxin. Hemolysis was detected when the color of mixed solution become red due to the leakage of hemopgobin from cell lysis.

The end point of wild type toxin was observed at 0.25 μg/ml of toxin concentration which is comparable to the end point of V32A, A80G, V109A, G141A, V186A, A190G and V223A mutant toxins. The mutants, A57G, L114A and H158A were found to have lower hemolytic activity than that of wild type. The activity for V46A, F131A and V193A mutants cannot be determined since they did not yield any activated toxin product from proteolytic processing.

Toxin	Solubility	Toxicity	
		Larvicidal toxicity LC_{50} (μg/ml)±SD	Hemolytic assay End point (μg/ml)
Cyt (Wild type)	++++	0.48±0.03	0.25
V32A (β1)	+++	1.57±0.28	0.125
V46A (β2)	++	122.66±31.60	No active toxin
A57G (αA)	++	>250	3.84
A80G (αB)	+++	2.22±0.07	0.55
V109A (αC)	++	>250	0.99
L114A (αC)	++	>250	15.62
F131A (αD)	+	>250	No active toxin
V135A (αD)	+++	>250	>250
G141A (αD)	+++	0.56±0.17	0.25
H158A (β4)	+++	69.77±2.96	31.25
Y168T (β5)	+++	>250	>250
V186A (β6)	+++	0.36±0.05	0.32
A190G (β6)	+++	0.49±0.05	0.25
V193A (β6)	+	>250	No active toxin
V223A (β7)	++	2.60±0.11	0.90

Number of experiment = 3

Table 5: Solubility, mosquito larvicidal and hemolytic activity of Cyt2Aa2 and mutants

CONCLUDING SUMMARY

1. We have characterized an unfolding pathway of cytolytic Cyt2Aa2 toxin from *Bacillus thuringiensis* subsp. *Darmstadiensis* by using a guanidinium hydrochloride denaturation.
2. Based on the observation of changes of circular dichroism and intrinsic fluorescence spectra, the determined unfolding curve of wild type Cyt2Aa2 was observed as three-state transition with 3 stable states of protein from native (N) to intermediate (I) and unfolded (U) states.
3. The conformational free energies for native and intermediate state unfolding are approximately 5.8 and 14.8 kcal/mol, respectively. Kinetic analysis suggested that the activation energy of both transitions was around 20-25 kcal/mol, with a rate-limiting step in the second transition. These results have established for the first time an energy profile of the Cyt2Aa2 toxin in various unfolding/refolding conformations.
4. Further characterization of the intermediate state by dye-binding assay, intrinsic fluorescence, and circular dichroism spectroscopy demonstrated characteristics of a molten globule state. This revealed intermediate may play an active role in structural folding and biological activity of the toxin.
5. We have successfully constructed 15 mutant toxins with amino acid substitution located throughout the protein secondary structure elements. They are V32A (on β1), V46A (on β2), A57G (on αA), A80C (on αB), V109A, L114A (on αC), F131A, V135A, G141A (on αD), H158A (on β4), Y168T (on β5), V186A, A190G, V193A (on β6), and V223A (β7]. Their mutated sequences were confirmed by **a**utomated DNA sequencing.
6. All mutant proteins were expressed as inclusion proteins in *E.coli* system under IPTG induction. Purification of the expressed toxin was accomplished by using size-exclusion chromatography.
7. The mutants, V32A, V46A, A80G, L114A, V135A, G141A, H158A, Y168T, V186A and A190G were soluble in 50 mM carbonate buffer (pH 10.8) comparable to that of wild

type. While the mutants, A57G, V109A and V223A were found with decreased solubility and F131A and V193A showed very low level of solubilization.

8. Proteolytic processing by proteinase K gave a 25-kDa active toxin product for V32A, A80G, V135A, G141A, Y168T and A190G 7, A57G, V109A, L114A, H158A, V186A and V223A. While the mutants, V46A, F131A and V193A were highly sensitive to the proteinase digestion, giving no active toxin product.
9. The LC50 against Stegomyia aegypti of V32A, A80G, G141A, V186A, A190G and V223A were comparable to wild type. The decreased toxicity was found for V46A and H158A. A complete loss of toxicity was observed for A57G, V109A, L114A, F131A, V135A, Y168T and V193A
10. Based on the data from these mutant toxins, It seems that the mutations on α helical elements has a significant effect on larvicidal toxicity, whereas the mutation on in the β-sheets did not affect the activity. These helical elements on toxin structure had been proposed to swing out and bind along the cell membrane.
11. Hemolytic activity of activated of V32A, A80G, V109A, G141A, V186A, A190G and V223A were comparable to that of wild type. Reduced activity was observed for A57G, L114A and H158A.
12. In an unfolding experiment, most of the mutants revealed the three-state transition similar to that of wild type. However A57G, L114A and V223A demonstrated the two-state transition.
13. The Φ-values of all mutants were found gradually decreased from native (Φ =1) to unfolded (Φ = 0) state indicating a progressive relaxation of the protein structure upon the given denaturant.
14. There are 5 states of Φ-values determined for V32A, A80G, V109A, V135A, G141A, H158A, Y168T, V186A and A190G mutant proteins, which are native (N), transition state I (TS I), intermediate (I), transition state II (TS II) and unfolded state (U). While A57G, L114A and V223A illustrated no observed intermediate state.
15. The far-UV CD spectra were found similar between the native and intermediate states of Cyt2Aa2 in 3.5 M GuHCl, while their fluorescence spectra were different. This data suggested the formation of molten globule in an intermediate state.

REFERENCES

[1] Butko P, Huang F, Pusztai-Carey M, Surewicz WK. Membrane permeabilization induced by cytolytic delta-endotoxin CytA from Bacillus thuringiensis var. israelensis. *Biochemistry.* 1996 Sep 3;35(35):11355-60.

[2] Hofte H, Whiteley HR. Insecticidal crystal proteins of *Bacillus thuringiensis. Microbiological reviews.* 1989 Jun; 53(2): 242-55.

[3] Knowles BH, White PJ, Nicholls CN, Ellar DJ. A broad-spectrum cytolytic toxin from *Bacillus thuringiensis* var. *kyushuensis.* PNAS, 1992 Apr 22; 248(1321):1-7.

[4] Boonserm P, Davis P, Ellar DJ, Li J. Crystal structure of the mosquito-larvicidal toxin Cry4Ba and its biological implications. J*ournal of molecular biology*. 2005 Apr 29; 348(2):363-82.

[5] Boonserm P, Mo M, Angsuthanasombat C, Lescar J. Structure of the functional form of the mosquito larvicidal Cry4Aa toxin from *Bacillus thuringiensis* at a 2.8-angstrom resolution. *Journal of bacteriology.* 2006 May; 188(9):3391-401.

[6] Galitsky N, Cody V, Wojtczak A, Ghosh D, Luft JR, Pangborn W, et al. Structure of the insecticidal bacterial delta-endotoxin Cry3Bb1 of *Bacillus thuringiensis. Acta crystallographica*. 2001 Aug; 57(Pt 8): 1101-9.

[7] Grochulski P, Masson L, Borisova S, Pusztai-Carey M, Schwartz JL, Brousseau R, et al. *Bacillus thuringiensis* CryIA(a) insecticidal toxin: crystal structure and channel formation. *Journal of molecular biology.* 1995 Dec 1; 254(3): 447-64.

[8] Li J, Derbyshire DJ, Promdonkoy B, Ellar DJ. Structural implications for the transformation of the *Bacillus thuringiensis* delta-endotoxins from water-soluble to membrane-inserted forms. *Biochemical Society Transactions.* 2001 Aug; 29(Pt 4):571-7.

[9] Morse RJ, Yamamoto T, Stroud RM. Structure of Cry2Aa suggests an unexpected receptor binding epitope. *Structure.* 2001 May 9;9(5):409-17.

[10] Bravo A, Gill SS, Soberon M. Mode of action of *Bacillus thuringiensis* Cry and Cyt toxins and their potential for insect control. *Toxicon.* 2007 Mar 15; 49(4):423-35.

[11] Bravo A, Gomez I, Conde J, Munoz-Garay C, Sanchez J, Miranda R, et al. Oligomerization triggers binding of a *Bacillus thuringiensis* Cry1Ab pore-forming toxin to aminopeptidase N receptor leading to insertion into membrane microdomains. *Biochimica Biophysica Acta.* 2004 Nov 17; 1667(1): 38-46.

[12] Li JD, Carroll J, Ellar DJ. Crystal structure of insecticidal delta-endotoxin from *Bacillus thuringiensis* at 2.5 A resolution. *Nature.* 1991 Oct 31; 353(6347): 815-21.

[13] Guerchicoff A, Delecluse A, Rubinstein CP. The *Bacillus thuringiensis* cyt genes for hemolytic endotoxins constitute a gene family. *Applied and Environmental Microbiology*. 2001 Mar; 67(3):1090-6.

[14] Koni PA, Ellar DJ. Cloning and characterization of a novel *Bacillus thuringiensis* cytolytic delta-endotoxin. *Journal of Molecular Biology.* 1993 Jan 20; 229(2):319-27.

[15] Waalwijk C, Dullemans AM, van Workum ME, Visser B. Molecular cloning and the nucleotide sequence of the Mr 28 000 crystal protein gene of *Bacillus thuringiensis* subsp. *israelensis*. *Nucleic Acids Research.* 1985 Nov 25; 13(22): 8207-17.

[16] Li J, Koni PA, Ellar DJ. Structure of the mosquitocidal delta-endotoxin CytB from *Bacillus thuringiensis* sp. *kyushuensis* and implications for membrane pore formation. *Journal of Molecular Biology.* 1996 Mar 22; 257(1): 129-52.

[17] Szabo E, Murvai J, Fabian P, Fabian F, Hollosi M, Kajtar J, et al. Is an amphiphilic region responsible for the haemolytic activity of *Bacillus thuringiensis* toxin? *International Journal of Peptide and Protein Research.* 1993 Dec;42(6):527-32.

[18] Lin SC, Lo YC, Lin JY, Liaw YC. Crystal structures and electron micrographs of fungal volvatoxin A2. *Journal of Molecular Biology.* 2004 Oct 15;343(2):477-91.

[19] Du J, Knowles BH, Li J, Ellar DJ. Biochemical characterization of *Bacillus thuringiensis* cytolytic toxins in association with a phospholipid bilayer. *The Biochemical Journal.* 1999 Feb 15; 338 (Pt 1):185-93.

[20] Knowles BH, Ellar DJ. Colloid-osmotic lysis is a general feature of the mechanism of action of *Bacillus thuringiensis* δ-endotoxin with different specificity. *Biochemical Biophysical Acta* 1987; 924: 509-18.

[21] Thiery I, Delecluse A, Tamayo MC, Orduz S. Identification of a gene for Cyt1A-like hemolysin from *Bacillus thuringiensis* subsp. *medellin* and expression in a crystal-negative B. thuringiensis strain. *Applied and Environmental Microbiology.* 1997 Feb; 63(2): 468-73.

[22] Knowles BH, Blatt MR, Tester M, Horsnell JM, Carroll J, Menestrina G, et al. A cytolytic delta-endotoxin from *Bacillus thuringiensis* var. *israelensis* forms cation-selective channels in planar lipid bilayers. *FEBS letters.* 1989 Feb 27; 244(2): 259-62.

[23] Promdonkoy B, Ellar DJ. Membrane pore architecture of a cytolytic toxin from *Bacillus thuringiensis. The Biochemical Journal.* 2000 Aug 15; 350 Pt 1: 275-82.

[24] Butko P. Cytolytic toxin Cyt1A and its mechanism of membrane damage: data and hypotheses. *Applied and Environmental Microbiology.* 2003 May; 69(5): 2415-22.

[25] Drobniewski FA, Knowles BH, Ellar DJ. Investigation of the membrane lesion induced in vitro by two mosquitocidal δ-endotoxins of *Bacillus thuringiensis. Current Microbiology* 1987; 15:295–9.

[26] Crickmore N, Bone EJ, Williams JA, Ellar DJ. Contribution of the Individual Components of the delta-endotoxin Crystal to the Mosquitocidal Activity of *Bacillus thuringiensis* subsp. *israelensis. FEMS Letters* 1995;131:249-54.

[27] Federici BA, Bauer LS. Cyt1Aa protein of *Bacillus thuringiensis* is toxic to the cottonwood leaf beetle, chrysomela scripta, and suppresses high levels of resistance to Cry3Aa. *Applied and Environmental Microbiology*. 1998 Nov; 64(11): 4368-71.

[28] Wu D, Chang FN. Synergism in mosquitocidal activity of 26 and 65 kDa proteins from *Bacillus thuringiensis* subsp. *israelensis* crystal. *FEBS Letters* 1985; 190:232–6.

[29] Wu D, Johnson JJ, Federici BA. Synergism of mosquitocidal toxicity between CytA and CryIVD proteins using inclusions produced from cloned genes of *Bacillus thuringiensis*. *Molecular Microbiology.* 1994 Sep; 13(6): 965-72.

[30] Manceva SD, Pusztai-Carey M, Russo PS, Butko P. A detergent-like mechanism of action of the cytolytic toxin Cyt1A from *Bacillus thuringiensis* var. *israelensis. Biochemistry.* 2005 Jan 18; 44(2): 589-97.

[31] Murphy KP. Noncovalent Forces Important to the Conformational Stability of Protein Structure. In: Shirley BA, ed. *Protien Stability and Folding, Theory and Practice*. Totowa, New Jersey: Humana Press 1995:1-34.

[32] Shirley BA. Urea and Guanidine Hydrochloride Denaturation Curves. In: Shirley BA, ed. *Protien Stability and Folding, Theory and Practice*. Totowa, New Jersey: Humana Press 1995:177-90.

[33] Maxwell KL, Wildes D, Zarrine-Afsar A, De Los Rios MA, Brown AG, Friel CT, et al. Protein folding: defining a "standard" set of experimental conditions and a preliminary kinetic data set of two-state proteins. *Protein Science.* 2005 Mar;14(3):602-16.

[34] Nolting B, Golbik R, Neira JL, Soler-Gonzalez AS, Schreiber G, Fersht AR. The folding pathway of a protein at high resolution from microseconds to seconds. *Proceedings of the National Academy of Sciences of the United States of America.* 1997 Feb 4;94(3):826-30.

[35] Nolting B. Phi-Value Analysis. *Protein Folding Kinetics*: Springer-Verlag Berlin Heidelberg 1999:105-7.

[36] Bradford MM. A rapid and sensitive method for the quantitation of microgram quantities of protein utilizing the principle of protein-dye binding. *Analytical Biochemistry.* 1976 May 7;72:248-54.

[37] Waddell WJ. A simple UV spectrophotometric method for the determination of protien. *J Lab Clin Med.* 1956; 48: 311-4.

[38] Nozaki, Y. (1972) A preparation of guanidine hydrochloride. *Method. Enzymol.* 26, 43-50.

[39] Ibarra-Molero, B. and Sanchez-Ruiz, J.M. (1996) A model-independent, nonlinear extrapolation procedure for the characterization of protein folding energetics from solvent-denaturation data. *Biochemistry* **35**, 14689-14702.

[40] Finney D. Probit analysis, third edition. London: Cambridge University Press 1971.

[41] Nolting B. Calculation and Interpretation of Phi-Values. *Protein Folding Kinetics*: Springer-Verlag Berlin Heidelberg 1999:120-3.

[42] Wang, G.F., Cao, Z.F., Zhou, H.M. and Zhao, Y.F. (2000) Comparison of inactivation and unfolding of methanol dehydrogenase during denaturation in guanidine hydrochloride and urea. *International Journal of Biochemistry and Cell Biology.* **32**, 873-878.

[43] Dignam, J.D., Qu, X. and Chaires, J.B. (2001) Equilibrium unfolding of Bombyx mori glycyl-tRNA synthetase. *Journal of Biological Chemistry.* **276**, 4028-4037.

[44] Chatterjee, A. and Mandal, D. K. (2003) Denaturant-induced equilibrium unfolding of concanavalin A is expressed by a three-state mechanism and provides an estimate of its protein stability. *Biochimical Biophysical Acta*. **1648**, 174-183.

[45] Gromiha, M.M., An, J., Kono, H., Oobatake, M., Uedaira, H. and Sarai, A. (1999) ProTherm: Thermodynamic Database for Proteins and Mutants. *Nucleic Acids Research.* **27**, 286-288.

[46] Vanhove, M., Guillaume, G., Ledent, P., Richards, J.H., Pain, R.H. and Frere, J.M. (1997) Kinetic and thermodynamic consequences of the removal of the Cys-77-Cys-123 disulphide bond for the folding of TEM-1 beta-lactamase. *Biochemistry Journal.* **321**, 413-417.

[47] Hornby, J.A., Luo, J.K., Stevens, J.M., Wallace, L.A., Kaplan, W., Armstrong, R.N., Dirr, H.W. (2000) Equilibrium folding of dimeric class mu glutathione transferases involves a stable monomeric intermediate. *Biochemistry* **39,** 12336-12344.

[48] Flaugh, S.L., Kosinski-Collins, M. S. and King, J. (2005) Contributions of hydrophobic domain interface interactions to the folding and stability of human gamma D-crystallin. *Protein Science.* **14**, 569-581.

[49] Krittanai, C., Bourchookarn, A., Pathaichindachote, W. and Panyim. S. (2003) Mutation of the hydrophobic residue on Helix 5 of the *Bacillus thuringiensis* Cry4B affects structural stability. *Protein and Peptide Letters*. **10**, 361-368.

[50] Goldberg M.E., Semisotnov, G.V. Friguet, B., Kuwajima, K., Ptitsyn, O.B. and Sugai, S. (1990) An early immunoreactive folding intermediate of the tryptophan synthease beta 2 subunit is a 'molten globule'. *FEBS Letters.* **263**, 51-56.

[51] Ptitsyn, O.B., Pain, R.H., Semisotnov, G.V., Zerovnik, E. and Razgulyaev, O.I. (1990) Evidence for a molten globule state as a general intermediate in protein folding. Evidence for a molten globule state as a general intermediate in protein folding. *FEBS Letters.* **262,** 20-24.

[52] Sugawara, T. Kuwajima, K. and Sugai, S. (1991) Folding of staphylococcal nuclease A studied by equilibrium and kinetic circular dichroism spectra. *Biochemistry* **30**, 2698-2706.

[53] Chenal, A., Savarin, P., Nizard, P., Gillet, D. and Forge, V. (2002) Membrane protein insertion regulated by bringing electrostatic and hydrophobic interaction into play: A case study with the translocation domain of diphtheria toxin. *Journal of Biological Chemistry.* **277**, 43425-43432.

[54] Gupta, P.K., Kurupati, R.K., Chandra, H., Gaur, R., Tandon, V., Singh, Y. and Maital, K. (2003) Acidic induced unfolding of anthrax protective antigen. *Biochemical Biophysical Research Communications.* **311**, 229-232.

[55] Zakharov, S.D. and Cramer, W.A. (1997) Insertion intermediates of pore-forming colicins in membrane two-dimension space. *Biochemistry* **36**, 12862-12868.

[56] Butko, P., Huang, F., Pusztai-Carey, M. and Surewicz, W.K. (1997) Interaction of the δ-endotoxin CytA from *Bacillus thuringiensis* var. *israelensis* with lipid membranes. *Biochemistry* **36**, 12862-12868.

[57] Butko, P., Huang, F., Pusztai-Carey, M. and Surewicz, W.K. (1996) Membrane permeabilization induced by cytolytic delta-endotoxin CytA from *Bacillus thuringiensis* var. *israelensis*. *Biochemistry* **35**, 11355-11360.

Research Outputs

Publications from the project

1. Thammachat, S., Pathaichindachote, W., Krittanai, C. and Promdonkoy, B. (2008) Amino acids at N- and C-termini are required for efficient production and folding of a cytolytic δ-endotoxin from Bacillus thuringiensis. **BMB Reports** 41: 820-5.
   Impact Factor (2005): 1.548

2. Promdonkoy B., Rungrod A., Promdonkoy P., Pathaichindachote W., Krittanai C. and Panyim S. (2008) Amino acid substitutions in aA and aC of Cyt2Aa2 alter hemolytic activity and mosquito-larvicidal specificity **J. Biotech**. 133, 287-293.
   Impact Factor (2005): 2.687

3. Sangcharoen A., Tepanant W., Kidsangaun S., Promdonkoy B. and Chartchai Krittanai. Investigation of the Unfolding Pathway of Bacillus thuringiensis Cyt2Aa2 Toxin Reveals an Unfolding Intermediate. (***Accepted by J. Biotech***)
   Impact Factor (2005): 2.687

Publications from indirect support of this TRF grant

1. Chongsatja, P. Bourchookarn, A. Lo, CF. Thongboonkerd, V. Krittanai, C. (2007) Proteomic analysis of differentially expressed proteins in Penaeus vannamei hemocytes upon Taura Syndrome Virus infection. **Proteomics.** Oct;7(19): 3592-601.
   Impact Factor (2005): 6.088

2. Kositanont, U. Saetun, P. Krittanai, C. Doungchawee, G. Tribuddharat, C, Thongboonkerd, V. (2007) Application of immunoproteomics to leptospirosis: towards clinical diagnostics and vaccine discovery. **Proteomics – Clin. Appl**; 1(4): 348-439.
   Impact Factor: -

3. Bourchookarn, A., Chongsatja, P. O., Thongboonkerd, V. and Krittanai, C. (2008) Proteomic analysis of altered proteins in lymphoid organ of yellow head virus infected Penaeus monodon. **Biochim. Biophys. Acta.** 1784, 504-511.
   Impact Factor (2005): 2.980

4. Junthorn, U., Unai, S., Kanthang, P., Ngamsaad, W., Modchang, C., Triampo, W., Krittanai, C., Triampo, D., Lenbury, Y. (2008) Single-Particle Tracking Method for Quantitative Tracking and Biophysical Studies of the MinE Protein. **J. Korean Phys Society.** 52(3) 639-648.

5. Unai, S., Kanthang, P., Junthon, U., Ngamsaad, W., Triampo, W., Modchang, C. and Krittanai, C. (2009) Quantitative analysis of time-series fluorescence microscopy using a spot tracking method: application to Min protein dynamics. **Biologia** 64: 27-42.

Presentations in research conferences

1. Chartchai Krittanai, Weerachon Tepanunt, Somruthai Kidsanguan, Boonhiang Promdonkoy. **Investigation of the Folding Pathway of Cyt2Aa2 Insecticidal Protein from *Bacillus thuringinesis.*** The 30th FEBS Congress and the 9th IUBMB Conference, Budapest, Hungary (July 2-7, 2005)

2. Anchanee Sangcharoen, Somruathai Kidsanguan and Chartchai Krittanai. **Protein Engineering of an Insecticidal Toxin Cyt2Aa2 by Disulfide Linkage.** The 31th Congress on Science and Technology of Thailand. (October 18-20, 2005)

3. Wanwarang Pathaichindachote, Chartchai Kritanai, Mongkon Audtho, Sakol Panyim and Boonhiang Promdonkoy. **Amino Acid Substitutions at a Possible Hinge Region Affect Conformational Changes and Biological Activity of A Cytolytic Toxin from *Bacillus thuringiensis.*** The 31th Congress on Science and Technology of Thailand. (October 18-20, 2005)

4. Anchanee Sangcharoen, and Chartchai Krittanai **Characterization of Structural Folding of Cyt2Aa2 Toxin in Intermediate State.** The 32th Congress on Science and Technology of Thailand. (October 18-20, 2006)

5. Siriya Thammachat and Chartchai Krittanai. **Mutagenesis Study of Residues on the N- and C-Terminal Ends of Cyt2Aa2 Toxin.** The 32th Congress on Science and Technology of Thailand. (October 18-20, 2006)

6. Boonsan Prasertkulchai and Chartchai Krittanai **Structure and Functional Investigation of the Outer Layer Helices of Cyt2Aa2 Toxin by Proteolytic Site Engineering.** The 32th Congress on Science and Technology of Thailand. (October 18-20, 2006)

7. Wanwarang Pathaichindachote, Chartchai Kritanai, Mongkon Audtho, Sakol Panyim and Boonhiang Promdonkoy. **Amino acids at the N-terminal are required for efficient expression and folding of a cytolytic toxin from *Bacillus thuringiensis.*** The 32th Congress on Science and Technology of Thailand. (October 18-20, 2006)

8. Amporn Rungrod, Patcharee Promdonkoy, Wanwarang Pathaichindachote, Chartchai Krittanai and Boonhiang Promdonkoy **Amino acids in αA and αC are invovled in specificity determinant of Cyt2Aa2.** The 32th Congress on Science and Technology of Thailand. (October 18-20, 2006)

9. Wanwarang Pathaichindachote, Chartchai Kritanai, Mongkon Audtho, and Boonhiang Promdonkoy **Phe143 and Leu146 of the *Bacillus thuringiensis* Cyt2Aa2 Toxin are required for Protein Folding and Crystal Packing.** The 33th Congress on Science and Technology of Thailand. (October 18-20, 2007)

10. Udorn Junthorn, Somrit Unai, Paisan Kanthang Waipot Ngamsaad, Wannapong Triampo, Charin Modchang, Chartchai Krittanai, and Yongwimon Lenbury. **How to Track MinE Protein Oscillations in *Escherichia coli.*** The 33th Congress on Science and Technology of Thailand. (October 18-20, 2007)

11. Somrit Unai, Pisan Khantang, Udon Junthorn, Waipot Ngamsaad, Narin Nattavut, Wanapong Triampo, and Chartchai Krittanai. **Single Particle Tracking: Application to Study MinD Protein Oscillation in Live *Escherichia coli.*** The 33th Congress on Science and Technology of Thailand. (October 18-20, 2007)

12. Wanwarang Pathaichindachote, Waristha Thuschana, Chartchai Kritanai, Mongkon Audtho, and Boonhiang Promdonkoy. **Role of Valine Residues at Position 193, 195 and 197 of Cyt2Aa2 Toxin from *Bacillus thuringiensis***. The 34th Congress on Science and Technology of Thailand. (October 31-November 2, 2008)

13. Anchanee Sangcharoen, Somruathai Kidsanguan and Chartchai Krittanai**. Structural Engineering of Cyt2Aa2 Toxin by Disulfide Bond** The Second Protein Research Network Symposium, Chulabhorn Research Institute (September 22-23, 2005)

14. Anchanee Sangcharoen, Somruathai Kidsanguan and Chartchai Krittanai**. Conformational Changes of the Mosquitocidal Cyt2Aa2 toxin Revealed during the Unfolding Pathway.** The 3rd Annual Symposium of Protein Society of Thailand. (August 28-29, 2008)

3. Graduate student training

Mr. Boonsan Prasertkulchai

Miss Anchanee Sangcharoen

Mr. Somrit Unai

Mr. Pisan Khantang

Mr. Udon Junthorn

Mr. Waipot Ngamsaad

ภาคผนวก

Reprint/Manuscript of Publication

Research Article

Investigation of the Unfolding Pathway of *Bacillus thuringiensis* Cyt2Aa2 Toxin Reveals an Unfolding Intermediate

Anchanee Sangcharoen[a], Weerachon Tepanant[a], Somruthai Kidsangaun[a], Boonhiang Promdonkoy[b] and Chartchai Krittanai [a,*]

[a] Institute of Molecular Biology and Genetics, Mahidol University, Salaya Campus, Putthamonthon 4 Road, Salaya, Nakhonpathom 73170, Thailand

[b] National Center for Genetic Engineering and Biotechnology (BIOTEC), National Science and Technology Development Agency, 113 Phahonyothin Road, Klong 1, Klong Luang, Pathumthani 12120, Thailand

Running Title: Unfolding pathway of Cyt2Aa2 toxin

---

* Corresponding Author: C. Krittanai, Tel: +662 800 3624 ext 1410, Fax: +662 441 9906, E-mail: stckt@mahidol.ac.th

Abstract

Cyt2Aa2 is a cytolytic toxin from *Bacillus thuringiensis* subsp. *darmstadiensis*. Its active form has a lethal activity against specific mosquito larvae. We characterized an unfolding pathway of Cyt2Aa2 using a guanidinium hydrochloride denaturation. The results revealed three-state transition with a detectable intermediate in a condition with 3-4 M of GuHCl. The conformational free energies for native and intermediate state unfolding were 5.82 ± 0.47 and 16.85 ± 1.47 kcal/mol, respectively. Kinetic analysis suggested that the activation energy of both transitions was around 23-25 kcal/mol, with a rate-limiting step in the second transition. These results have established an energy profile of the Cyt2Aa2 toxin in various conformations involved in the unfolding/refolding pathway. Further characterization of the intermediate state by dye-binding assay, intrinsic fluorescence, and circular dichroism spectroscopy demonstrated characteristics of a molten globule state. This revealed intermediate could play an active role in the structural folding and biological activity of the toxin.

Keywords: Cyt2Aa2, *Bacillus thuringiensis*, protein unfolding, molten globule, intrinsic fluorescence, circular dichroism.

Introduction

Bacillus thuringiensis is a spore-forming, Gram-positive soil bacterium which produces parasporal proteins during sporulation (Nickerson et al., 1975). The produced endotoxins can be solubilized in alkaline pH, and become insecticidal after proteolysis by insect gut proteases (Murphy et al., 1976; Bulla et al., 1977; Andrews et al., 1985; Armstrong et al., 1985). The binding of an active toxin on the brush border membrane of a susceptible insect could result in the formation of ion channels or pores, leading to osmotic imbalance, cell swelling and osmotic lysis (Hofte and Whiteley, 1989; Schnepf et al., 1998).

The cytolytic toxin Cyt2Aa2 is produced by *B. thuringiensis* subsp. *darmstadiensis* (Promdonkoy et al., 2003). This toxin is synthesized as a 29-kDa protoxin and then proteolytically processed into a 25-kDa active form. Its toxicity is found against *Stegomyia* and *Culex* sp. mosquito larvae (Galjart et al., 1987). The x-ray structure of Cyt2 toxin contains a single domain of α/β architecture comprising six α-helices and seven β-sheets (Li et al., 1996). Cyt toxin can bind and form pores in a synthetic lipid membrane without the requirement of a receptor (Thomas and Ellar, 1983). The precise mechanism of action for Cyt toxin is still unclear, and may be based on either pore-forming (Promdonkoy and Ellar, 2000; 2003) or detergent-like model (Butko, 2003). To study the details of membrane interaction, stable conformational states of the toxin should be identified and characterized. The present study aims to analyze the conformational states of Cyt2Aa2 toxin using a chemically induced unfolding experiment. The identified conformational states and calculated transitional free energy between each state in the unfolding pathway could help reveal an energy map of the toxin. In addition, the stable intermediate state can also be characterized further to provide a clue to its possible involvement in the structural folding and biological function of Cyt2Aa2 toxin.

Materials and Methods

Protein expression and purification: Cyt2Aa2 protein was expressed at 37 ^{o}C in *Escherichia coli* strain JM 109 (Promdonkoy et al., 2003) in the presence of 0.1 mM IPTG. The culture media was LB broth containing 100-μg/ml ampicillin. The cell culture was disrupted using a French pressure cell. The harvested inclusion protein was solubilized in 50 mM carbonate buffer (pH 10.0). The soluble toxin was then chromatographically purified using a Superdex-200 HR10/30 size-exclusion column (Amersham). Protein concentration was determined based on Bradford dye-binding assay and far-UV absorption (Waddell, 1956).

Circular dichroism spectroscopy: CD spectra were obtained by a Jasco J-715 spectropolarimeter, purged with oxygen-free nitrogen (Jasco, Japan). The instrument was calibrated daily with 1.0 mg/ml (+)-10-camphorsulphonic acid (CSA), yielding an intensity ratio between 192 and 290 nm greater than 2.0. A sample of 0.4-0.6 mg/ml was loaded into a cylindrical quartz cuvette of 0.02-cm path length (Hellma, USA) and analyzed from 190 to 260 nm. Scanning was set at a rate of 20 nm/min, with 1.0-second response time, 50-millidegree sensitivity and four accumulations. All spectra were subtracted by baseline spectra of buffers containing an appropriate concentration of GuHCl.

Intrinsic fluorescence spectroscopy: Emission spectra were monitored from 300 to 500 nm on Jasco FP-6300 and Perkin Elmer LS-50B spectrofluorometers, based on an excitation of intrinsic fluorescence from aromatic side chains at 280 nm. Samples containing 20-40 μg/ml of protein were analyzed in a rectangular quartz cuvette of 0.5-cm path length. Scanning rate was 50 nm/min. At least three repetitive scans were obtained and averaged.

Steady-state unfolding: A series of GuHCl stock from 0-6.0 M was freshly prepared and used to unfold the protein at 4 ^{o}C. The purified toxin was incubated overnight in various

concentrations of GuHCl, and then monitored for conformational state by fluorescence spectroscopy. An accurate concentration of GuHCl in each individual condition was confirmed by a refractive index, as described by Nozaki (Nozaki, 1972). An unfolding curve of the toxin was constructed from a fluorescence intensity ratio between 330 and 350 nm ($F_{330/350}$). The apparent fraction of unfolding (f_{app}) was determined based on the equation:

$$f_{app} = \frac{I_{obs} - (\alpha_N + \beta_N [C])}{(\alpha_U + \beta_U [C]) - (\alpha_N + \beta_N [C])}$$

where I_{obs} is the observed intensity; α_N and α_U are Y-intercepts for the native and unfolded states; β_N and β_U are slopes at low and high GuHCl concentrations; and [C] is the GuHCl concentration. The transitional midpoint $[C]^{50\%}$ and unfolding free energy of the protein in the absence of denaturant $\Delta G^{o}_{w} = m[C]^{50\%}$ at 25 °C were obtained by curve fitting using the model equation (Ibarra-Molero and Sanchez-Ruiz, 1996):

$$f_{app} = \frac{(\alpha_N + \beta_N [C]) + (\alpha_U + \beta_U [C]) \, exp^{[\, m\, (\, [C] - [C]^{50\%}\,)\,]/RT}}{1 + exp^{[\, m\, (\, [C] - [C]^{50\%}\,)\,]/RT}}$$

Kinetic unfolding: The toxin (20-40 µg/ml) was mixed with various concentrations of GuHCl. The fluorescence spectra decay was recorded at 340 nm over a time course from 2000 to 5000 sec, using an excitation wavelength of 280 nm. The bandwidths of excitation and emission were 5 nm. The fluorescence decay spectra were subtracted by baseline spectra obtained in the first 50 seconds. Each curve was then fitted to the first order single exponential equation (using the SigmaPlot 6.0 software suite):

$$I_t = I_\alpha + \Delta I \exp^{(-k_{obs})t}$$

where I_t is the signal intensity at a given time, I_α is the signal intensity at the plateau, I_o is the initial intensity, ΔI is the difference of I_α and I_o, k_{obs} is the kinetic rate constant (which is denaturant dependent), and t is time. The ln k_{obs} was plotted against the GuHCl concentration and fitted with the linear equation

$$\ln k_{obs} = m[\text{GuHCl}] + \ln k_w$$

where $\ln k_w$ is the natural log of the kinetic rate constant in water, m is the slope, and [GuHCl] is the concentration of GuHCl. The k_w value was used for the activation energy calculation

$$k_w = (k_B T/h) \exp^{(-E_{ac,w})/RT}$$

where k_B is Boltzmann's constant (1.3807×10^{-23} J/K), h is Planck's constant (6.6261×10^{-34}), T is absolute temperature (°K), R is the gas constant (1.987 cal/mol K) and $E_{ac,w}$ is the activation energy.

ANS binding assay: 1-anilino-8-naphthalene-sulfonate (ANS; Sigma) was applied to determine the conformational state of an unfolding intermediate. Cyt2Aa2 protoxin (30 µg/ml) was incubated in various concentrations of GuHCl for 16-18 hrs. ANS was then added to a final concentration of 100 µM, mixed and incubated for 5 minutes in the dark. The samples were scanned for emission spectra from 420-600 nm at an excitation wavelength of 350 nm. Slit width for excitation and emission spectra was 5 nm. The spectra of blank solution (without protein) were recorded for subtraction. Intensity changes at a particular wavelength (465 nm) versus GuHCl concentrations were documented.

Results and Discussion

Steady-state unfolding and transitional free energy analysis

We employed intrinsic fluorescence spectroscopy to monitor for conformational states of Cyt2Aa2 in various GuHCl concentrations. The toxin in an initial condition of carbonate buffer gave a fluorescence emission spectrum with λ_{max} around 330 nm. When the denaturant

was gradually increased in the unfolding condition, the spectra progressively changed, with a reduction of emission intensity and a red shift of λ_{max} toward 350 nm (Figure 1). The shifting of λ_{max} to a longer wavelength was similar to other reported unfolding proteins such as concanavalin A, methanol dehydrogenase, and glycyl-tRNA synthetase, indicating a conformational change of tryptophan residues from an apolar to a polar environment (Wang et al., 2000; Dignam et al., 2001; Chatterjee and Mandal, 2003). With a series of intensity ratio between 330 and 350 nm representing native and unfolded conformations, an unfolding curve was then established as a function of the denaturant (Figure 2). The resulting curve demonstrated a well-defined feature corresponding to a three-state transitional model. These three revealed conformational states could be assumed to represent the native (N), intermediate (I) and unfolded states (U). This suggests that GuHCl could bind and help stabilize intermediate and unfolded conformations of the toxin. The steady-state conformations for N, I and U can be obtained at approximately 0-2, 3-4 and 6-7 M of GuHCl, respectively. Based on the three-state model equation, a curve fitting was performed which yielded values for denaturant concentration at a half unfolding ($[GuHCl]^{50\%}$) and transitional slope (m). These data were then used to determine the conformational free energy of protein in a denaturant-free condition (ΔG_w). After a number of independent repeats, we could report a conformational free energy of the native state at 5.82±0.47 kcal/mol, while the free energy of the intermediate against the fully unfolded state was 16.85±1.47 kcal/mol. The reverse process of these conformational changes was also analyzed by a refolding experiment. Interestingly, the derived refolding curve and free energy values were found to be very similar to those obtained from the unfolding study. These results confirmed that the two investigated pathways are simply a reversal process of the same route and existing conformations. When considering the completed transition, starting from native to unfolded state, the summation of conformational free energy found for Cyt2Aa2 toxin was 22.67±1.94 kcal/mol. This total unfolding free energy was comparable to the stabilizing energy of other native proteins with a similar molecular weight, as reported in the database (Gromiha et al., 1999), such as 25-kDa glutathione s-transferase, 21-kDa γD crystallin, and 28-kDa β-lactamase (Vanhove et al., 1997; Hornby et al., 2000; Flaugh et al., 2005). These proteins undergo a three-state unfolding involving 12 to 27 kcal/mol of free energy. Moreover, the total unfolding free energy for Cyt2Aa2 toxin was also found to be similar to the previously reported data from the two-state unfolding of *B. thuringiensis* Cry4Ba toxin (Krittanai et al., 2003).

Kinetics of unfolding and activation energy analysis

In order to investigate the kinetics among these identified conformational states, a rapid mixing of purified toxin in carbonate buffer with various GuHCl concentrations was performed. During the mixing, intensity changes of fluorescence emission spectra were monitored over a period of time, as shown in Figure 3. The emission intensity corresponding to the native state at 330 nm was found to decrease obviously and rapidly after the addition of a denaturant. In addition, a more significant change of 330-nm intensity was repeatedly obtained when using a higher concentration of GuHCl. Based on the first order of single exponential equation, we were able to obtain an apparent rate constant (k_{obs}) for each denaturant condition. A linear plot between $\ln k_{obs}$ and GuHCl concentrations provided rate constants in a denaturant-free condition (k_w) of 3.62×10^{-6} and 5.83×10^{-10} sec^{-1} for the first and second transitions. Then the activation energy ($E_{ac,w}$) for these two transitions was finally obtained: 23.10 ± 0.28 and 24.89 ± 0.10 kcal/mol, respectively. Despite the activation energy for both transitions being very similar, the rate constant of the second transition was

much slower than that of the first one. Thus this transition from an intermediate to an unfolded state could be identified as a rate-limiting step of the unfolding pathway.

Construction of an energy map

The combined data from steady-state and kinetic analyses can provide necessary information for the construction of a conformational energy map of the unfolding toxin. Conformational free energy (ΔG_w) of the three conformational states together with the activation energy ($E_{ac,w}$) of both transitions were mapped along the pathway progression, as shown in Figure 4. This energy map displays an unfolding pathway starting from a lower-energy native state, and proceeding to higher-energy intermediate and unfolded states, respectively. The transition between each conformational state involves thermodynamic free energy around 5 and 16 kcal/mol, and activation energy around 23-24 kcal/mol. This energy map for the Cyt toxin family was experimentally established for the first time in this study. It could provide relative energy characteristics for the study of protein structure and stability, and could be used as a reference for structural engineering of the mutant toxins.

Characterization of intermediate state

ANS binding assay was applied to probe for an exposure of the protein hydrophobic core upon a conformational change. When fluorescent dye binds to the toxin, its emission spectrum is experimentally established with a λ_{max} of 465 nm. When this assay was performed for each denaturing condition, the results showed the maximal intensity of binding when the toxin was in 3.0-3.5 M GuHCl. It is apparent that the adopted intermediate state in this denaturing condition has a relaxed structure, and extensively exposes its hydrophobic core to the environment. We also analyzed the secondary structure of the toxin using circular dichroism spectroscopy. The CD spectra obtained for the native, intermediate and unfolded states are shown in Figure 5. Interestingly, while the CD spectrum for the unfolded state indicated a significant loss of protein secondary structure, the spectra for the intermediate and native states were found to be very similar. This result suggested that the same secondary structure element is maintained in both native and intermediate states. In addition, our intrinsic fluorescence data for the intermediate state showed a red shift of λ_{max} toward 340 nm, indicating a detectable loss of the toxin's tertiary structure. Taking these data together, we were able to demonstrate that the intermediate state was present as a loose folding of the native-like secondary structure and the exposed hydrophobic core. Thus, this stable intermediate can be characterized molten globule state.

Several reports on the protein folding pathway (Goldberg et al., 1990; Ptitsyn et al., 1990; Sugawara et al., 1991) involve a molten globule state formation. Moreover, the molten globule states for diphtheria toxin (Chenal et al., 2002), anthrax protective antigen (Gupta et al., 2003) and colicins (Zakharov and Cramer, 1997) had been shown to be responsible for their functions in protein-lipid membrane interactions. For *B. thuringiensis* toxin, a molten globule has been proposed for Cyt1A toxin in the presence of liposome vesicles, using differential scanning calorimetry and CD spectroscopy (Butko et al., 1997). The toxin binds and releases the dye from lipid membrane vesicles at low pH (Butko et al., 1996; Butko et al., 1997). It has been proposed that the molten globule structure binds to the lipid membrane independent from the net charge of the membrane. The importance of a molten globule for biological functions could also be inferred for Cyt2Aa2. Our data directly suggest a presence of molten globule in its unfolding and refolding pathway. When the native and intermediate states of the toxin are related in terms of mechanism of action, it is clear that the native conformation is required for the production of toxin, providing a stable form of protease

resistance. However when the toxin undergoes a proteolytic activation and conformational change, a formation of molten globule could then be required for an active role in toxin and membrane interaction. Future investigation of the functional role and interacting mechanism of the intermediate revealed in this work could help provide a basic understanding of the toxin structure as well as a better mechanism model to be used for the application of Cyt2A toxin.

Acknowledgements

This work was supported by the Thailand Research Fund (TRF) and the Thailand Center of Excellence for Physics (Integrated Physics Cluster). Graduate Scholarships from the Commission on Higher Education Staff Development program to A.S. and the Thailand Graduate Institute of Science and Technology (TGIST) to W.T were gratefully acknowledged.

References

Andrews, R.E., Bibilos, M.M. and Bulla, L.A. (1985) Protease activation of the entomocidal protoxin of *Bacillus thuringiensis* subsp. *kurstaki*. *Appl. Environ. Microb*. **50**, 737-742.

Armstrong, J.L., Rohrmann, G.F. and Beaudreau, G.S. (1985) Delta endotoxin of *Bacillus thuringiensis* subsp. *israelensis*. *J. Bacteriol.* **161**, 39-46.

Bulla, L.A., Kramer, K.J. and Davidson, L.I. (1977) Characterization of the entomocidal parasporal crystal of *Bacillus thuringiensis*. *J. Bacteriol.* **130**, 375-383.

Butko, P., Huang, F., Pusztai-Carey, M. and Surewicz, W.K. (1996) Membrane permeabilization induced by cytolytic delta-endotoxin CytA from *Bacillus thuringiensis* var. *israelensis*. *Biochemistry* **35**, 11355-11360.

Butko, P., Huang, F., Pusztai-Carey, M. and Surewicz, W.K. (1997) Interaction of the δ-endotoxin CytA from *Bacillus thuringiensis* var. *israelensis* with lipid membranes. *Biochemistry* **36**, 12862-12868.

Butko, P. (2003) Cytolytic toxin Cyt1A and its mechanism of membrane damage: data and hypotheses. *Appl. Environ. Microb*. **69**, 2415-2422.

Chatterjee, A. and Mandal, D. K. (2003) Denaturant-induced equilibrium unfolding of concanavalin A is expressed by a three-state mechanism and provides an estimate of its protein stability. *Biochim Biophys Acta*. **1648**, 174-183.

Chenal, A., Savarin, P., Nizard, P., Gillet, D. and Forge, V. (2002) Membrane protein insertion regulated by bringing electrostatic and hydrophobic interaction into play: A case study with the translocation domain of diphtheria toxin. *J Biol Chem.* **277**, 43425-43432.

Dignam, J.D., Qu, X. and Chaires, J.B. (2001) Equilibrium unfolding of Bombyx mori glycyl-tRNA synthetase. *J Biol Chem.* **276**, 4028-4037.

Flaugh, S.L., Kosinski-Collins, M. S. and King, J. (2005) Contributions of hydrophobic domain interface interactions to the folding and stability of human gamma D-crystallin. *Protein Sci.* **14**, 569-581.

Galjart, N.J., Sivasubramanian, N. and Federici, B.A. (1987) A plasmid location, cloning, and sequence analysis of the gene encoding a 27.3-kilodalton cytolytic protein from *Bacillus thuringiensis* subsp. *morrisoni* (PG-14). *Curr. Microbiol.* **16**, 171-177.

Goldberg M.E., Semisotnov, G.V. Friguet, B., Kuwajima, K., Ptitsyn, O.B. and Sugai, S. (1990) An early immunoreactive folding intermediate of the tryptophan synthease beta 2 subunit is a 'molten globule'. *FEBS Lett.* **263**, 51-56.

Gromiha, M.M., An, J., Kono, H., Oobatake, M., Uedaira, H. and Sarai, A. (1999) ProTherm: Thermodynamic Database for Proteins and Mutants. *Nucleic Acids Res.* **27**, 286-288.

Gupta, P.K., Kurupati, R.K., Chandra, H., Gaur, R., Tandon, V., Singh, Y. and Maital, K. (2003) Acidic induced unfolding of anthrax protective antigen. *Biochem. Bioph. Res. Com.* **311**, 229-232.

Hofte, H. and Whiteley, H.R. (1989) Insecticidal crystal proteins of *Bacillus thuringiensis*. *Microbiol. Mol. Biol. Rev.* **53**, 242-255.

Hornby, J.A., Luo, J.K., Stevens, J.M., Wallace, L.A., Kaplan, W., Armstrong, R.N., Dirr, H.W. (2000) Equilibrium folding of dimeric class mu glutathione transferases involves a stable monomeric intermediate. *Biochemistry* **39,** 12336-12344.

Ibarra-Molero, B. and Sanchez-Ruiz, J.M. (1996) A model-independent, nonlinear extrapolation procedure for the characterization of protein folding energetics from solvent-denaturation data. *Biochemistry* **35**, 14689-14702.

Krittanai, C., Bourchookarn, A., Pathaichindachote, W. and Panyim. S. (2003) Mutation of the hydrophobic residue on Helix 5 of the *Bacillus thuringiensis* Cry4B affects structural stability. *Protein Peptide Lett*. **10**, 361-368.

Li, J., Koni, P.A. and Ellar, D.J. (1996) Structure of the mosquitocidal δ-endotoxin CytB from *Bacillus thuringiensis* sp. *kyushuensis* and implication for membrane pore formation. *J. Mol. Biol.* **257,** 129-152.

Murphy, D.W., Sohi, S.S. and Fast, P.G. (1976) *Bacillus thuringiensis* enzyme-digested delta endotoxin: effect on cultured insect cells. *Science.* **194**, 954-956.

Nickerson, K.W., De Pinto, J. and Bulla, L.A. (1975) Lipid metabolism during bacterial growth, sporulation, and germination: kinetics of fatty acid and macromolecular synthesis during spore germination and outgrowth of *Bacillus thuringiensis*. *J. Bacteriol.* **121**, 227-233.

Nozaki, Y. (1972) A preparation of guanidine hydrochloride. *Method. Enzymol.* 26, 43-50.

Promdonkoy, B., Ellar, DJ. (2000) Membrane pore architecture of a cytolytic toxin from *Bacillus thuringiensis*. *Biochem J.* **350** (Pt) 1:275-282.

Promdonkoy, B., Chewawiwat, N., Tanapongpipat, S., Luxananil, P. and Panyim, S. (2003) Cloning and characterization of a cytolytic and mosquito larvicidal delta-endotoxin from *Bacillus thuringiensis* subsp. *Darmstadiensis*. *J. Curr. Microbiol*. **46**, 94-98.

Promdonkoy, B., Ellar, DJ. (2003) Investigation of the pore-forming mechanism of a cytolytic delta-endotoxin from *Bacillus thuringiensis*. *Biochem J.* **374** (Pt 1): 255-259.

Ptitsyn, O.B., Pain, R.H., Semisotnov, G.V., Zerovnik, E. and Razgulyaev, O.I. (1990) Evidence for a molten globule state as a general intermediate in protein folding. Evidence for a molten globule state as a general intermediate in protein folding. *FEBS Lett.* **262,** 20-24.

Schnepf, E., Crickmore, N., Van Rie, J., Lereclus, D., Baum, J., Feitelson, J., Zeigler, D.R. and Dean, D.H. (1998) *Bacillus thuringiensis* and its pesticidal crystal proteins. Microbiol. *Mol. Biol. Rev*. **62**, 775-806.

Sugawara, T. Kuwajima, K. and Sugai, S. (1991) Folding of staphylococcal nuclease A studied by equilibrium and kinetic circular dichroism spectra. *Biochemistry* **30**, 2698-2706.

Thomas, W.E. and Ellar, D.J. (1983) *Bacillus thuringiensis* var *israelensis* crystal delta-endotoxin: effects on insect and mammalian cells in vitro and in vivo. *J. Cell Sci.* **60**, 181-197.

Vanhove, M., Guillaume, G., Ledent, P., Richards, J.H., Pain, R.H. and Frere, J.M. (1997) Kinetic and thermodynamic consequences of the removal of the Cys-77-Cys-123 disulphide bond for the folding of TEM-1 beta-lactamase. *Biochem J.* **321**, 413-417.

Waddell, W.J. (1956) A simple ultraviolet spectrophotometric method for the determination of protein. *J. Lab. Clin. Med*. **48,** 311-314.

Wang, G.F., Cao, Z.F., Zhou, H.M. and Zhao, Y.F. (2000) Comparison of inactivation and unfolding of methanol dehydrogenase during denaturation in guanidine hydrochloride and urea. *Int J Biochem Cell Biol.* **32**, 873-878.

Zakharov, S.D. and Cramer, W.A. (1997) Insertion intermediates of pore-forming colicins in membrane two-dimension space. *Biochemistry* **36**, 12862-12868.

Figure Legends

Figure 1: Intrinsic fluorescence spectra of Cyt2Aa2 toxin in various concentrations of guanidinium hydrochloride. Purified toxin of 20-40 μg/ml was incubated overnight in 0.0-6.4 M GuHCl. The emission spectra were obtained from 300 to 500 nm, with an excitation at 280 nm.

Figure 2: An unfolding curve of Cyt2Aa2 toxin derived from a plot of the fluorescence intensity ratio for native (N) and unfolded (U) states between 330 and 350 nm, respectively. The three-state transition model was demonstrated to be a function of the denaturant.

Figure 3: Exponential decay of the fluorescence intensity at 330 nm from a rapid mixing of Cyt2Aa2 with various concentration of GuHCl. The faster (darker color) and slower (lighter color) decays were observed when using higher and lower concentrations of GuHCl, respectively.

Figure 4: The energetic map of Cyt2Aa2 unfolding/refolding, showing the relative energy levels for native (N), intermediate (I) and unfolded (U) states. The activation energy was also labeled for each conformational transition.

Figure 5: Circular dichroism spectra of Cyt2Aa2 toxin in the native, intermediate and unfolded states. Purified toxin of 0.3 mg/ml was applied, and the spectra expressed in $[\theta]_{MRE}/deg \cdot cm^2 \cdot dmol^{-1.}$

Figure 1

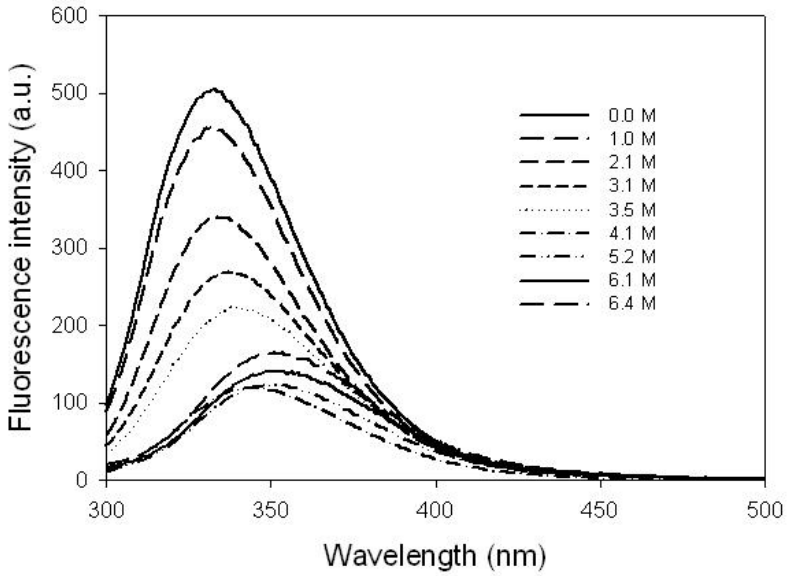

Figure 2

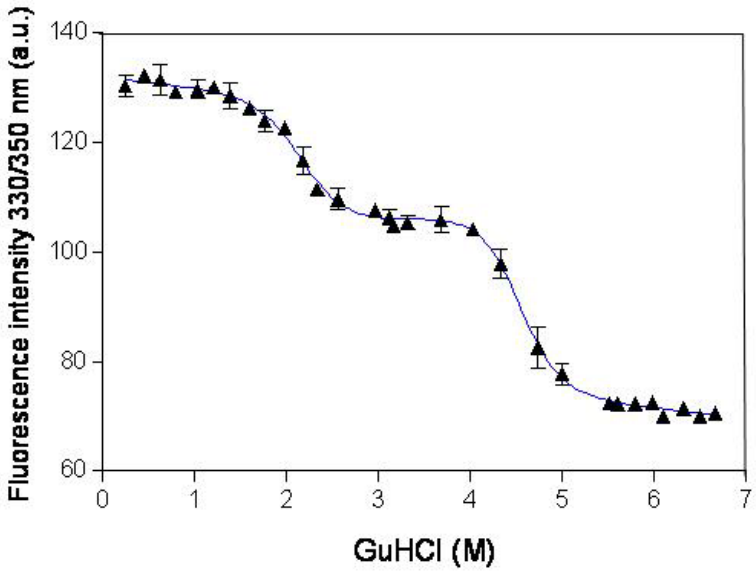

Figure 3

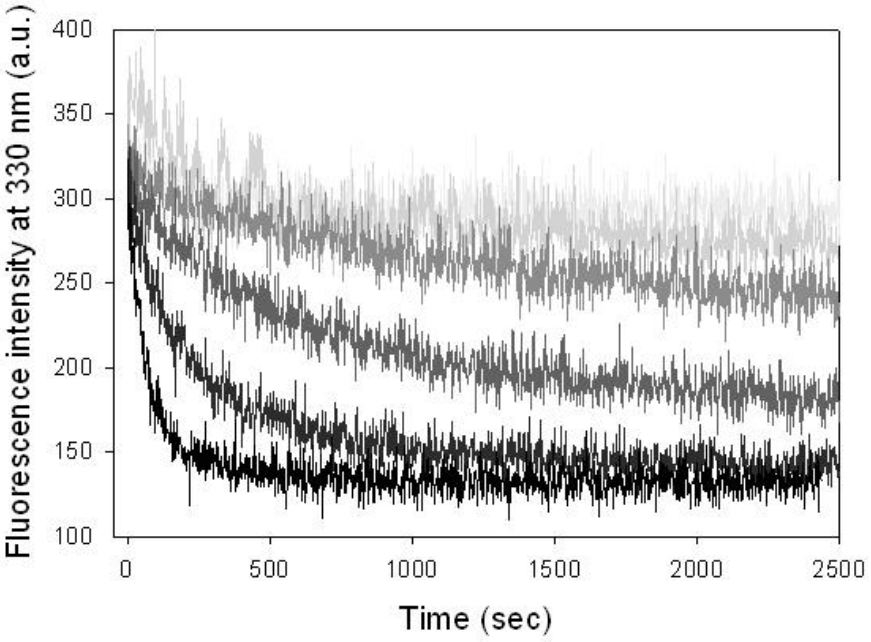

Figure 4

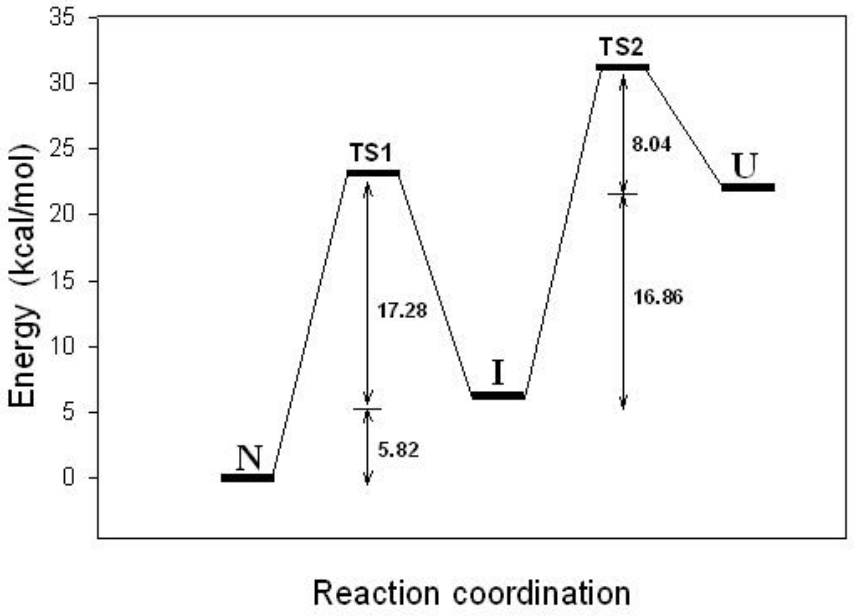

Figure 5

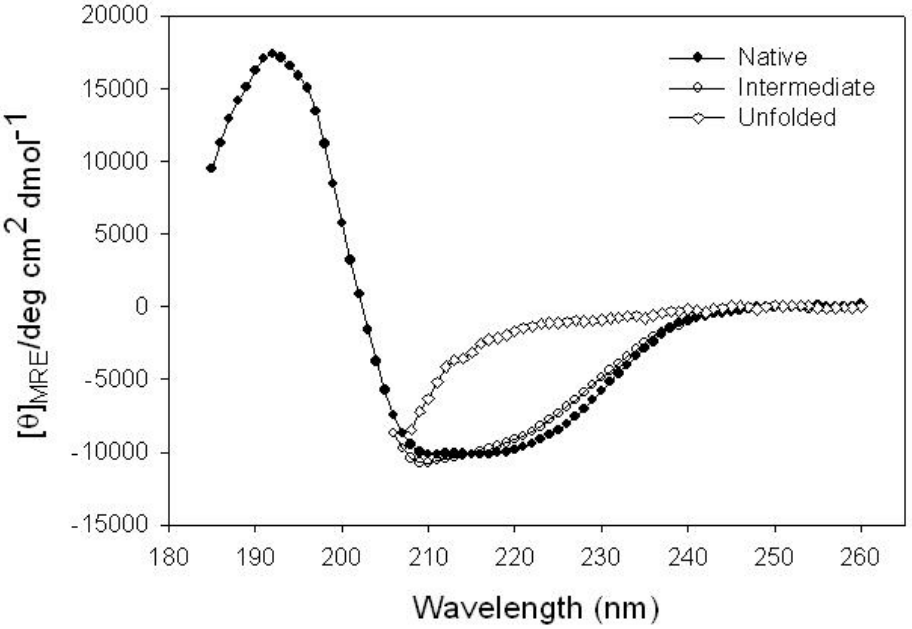
20000
15000
10000
5000
0
-5000
-10000
-15000
180
190
200
210
220
230
240
250
260
Native
Intermediate
Unfolded
$[\theta]_{MRE}$/deg cm^{-2} dmol^{-1}
Wavelength (nm)

BMB
reports

Amino acids at N- and C-termini are required for the efficient production and folding of a cytolytic δ-endotoxin from *Bacillus thuringiensis*

Siriya Thammachat[1], *Wanwarang Pathaichindachote*[2], *Chartchai Krittanai*[1] *& Boonhiang Promdonkoy*[2,*]

[1]Institute of Molecular Biology and Genetics, Mahidol University, Salaya Campus, Nakhonpathom 73170, Thailand, [2]National Center for Genetic Engineering and Biotechnology, National Science and Technology Development Agency, Pathumthani 12120, Thailand

Bacillus thuringiensis **Cyt2Aa toxin is a mosquito-larvicidal and cytolytic δ-endotoxin, which is synthesized as a protoxin and forms crystalline inclusions within the cell. These inclusions are solubilized under alkaline conditions and are activated by proteases within the larval gut. In order to assess the functions of the N-and C-terminal regions of the protoxin, several N- and C-terminal truncated forms of Cyt2Aa were constructed. It was determined that amino acid removal at the N-terminal, which disrupts the β1 structure, might critically influence toxin production and inclusion formation. The deletion of 22 amino acids from the C-terminus reduced the production and solubility of the toxin. However, the removal of more than 22 amino acids from the C-terminus or the addition of a bulky group to this region could result in the inability of the protein to adopt the proper folding. These findings directly demonstrated the critical roles of N- and C- terminal amino acids on the production and folding of the *B. thuringiensis* cytolytic δ-endotoxin. [BMB reports 2008; 41(11): 820-825]**

INTRODUCTION

Bacillus thuringiensis (Bt) is a gram-positive soil bacterium which can synthesize insecticidal crystal proteins during sporulation (1). The toxic proteins have been classified into two major groups, referred to as the Cry and Cyt toxins (2). The receptor-specific Cry proteins are generally toxic to insect larvae in the orders *Lepidoptera, Diptera*, and *Coleoptera*. The toxins in the other group, the Cyt toxins, are specifically toxic to *Dipteran* larvae including mosquito and blackfly larvae, *in vivo*. The toxins in this group also evidence cytolytic activity to a broad range of cells, including erythrocytes, *in vitro* (3-6). The amino acid sequences of all Cyt toxins show a high degree of homology with each other (7), and therefore all of them should evidence similar 3D structures. On the basis of the X-ray crystallographic structure of Cyt2Aa1 (8), all Cyt toxins should be single domain proteins with alpha-beta architectures, comprised of six helices and seven beta sheets, in which the two outer-layers of the alpha helix hairpins are wrapped around a mixed beta sheet (8).

The Cyt toxins are generated as protoxins in the form of crystalline inclusions. The crystal protoxin can be solubilized under alkaline conditions, and then proteolysis is processed by proteases in the mid-gut tracts of susceptible larvae (9). The activated toxin will bind to the epithelial cell membranes and form an oligomeric complex prior to the breakage of the cell. Two possible hypotheses have been currently proposed to explain its mode of action, and these hypotheses are referred to as the detergent-liked and pore-forming models. The detergent-like model proposes that the activated toxin molecules aggregate on the membrane surface, thereby inducing membrane fragmentation and releasing intracellular molecules (10, 11), whereas the pore-forming model suggests that parts of the toxin molecule are inserted into the lipid bilayers in order to form transmembrane pores, thus resulting in osmotic imbalances and cell lysis (12, 13).

Although no model has yet been developed in which the Cyt toxin is employed to disrupt the cell membrane, the toxin inclusions must be solubilized and the soluble protoxin must be activated by gut proteases. For Cyt2Aa, 33-37 and 22-31 amino acids at the N- and C-termini are removed in order to convert the inactive protoxin into the active toxin (9). This clearly demonstrates that amino acids at both termini are not crucial for biological activity. However, they may be required to facilitate the production and folding of the toxin within the host cell. In order to assess the functions of the N- and C-terminal regions, several N- and C-terminal truncated forms of Cyt2Aa were constructed. The truncated fragments and full-length protein were designed to be generated independently (non-fusion), and as N-terminal fusion proteins to glutathione S-transferase (GST) or C-terminal fusion proteins to green fluorescent protein (GFP).

*Corresponding author. Tel: 662-564-6700(ext 3340); Fax: 662-564-6707; E-mail: boonhiang@biotec.or.th

Received 1 July 2008, Accepted 4 September 2008

Keywords: *Bacillus thuringiensis*, Cytolytic toxin, Gene expression, Larvicidal toxin, Truncated protein

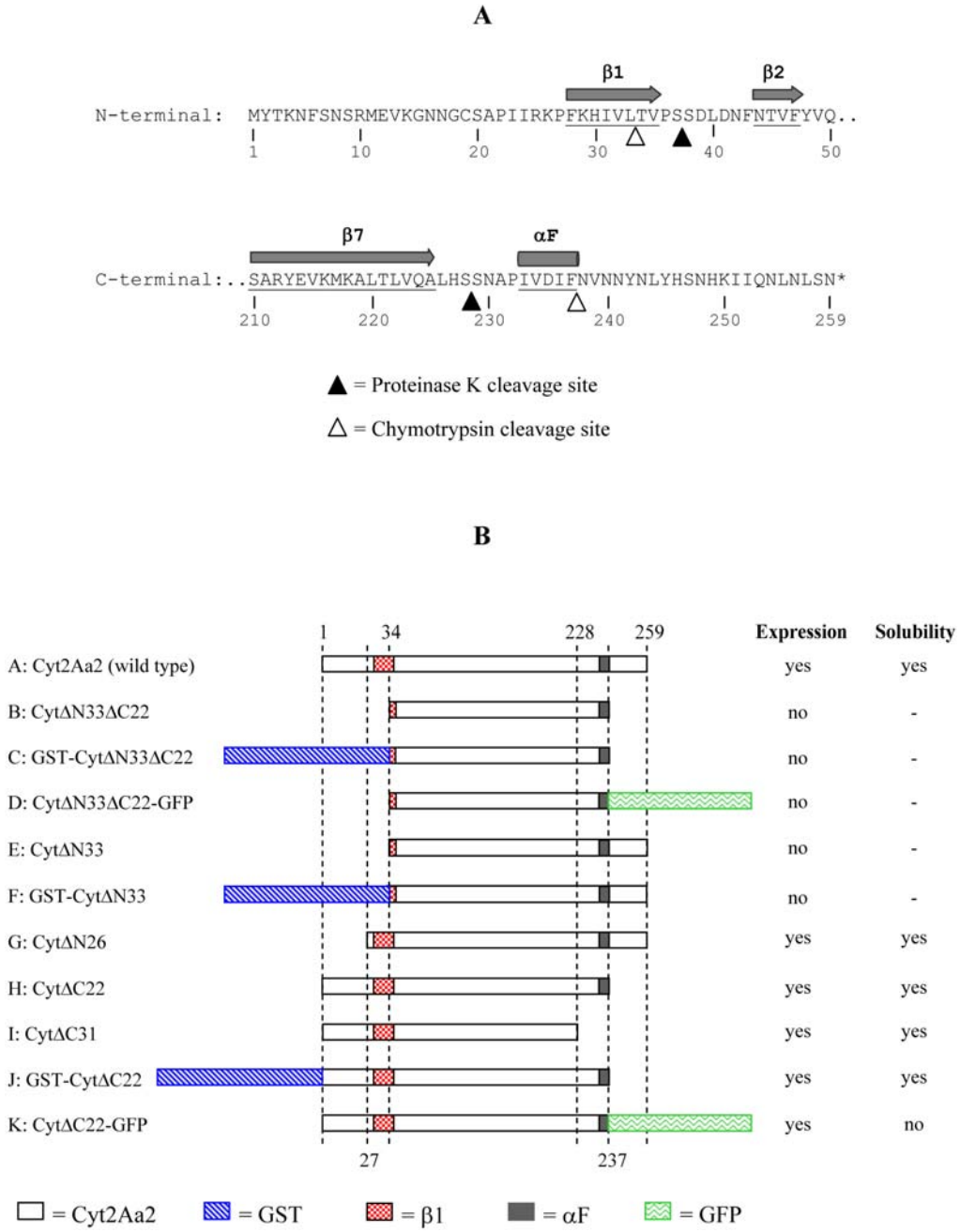

Fig. 1. (A) The deduced amino acid sequence at the N- and C-termini of Cyt2Aa. The secondary structures of the Cyt2Aa protein are shown on top of the sequence. Arrows and rod represent β-sheets and α-helix. Proteinase K and chymotrypsin cleavage sites are shown as filled and open triangles, respectively. (B) Schematic diagram representation of truncated and fusion proteins of Cyt2Aa2 toxin. Upper and lower numbering represents the definite amino acids for the design of truncated toxins. The non-fusion forms of truncated toxins were cloned into pGEM-Teasy to be expressed under the control of the *lac* promoter. Some truncated forms were subcloned into pGEX-4T-3 between the *Bam*HI and *Xho*I sites to be expressed as GST-fusion proteins. The GFP was fused to the C-terminus of truncated toxin genes (CytΔN33ΔC22 and CytΔC22) and cloned in pTZ57R.

RESULTS AND DISCUSSION

Production of truncated Cyt2Aa2 fragment similar to the protease activated toxin

The gene encoding for Cyt2Aa2 from *Bacillus thuringiensis* subsp. *darmstadiensis* has been cloned and sequenced in our laboratory (4). It comprises 259 amino acids, identical to that of Cyt2Aa1 (14). The gene was placed downstream of the *lac* promoter in pGEM-Teasy vector and transformed into *E. coli* JM109, so that it could be induced by IPTG. The full-length Cyt2Aa2 was abundantly generated as inclusion bodies within the *E. coli* cells (4). These inclusions can be readily solubilized in alkaline buffers such as 50 mM Na_2CO_3 pH 10.5. The soluble toxin can be activated *in vitro* by proteinase K or chymotrypsin. The cleavage sites for both enzymes in Cyt2Aa2 are shown in Fig. 1. Digestion with proteinase K removes up to 37 and 31 amino acids from the N- and C-terminal regions, respectively, whereas activation by chymotrypsin deletes 33 and 22 amino acids from the N- and C-terminal regions, respectively (9). Activated products from both enzymes evidenced similar activity. In order to generate truncated proteins similar to the chymotrypsin-activated toxin (CytΔN33ΔC22), the gene encoding for truncated Cyt2Aa2 between Thr34-Phe237 was amplified via PCR with a pair of specific primers. The PCR product was cloned into pGEM-Teasy vector, to be expressed under the control of the *lac* promoter. The production of the truncated fragment was not detected (not shown), although this system has already proven successful for the abundant expression of full-length Cyt2Aa2 (4). This result indicates that amino acids at either the N- or C-terminus, or both, are required for protein folding and inclusion formation. The truncated protein may fail to fold properly or may be unable to form inclusions, and could be completely digested by the proteases of the host. Amino acids at the N- and C-termini of other *B. thuringiensis* crystal toxins, such as Cry4Ba, also perform a crucial function in inclusion formation and solubilization (15, 16).

The production of several proteins in *E. coli* has been improved when expressed as GST-fusion proteins, including mosquitocidal toxin 1 (Mtx1) (17), chitinases (18), and HIV proteins (19). This approach was therefore employed to improve the production of the truncated Cyt2Aa2. The truncated gene was cloned into pGEX-4T-3 between the *Bam*HI and *Xho*I sites in order to be expressed as the GST-CytΔN33ΔC22 fusion protein (Fig. 1, fragment C). Unfortunately, no recombinant proteins were generated in this system. The truncated Cyt2Aa2 gene was also linked to the GFP gene in order to be expressed as the CytΔN33ΔC22-GFP fusion protein (Fig. 1, fragment D). However, this construct proved unable to generate the recombinant protein (not shown). Our results showed that the N- or C-terminus, or both, perform a crucial function in the production of Cyt2Aa2.

Role of N-terminal region of the Cyt toxin

In order to assess the functions of the N-terminal region of the protoxin, 3 different truncated forms of the Cyt2Aa2 toxin were constructed. The first N-terminal truncated toxin, CytΔN33, corresponding to amino acids Thr34 through Asn259 (Fig. 1, construct E), was generated in respect to the chymotrypsin cleavage site at the C-terminus of β1. The production of this truncated fragment could not be detected when the truncated gene was positioned downstream of strong promoters including lacZ (in pGEM-Teasy) and T7 (in pET-17b). The truncated gene was subsequently cloned in pGEX-4T-3, to be expressed as the GST-CytΔN33 fusion protein (Fig. 1, construct F). However, the fusion protein could not be generated in *E. coli* (not shown). The results demonstrated that the removal of 33 amino acids from the N-terminal region of Cyt2Aa2 disrupted the formation of the first β-sheet, which may be required for nucleation and subsequent folding. The misfolded protein is unstable, and could be digested completely by the host cell proteases.

Our results showed that β1 may perform a central function in protein folding. In order to evaluate this possibility, another truncated toxin harboring β1 was constructed via the deletion of the first 26 amino acids from the N-terminus (Fig. 1, construct G). This fragment (CytΔN26) was generated abundantly in *E. coli*. However, the majority of the fragments were produced in soluble form. This result suggested that amino acids at the N-terminal region upstream of β1 are required for inclusion formation, and β1 is required for protein folding or the stabilization of the protein structure.

Helix αF at the C-terminus of Cyt toxin is required for folding

The C-terminal truncated toxins were constructed on the basis of proteolytic cleavage sites (Fig. 1). Activation by chymotrypsin removes 22 amino acids from the C-terminus and leaves the αF helix intact, whereas digestion with proteinase K removes 31 amino acids from the C-terminus, including αF (Fig. 1). In order to generate C-terminal truncated toxins similar to these fragments, nucleotides encoding for Asn and Ser at positions 238 and 229 were mutated to stop codons (Fig. 1, constructs H and I). It was determined that the removal of 22 amino acids from the C-terminus (CytΔC22) exerted no detectable effects on protein production. The truncated protein was generated at a high level, and formed inclusion bodies similar to that of the full-length toxin (Fig. 2). However, protein production was reduced significantly when an additional 9 amino acids were deleted (CytΔC31). This suggested that helix αF at the very end of the molecule performs a crucial function in the efficient folding and crystal packing of the Cyt toxin. The overall conformation of the purified CytΔC31 protoxin was investigated in comparison with that of the full-length toxin via intrinsic fluorescence spectroscopy. It was determined that the CytΔC31 protoxin evidenced significantly different emission spectra as compared to the full-length protein (Fig. 3). The

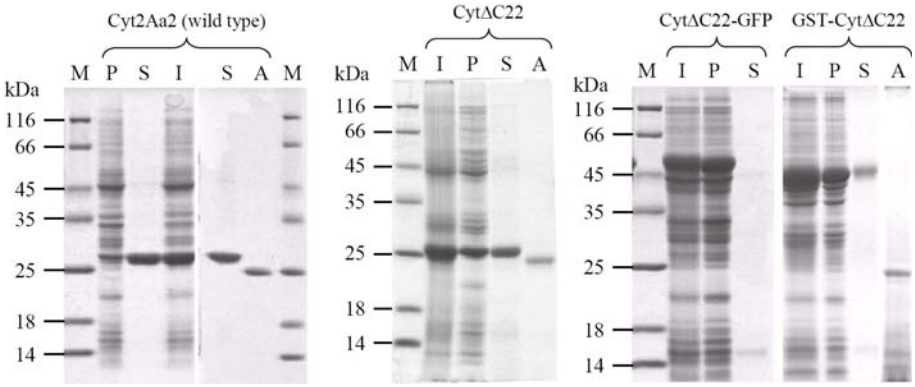

Fig. 2. Coomassie-stained SDS-polyacrylamide gel of inclusions, soluble and protease-activated Cyt2Aa2 and its truncated forms. Toxin inclusions (I) were extracted and partially purified from *E. coli*. The inclusions were solubilized in 50 mM Na_2CO_3 buffer at a pH of 10.5 plus 10 mM DTT, and the soluble fraction (S) was separated from insoluble materials or pellets (P) via centrifugation. Soluble proteins were activated (A) for 1 hour with 1% (w/w) proteinase K at 37°C. Protein molecular weight markers (M) were shown alongside in kDa.

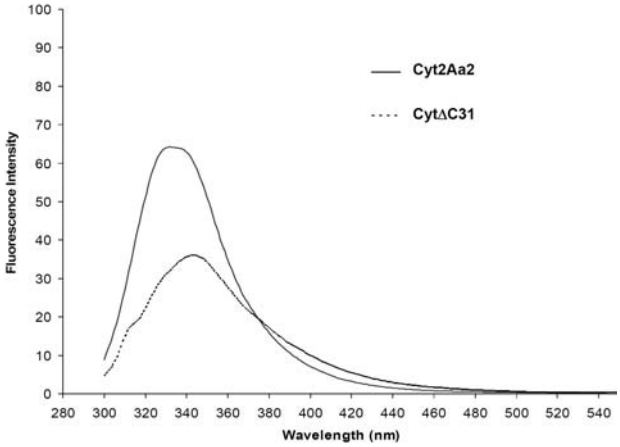

Fig. 3. Intrinsic fluorescent spectra of solubilized toxins. Solubilized toxin in carbonate buffer was excited at 280 nm and the emission spectra were scanned at between 300-500 nm.

emission spectra of the CytΔC31 protoxin evidenced a maximum peak at 342 nm, whereas that of Cyt2Aa2 was observed at 332 nm. This result showed that the overall structure of CytΔC31 differed significantly from the full-length toxin. This result suggested that the abrogation of the αF structure could effectively result in the misfolding and formation of inclusions that are more difficult to solubilize.

The addition of a bulky group, such as GST and GFP, to either end of the C-terminal truncated toxin, CytΔC22 (Fig. 1, constructs J and K), exerted no significant effects on the levels of protein production, but interfered significantly with the solubility of the toxin inclusions. The solubility of the GST-CytΔC22 inclusion was reduced and inclusions of the CytΔC22-GFP fusion protein could not be solubilized (Fig. 2). The solubilized GST-CytΔC22 fusion protein could be processed into an activated form similar to that of the wild-type (Fig. 2). These results showed that a bulky group added to the N- or C-terminus of the Cyt toxin influenced the solubility of the toxin inclusion. This indicated that both termini are involved in inclusion formation.

Biological activity of truncated proteins

Only 5 constructs were determined to be able to generate the truncated proteins, CytΔN26, CytΔC22, GST-CytΔC22, CytΔC22-GFP and CytΔC31. The mosquito larvicidal activity of these proteins was assessed by feeding to *A. aegypti* and *C. quinquefasciatus* larvae, and the results are provided in Table 1. We detected only 2 constructs that evidenced larvicidal activity, namely CytΔC22 and GST-CytΔC22. However, both of these evidenced toxicity approximately 2-5 times lower than that of the full-length toxin. Other constructs were unable to kill larvae at toxin concentrations of up to 250 μg/ml. It should be noted that the 2 truncated forms that retain larvicidal activity were generated abundantly as inclusion bodies, and the inclusions could be solubilized and activated by proteinase K. The reduction in toxicity may be attributable to the lower solubility of both truncated forms as compared to that of the full-length toxin (Fig. 2). The results of the *in vitro* solubilization test showed that CytΔC22-GFP was insoluble, and that only a minute amount of CytΔC31 could be solubilized. This showed that both of them might not be solubilized in the larval gut, and thus should not evidence any activity. The N-terminal truncated form that retains β1 (CytΔN26) exhibited no toxicity to mosquito larvae. Although it was generated at a high level, it exists in soluble form and is incapable of resisting proteinase K digestion. This protein could be digested completely by the larval gut proteases prior to exhibiting any toxicity. Hemolytic activity assays of the proteinase K-activated fragments evidenced a trend similar to that of larvicidal toxicity (Table 1).

In summary, amino acids at both termini of Cyt2Aa2 perform a crucial function during protein folding and inclusion formation. The first 26 amino acids at the N-terminal region upstream of β1 may be required for intermolecular interaction and inclusion formation. The deletion of this part might disrupt such interactions and the truncated protein could be generated in soluble form. Amino acids in β1 could be responsible for initial folding or nucleation. The truncated protein lacking β1 may not be capable of folding properly, and the misfolded protein is unstable and degraded. The final 22 amino acids at the

Table 1. Biological activities of the truncated proteins. Mosquito larvicidal activity of the mutant toxins against *A. aegypti* and *C. quinquefasciatus* larvae were reported as LC_{50}. The fiducial limits at 95% confident were shown in parentheses. Hemolytic activity against sheep red blood cells was recorded after 24 hours.

Toxin	Mosquito larvicidal activity; LC_{50} (ng/ml)[a]		Hemolysis end-point (μg/ml)
	A. aegypti	*C. quinquefasciatus*	
Full-length	286 (261-314)	313 (271-363)	0.25-0.50
CytΔC22	491 (430-559)	1,075 (941-1,230)	0.25-0.50
GST-CytΔC22	717 (570-904)	1,433 (1,172-1,755)	1.0-2.0
CytΔC22-GFP	inactive	inactive	ND[b]
CytΔC31	inactive	inactive	2.0-4.0
CytΔC26	inactive	inactive	2.0-4.0

[a] inactive means no mortality was observed when using toxin up to 250,000 ng/ml.
[b] ND means not determined (no activated toxin available)

C-terminus of Cyt2Aa2 downstream of the αF helix should not perform a major function in protein production and biological activity. However, the removal of 31 amino acids from the C-terminal region (including αF) or the addition of a bulky group to this region have resulted in the production of inclusion bodies that are insoluble within the larvae gut. The αF helix is, therefore, required for the formation of a uniform or crystalline inclusion, in order to be solubilized in the larvae gut.

MATERIALS AND METHODS

Bacterial strain, plasmid, and oligonucleotides

Escherichia coli JM109 was utilized for the cloning and expression of the full-length and truncated Cyt2Aa2 throughout this experiment. The recombinant plasmid pGEM-Cyt2Aa2 (4), containing the full-length of the *cyt2Aa2* gene from *B. thuringiensis* subsp. *darmstadiensis* 73E10-2, was utilized as a template for the construction of the truncated *cyt2Aa2* gene. The recombinant plasmid pBCgfp (20) was utilized as a source for the *gfp* gene. The plasmid pGEM-Teasy (Promega), pTZ57R (Fermentas) and pGEX-4T-3 (GE Healthcare) were utilized for the cloning and expression of truncated and fusion proteins. The oligonucleotide primers employed in this experiment were obtained from Sigma Proligo, Singapore.

Construction of recombinant plasmids expressing truncated *Cyt2Aa2* and fusion proteins

Genes encoding for truncated proteins were generated via polymerase chain reaction (PCR) using a high fidelity *Pfu* polymerase. The PCR reactions were conducted using pGEM-Cyt2Aa2 as a template, together with specific primers designed for each of the constructs. The PCR products of the gene encoding for truncation at the N-terminal region, CytΔN26 and CytΔN33, as well as the active core protein, CytΔN33ΔC22, were cloned into pGEM-Teasy vector. The construction of the C-terminal truncated toxin was based on Stratagene's QuikChange™ Site-directed mutagenesis Kit. Codons encoding for Asn at position 238 and Ser at position 229 were substituted with stop codons to generate the C-terminal truncated mutants (CytΔC22 and CytΔC31). Genes encoding for CytΔN33, CytΔC22, and the active core proteins were fused to the C-terminus of the GST gene in pGEX-4T-3 vector between the *Bam*HI and *Xho*I sites, to be expressed as GST-CytΔN33, GST-CytΔC22, and GST-CytΔN33ΔC22, respectively. The GFP gene was also tagged to the end of genes encoding for CytΔC22 and CytΔN33ΔC22 using SOE-PCR and cloned into the pTZ57R vector. The DNA sequences of all constructs were confirmed via automated DNA sequencing (Macrogen Inc, Korea). Schematic diagrams representing protease cleavage sites and the construction of truncated and fusion proteins are provided in Fig. 1.

Expression, purification, and solubilization

E. coli cells harboring mutant plasmids were inoculated in LB broth containing 100 μg of ampicillin/ml and were grown at 37°C until the OD_{600} of the culture reached 0.4-0.5. One mM IPTG was added in order to induce the expression of the toxin gene, and the culture was grown for at least an additional 5 hr. Toxin inclusions were released from cells using a French press and ultrasonication, as previously described (21). Inclusions were solubilized for 1 hour in 50 mM Na_2CO_3 pH 10.5 containing 10 mM DTT at 37°C. After 5 min of centrifugation at 12,000xg, soluble protoxin in the supernatant was collected. For proteolytic activation, the soluble protoxin was processed for 1 hour with 1% proteinase K (w/w) at 37°C.

Intrinsic fluorescence spectroscopy analysis

The comparative overall conformations of the truncated and full-length toxins were analyzed via fluorescent spectroscopy. One μM of purified toxin in carbonate buffer was added to a quartz cuvette, then placed in a Jasco FP-6500 fluorospectrometer. The protein sample was excited at 280 nm and the emission spectrum was monitored between 300-550 nm using an excitation and emission slit width of 3 nm. All emission spectra were subtracted with buffer prior to comparison with that of the full-length Cyt2Aa2.

Hemolysis activity assay

The hemolysis assay was conducted as previously described (21), with minor modifications. Sheep red blood cells were washed twice in PBS at a pH of 7.4, and diluted to a 2% suspension in the same buffer. Proteinase K-activated toxin was placed in each well of a 96-well microtiter plate as a two-fold serial dilution (100 μl/well). An equal volume of the diluted red blood cells was added to each well and incubated for 24 h at room temperature. The hemolysis end-point was judged at the last well at which coloration remained visible.

Mosquito larvicidal activity assay

Toxin inclusions were diluted in distilled water as two-fold serial dilutions from 500 to 0.25 μg/ml. One milliliter of diluted inclusion was fed to ten 3rd-instar larvae (*Culex quinquefasciatus* and *Aedes aegypti*) in 1 ml of water. The mortality of larvae in each well was recorded after 24 h of feeding with the toxin. The LC_{50} (50% lethal concentration) was calculated via Probit analysis (22).

Acknowledgements

The authors would like to thank Chawewan Chimwai for supplying the mosquito larvae. This work was supported by the Thailand Research Fund (TRF) and the National Center for Genetic Engineering and Biotechnology, National Science and Technology Development Agency, Thailand.

REFERENCES

1. Schnepf, E., Crickmore, N., Van, R. J., Lereclus, D., Baum, J., Feitelson, J., Zeigler, D. R. and Dean, D. H. (1998) Bacillus thuringiensis and its pesticidal crystal proteins. *Microbiol. Mol. Biol. Rev.* **62**, 775-806.
2. Crickmore, N., Zeigler, D. R., Feitelson, J., Schnepf, E., Van, R. J., Lereclus, D., Baum, J. and Dean, D. H. (1998) Revision of the nomenclature for the Bacillus thuringiensis pesticidal crystal proteins. *Microbiol. Mol. Biol. Rev.* **62**, 807-813.
3. Juarez-Perez, V., Guerchicoff, A., Rubinstein, C. and Delecluse, A. (2002) Characterization of Cyt2Bc toxin from Bacillus thuringiensis subsp. *medellin*. *Appl. Environ. Microbiol.* **68**, 1228-1231.
4. Promdonkoy, B., Chewawiwat, N., Tanapongpipat, S., Luxananil, P. and Panyim, S. (2003) Cloning and characterization of a cytolytic and mosquito larvicidal delta-endotoxin from Bacillus thuringiensis subsp. *darmstadiensis*. *Curr. Microbiol.* **46**, 94-98.
5. Thomas, W. E. and Ellar, D. J. (1983) Bacillus thuringiensis var israelensis crystal delta-endotoxin: effects on insect and mammalian cells *in vitro* and *in vivo*. *J. Cell Sci.* **60**, 181-197.
6. Knowles, B. H., White, P. J., Nicholls, C. N. and Ellar, D. J. (1992) A broad-spectrum cytolytic toxin from *Bacillus thuringiensis* var. *kyushuensis*. *Proc. Biol. Sci.* **248** ,1-7.
7. Guerchicoff, A., Delecluse, A. and Rubinstein, C. P. (2001) The Bacillus thuringiensis cyt genes for hemolytic endotoxins constitute a gene family. *Appl. Environ. Microbiol.* **67**, 1090-1096.
8. Li, J., Koni, P. A. and Ellar, D. J. (1996) Structure of the mosquitocidal delta-endotoxin CytB from *Bacillus thuringiensis* sp. *kyushuensis* and implications for membrane pore formation. *J. Mol. Biol.* **257**, 129-152.
9. Koni, P. A. and Ellar, D. J. (1994) Biochemical characterization of *Bacillus thuringiensis cytolytic delta-endotoxins*. *Microbiology* **140** (Pt 8), 1869-1880.
10. Butko, P. (2003) Cytolytic toxin Cyt1A and its mechanism of membrane damage: data and hypotheses. *Appl.* Environ. *Microbiol.* **69**, 2415-2422.
11. Manceva, S. D., Pusztai-Carey, M., Russo, P. S. and Butko, P. (2005) A detergent-like mechanism of action of the cytolytic toxin Cyt1A from *Bacillus thuringiensis* var. *israelensis*. *Biochemistry* **44**, 589-597.
12. Promdonkoy, B. and Ellar, D. J. (2003) Investigation of the pore-forming mechanism of a cytolytic delta-endotoxin from *Bacillus thuringiensis*. *Biochem. J.* **374**, 255-259.
13. Knowles, B. H., Blatt, M. R., Tester, M., Horsnell, J. M., Carroll, J., Menestrina, G. and Ellar, D. J. (1989) A cytolytic delta-endotoxin from *Bacillus thuringiensis* var. *israelensis* forms cation-selective channels in planar lipid bilayers. *FEBS Lett.* **244**, 259-262.
14. Koni, P. A. and Ellar, D. J. (1993) Cloning and characterization of a novel *Bacillus thuringiensis* cytolytic delta-endotoxin. *J. Mol. Biol.* **229**, 319-327.
15. Moonsom, S., Chaisri, U., Kasinrerk, W. and Angsuthanasombat, C. (2007) Binding characteristics to mosquito-larval midgut proteins of the cloned domain II-III fragment from the Bacillus thuringiensis Cry4Ba toxin. *J. Biochem. Mol. Biol.* **40**, 783-790.
16. Chayaratanasin, P., Moonsom, S., Sakdee, S., Chaisri, U., Katzenmeier, G. and Angsuthanasombat, C. (2007) High level of soluble expression in Escherichia coli and characterisation of the cloned Bacillus thuringiensis Cry4Ba domain III fragment. *J. Biochem. Mol. Biol.* **40**, 58-64.
17. Promdonkoy, B., Promdonkoy, P., Tanapongpipat, S., Luxananil, P., Chewawiwat, N., Audtho, M. and Panyim, S. (2004) Cloning and characterization of a mosquito larvicidal toxin produced during vegetative stage of *Bacillus sphaericus* 2297. *Curr. Microbiol.* **49**, 84-88.
18. Huang, C. J. and Chen, C. Y. (2005) High-level expression and characterization of two chitinases, ChiCH and ChiCW, of *Bacillus cereus* 28-9 in *Escherichia coli*. *Biochem. Biophys. Res. Commun.* **327**, 8-17.
19. Jensen, T. H., Jensen, A. and Kjems, J. (1995) Tools for the production and purification of full-length, N- or C-terminal 32P-labeled protein, applied to HIV-1 Gag and Rev. *Gene* **162**, 235-237.
20. Matthysse, A. G., Stretton, S., Dandie, C., McClure, N. C. and Goodman, A. E. (1996) Construction of GFP vectors for use in gram-negative bacteria other than *Escherichia coli*. *FEMS Microbiol. Lett.* **145**, 87-94.
21. Promdonkoy, B. and Ellar, D. J. (2000) Membrane pore architecture of a cytolytic toxin from *Bacillus thuringiensis*. *Biochem.* J. **350 Pt 1**, 275-282.
22. Finney D. (1971) Probit Analysis, Cambridge University Press, London, UK.

Available online at www.sciencedirect.com
ScienceDirect
Journal of Biotechnology 133 (2008) 287–293
Journal of BIOTECHNOLOGY
www.elsevier.com/locate/jbiotec

Amino acid substitutions in αA and αC of Cyt2Aa2 alter hemolytic activity and mosquito-larvicidal specificity

Boonhiang Promdonkoy [a,*], Amporn Rungrod [a], Patcharee Promdonkoy [a], Wanwarang Pathaichindachote [a], Chartchai Krittanai [b], Sakol Panyim [b,c]

[a] *National Center for Genetic Engineering and Biotechnology, National Science and Technology Development Agency, 113 Phahonyothin Road, Klong 1, Klong Luang, Pathumthani 12120, Thailand*
[b] *Institute of Molecular Biology and Genetics, Mahidol University, Salaya Campus, Nakhonpathom 73170, Thailand*
[c] *Department of Biochemistry, Faculty of Science, Mahidol University, Rama 6 Road, Bangkok 10400, Thailand*

Received 13 July 2007; received in revised form 5 October 2007; accepted 13 October 2007

Abstract

Cyt2Aa2 produced by *Bacillus thuringiensis* subsp. *darmstadiensis* exhibits *in vitro* cytolytic activity against broad range of cells but shows specific *in vivo* toxicity against larvae of Dipteran insects. To investigate the role of amino acids in αA and αC of this toxin, 3 single-point mutants (A61C, S108C and V109A) were generated. All 3 mutant proteins were highly produced as inclusion bodies that could be solubilized and activated by proteinase K similar to that of the wild type. Hemolytic activity of A61C and S108C mutants was significantly reduced whereas the V109A mutant showed comparable hemolytic activity to the wild type. Interestingly, the A61C mutant exhibited high larvicidal activity to both *Aedes aegypti* and *Culex quinquefasciatus*. S108C and V109A mutants showed low activity against *C. quinquefasciatus* but relatively high toxicity to *A. aegypti*. These results demonstrated for the first time that amino acids in αA and αC are involved in the selectivity of the Cyt toxin to the targeted organism.

Keywords: *Bacillus thuringiensis*; Cyt toxin; Hemolytic; Larvicidal protein; Mosquito; Specificity determinant

1. Introduction

Cyt toxins are mosquito-larvicidal and cytolytic toxins produced by a minor group of *Bacillus thuringiensis* (Bt) mostly in subspecies that are toxic to Dipteran insects (Cheong and Gill, 1997; Juarez-Perez et al., 2002; Promdonkoy et al., 2003). All Cyt toxins discovered from different *B. thuringiensis* subspecies show high amino acid sequence homology (Guerchicoff et al., 2001). Therefore, all of them should have similar structure and function (Li et al., 1996). Cyt toxins showed specific activity against Dipteran insects *in vivo* but have cytolytic activity to broad range of cells *in vitro* (Knowles et al., 1992; Maddrell et al., 1989). The ability of these toxins to bind and form pore in the membrane prepared from pure lipids indicated that they do not need a specific receptor (Drobniewski and Ellar, 1989; Thomas and Ellar, 1983). X-ray crystallographic analysis of soluble toxin showed no receptor-binding motif (Li et al., 1996). However, the receptor-binding motif may be formed after conformation changes which occur upon the toxin approaching the membrane.

Several evidences suggested that Cyt toxins form an oligomeric pore but the number of molecule required to form a pore is still unclear (Chow et al., 1989; Promdonkoy and Ellar, 2000). Diameter of the pore formed by Cyt toxin was estimated to be 1–2 nm (Drobniewski and Ellar, 1988). Digestion of the membrane-bound toxin by several proteases revealed that the C-terminal half was protected from proteolysis digestion and should be inserted into the membrane (Du et al., 1999). Investigation by labeling selected residues by polarity sensitive chemical, acrylodan, showed that β5, β6 and β7 should insert into the membrane (Promdonkoy and Ellar, 2000). From the above evidences together with the X-ray crystal structure of Cyt toxin in solution, Li et al. (2001) proposed that β5, β6 and β7 which are long enough to span the membrane

* Corresponding author. Tel.: +66 2 564 6700; fax: +66 2 564 6707.
E-mail address: boonhiang@biotec.or.th (B. Promdonkoy).

0168-1656/$ – see front matter © 2007 Elsevier B.V. All rights reserved.
doi:10.1016/j.jbiotec.2007.10.007

Table 1
Mutagenic primers for site-directed mutagenesis

Primer	Sequence (5′–3′)	Restriction enzyme
A57L	ATACATTAATCAG**CTG**CTTCATTTAGCA	PvuII
A61C	GGCGCTTCATTTA**TGC**AATGCTTTTCAAGG	BsrDI
S108C	GCAAACAGTTGA**GATCTGC**GTTATGGTTGA	BglII
V109A	CAGTTGAAATTTC**GGCC**ATGGTTGAGCA	HaeIII
M110A	GAAATTTCAGTTG**CCGTGG**AGCAACTTAA	SecI
L114A	ATGGTTGAGCA**GGCC**AAAAAGATTATTCA	HaeIII
I118A	AACTTAAAAAGATT**GCT**CAGGAGGTTTTAGG	DdeI

Primers were designed based on *cyt2Aa2* gene (GenBank accession no. AF472606). Mutated nucleotides were shown in bold and restriction enzyme recognition sites were underlined. This table showed only the forward primers. DNA sequences of the reverse primers are complementary to their forward primers.

should insert into the membrane. These sheets from several molecules may oligomerise and form "β-barrel" pore similar to that of α-hemolysin (Song et al., 1996). Reversion mutagenesis study suggested that amino acids in αA–αD may involve with oligomerization and αD-β4 loop and β6-β7 loop could facilitate conformational changes during membrane insertion (Promdonkoy and Ellar, 2005). Although several reports have suggested that Cyt toxins form pore on the membrane, Butko (2003) proposed that Cyt toxin may not form a well-defined pore but rather aggregates nonspecifically on the membrane surface, causing the lipid membrane to be more disordered or even completely destroy the membrane in a detergent-like manner. This hypothesis was further supported by analyses of the membrane-bound toxin on SDS-PAGE, fluorescence spectroscopy and fluorescence microscopy (Manceva et al., 2005).

Secondary structure analysis revealed that αA and αC are amphiphatic. Study of the synthetic peptides corresponding to these helices showed that they could interact to lipid membrane and self-aggregate (Gazit et al., 1997). It is therefore possible that amino acids in these regions are involved with membrane binding and oligomerization. To investigate the role of amino acids in these helices, several single amino acid substitutions in αA and αC were generated. Effect of the replacement on protein production, inclusion formation, solubilization, protease activation, hemolytic and mosquito-larvicidal activities were investigated.

2. Materials and methods

2.1. Bacterial strain, plasmid and oligonucleotides

Escherichia coli JM109 (Promega) was used throughout the experiment. Recombinant plasmid pGEM-Cyt2Aa2 containing full-length *cyt2Aa2* gene was as described elsewhere (Promdonkoy et al., 2003). Oligonucleotide primers for site-directed mutagenesis were from BioService Unit, National Center for Genetic Engineering and Biotechnology, Thailand and from Sigma Proligo Ltd., Singapore. The primer sequences and additional information are shown in Table 1.

2.2. Site-directed mutagenesis

The method used in this work was based on Stratagene's QuikChange™ Site-Directed Mutagenesis. The recombinant plasmid pGEM-Cyt2Aa2 was used as a template for single substitution together with appropriate primers described in Table 1. The recombinant plasmids obtained for each mutant was analyzed by restriction endonuclease digestion with the enzyme shown in Table 1. DNA sequences of the full-length *cyt2Aa2* gene from all mutants were verified by automated DNA sequencer at the BioService Unit, National Center for Genetic Engineering and Biotechnology, Thailand and Macrogen Inc., Korea.

2.3. Protein preparation

The *E. coli* culture was grown at 37 °C for 16–24 h with shaking at 220–250 rpm in a litre of LB containing 100 μg ampicillin ml^{-1} and 1 mM IPTG using a 0.1% inoculum from a freshly grown culture. The toxin inclusions were isolated as described previously (Promdonkoy et al., 2004) and stored at −20 °C in 1 ml aliquots until required. The inclusion was solubilized in 50 mM Na_2CO_3 pH 10.5 plus 10 mM DTT at 37 °C for 1 h with occasional shaking. Solubilized toxin was then separated from insoluble material by centrifugation at 13,000 × *g* for 3 min and stored at −20 °C in 1 ml aliquots. Concentrations of solubilized proteins were determined by the method of Bradford (1976) using the Bio-Rad protein assay kit and BSA as standard. For proteolytic processing, the solubilized material was mixed with 1% (w/w) proteinase K and incubated at 37 °C for 1 h.

2.4. Intrinsic fluorescent property analysis

Fluorescence spectra of Cyt2Aa2 and its mutants were obtained by emission scanning of protein solution in a 10 mm path length square quartz cell. The protein samples were excited at 280 nm using a Jasco FP-6500 spectrofluorometer. The Emission spectra were recorded from 300–500 nm with medium scanning speed using 3 nm of excitation and emission slit width. All spectra were subtracted with baseline spectra from buffer.

2.5. Hemolytic assay in microtitre plate

The hemolysis assay in microtitre plates was as described by Thomas and Ellar (1983) except that a 2% (v/v) sheep blood cell suspension in PBS buffer (8 mM Na_2HPO_4, 1.5 mM KH_2PO_4, 140 mM NaCl, 2.7 mM KCl, pH 7.4) was used. Toxin inclusions from *E. coli* were solubilized and proteolytically processed as described earlier then diluted in two-fold serial dilutions with

PBS buffer in a 96-well, U-bottom shape microtitre plate. 0.1-ml aliquots of the diluted toxin were mixed with 0.1 ml of diluted blood cells and left at room temperature. The end-point of hemolysis was judged after 24 h as the last well at which colouration of the liquid was still visible.

2.6. Hemoglobin release assay

Hemoglobin release assays were performed as described previously (Promdonkoy and Ellar, 2003). Sheep RBCs (1% in PBS pH 7.4) were pre-incubated at room temperature (25 °C). The cells were then treated with proteolytically processed Cyt2Aa2 at varying concentrations (0.125–256 μg ml^{-1}) and incubated at room temperature. Samples of 1 ml were taken out at indicated times and the unbroken cells and cell debris were removed from these samples by centrifugation at 12,000 × *g* for 30 s. The hemoglobin containing supernatant was removed and hemoglobin release was quantified at A_{540}. The supernatant from 1% RBC treated with 0.1% Triton X-100 was used as a 100% hemolysis control and the supernatant from untreated 1% RBC was used as a 0% lysis (blank).

2.7. Mosquito-larvicidal assay

Mosquito-larvicidal assays were carried out 3 times in duplicate using 3rd instar *Aedes aegypti* and *Culex quinquefasciatus* larvae supplied by the Institute of Molecular Biology and Genetics, Mahidol University. Mosquito-larvicidal activity of the toxin was tested by diluting the toxin inclusions in water as two-fold serial dilutions from 512 to 0.125 μg ml^{-1}. One millilitre of diluted inclusions was added to 1 ml of water with 10 larvae in each well of tissue culture plate (24-well plate, diameter of the well = 1.5 cm). Proteins extracted from *E. coli* JM109 containing pGEM-Teasy were used as negative control. Mortality was recorded after incubation at 30 °C for 24 h. LC_{50} (50% lethal concentration) was calculated using Probit analysis (Finney, 1971).

2.8. Liposomes preparation

Multilamellar phospholipid liposome vesicles were prepared according to the method described by Thomas and Ellar (1983) with modification. The lipid mixture of egg yolk phosphatidyl choline:cholesterol:stearylamine in a molar ratio of 4:3:1 in chloroform/methanol (2:1) was added to a glass bottle and mixed. The solvent was removed by flushing with nitrogen gas. An appropriate buffer was added and the lipid resuspended by gentle swirling of the bottle until all lipid had been resuspended. The liposomes were stored at −80 °C in 0.5 ml aliquots.

2.9. Toxin-membrane interaction assay

Liposomes (100–1000 μg total lipid ml^{-1}) were incubated with activated toxin (10–100 μg ml^{-1}) in PBS buffer at 25 °C for 1 h. The samples were then centrifuged at 20,000 × *g* for 15 min and the supernatant removed. The pellets were washed twice with PBS buffer and centrifuged as above. Final pellets were subjected to SDS-PAGE or stored at 4 °C for subsequent analysis.

3. Results and discussion

Cyt2Aa2 protoxin consists of 259 amino acids that show identical sequence to Cyt2Aa1 (Koni and Ellar, 1993; Promdonkoy et al., 2003). Therefore, Cyt2Aa2 should adopt the same 3D structure as reported for Cyt2Aa1 (Li et al., 1996). The toxin is a single domain protein with β-sheets at the middle and are sandwiched both sides by 4 major α-helices (Fig. 1). Several experiments suggested that Cyt toxin molecules bind to lipid membrane, oligomerize and some part of the toxin insert into the membrane to form pores (Du et al., 1999; Promdonkoy and Ellar, 2003). Since all α-helices is too short to span the width of the membrane, it is more likely that the β-sheets insert into the membrane. Investigation using synthetic peptides corresponding to αA, αC, β5, β6 and β7 revealed that only αA and αC could undergo self-oligomerization and interact with lipid membrane (Gazit et al., 1997). Structural analysis of these helices found that they are amphiphatic helices. Amino acids in these helices could play important role during oligomerization and membrane binding. To investigate this possibility, selected amino acids in both helices were substituted (A57L and A61C in αA and S108C, V109A, M110A, L114A and I118A in αC). Positions of these residues on the molecule are shown in Fig. 1.

E. coli cells containing mutated gene were induced by 1 mM IPTG to produce the toxin. Analysis of the whole cell lysate on SDS-PAGE revealed that all mutants express at high level similar to the wild type toxin. All mutants were produced as inclusion bodies inside the cell and could be easily visible under phase-contrast microscope. The total yield of inclusions extracted from *E. coli* was approximately 20–30 mg l^{-1} of the culture cells. Solubility test in 50 mM Na_2CO_3 pH 10.5 plus 10 mM DTT revealed that only 3 mutants (A61C, S108C and V109A) could be solubilized in this buffer similar to the wild type (Fig. 2). Inclusions from 3 mutants (M110A, L114A and I118A) showed very low solubility (less than 10%) and 1 mutant (L57A) was unable to solubilize in this buffer. The soluble proteins from 3 mutants were activated by proteinase K (1%, w/w) at 37 °C for 1 h. All of them were processed and yielded similar product to that of the wild type (Fig. 2). Results indicated that replacement at these positions (A61C, S108C and V109A) did not affect folding of the toxin. Intrinsic fluorescence emission spectrum analyses revealed that the overall conformation of these mutants was not different from that of the wild type (not shown). Soluble fraction from 3 low solubility mutants (M110A, L114A and I118A) was not stable upon activation. These proteins were completely degraded after incubation with proteinase K or chymotrypsin (not shown). This suggests that substitution at these positions disturbed protein folding and inclusion formation. These residues are located in the hydrophobic face of helix αC pointing inside the molecule. Replacement these positions with smaller and less hydrophobic side-chain may destabilize the Van der Waal contact required to hold the right conformation. Substitution Ala57 by Leu in αA may affect protein folding in opposite direction to the above mutants.

(A)

```
MYTKNFSNSRMEVKGNNGCSAPIIRKPFKHIVLTVPSSDL 40
                                  β1

DNFNTVFYVQPQYINQALHLANAFQGAIDPLNLNFNFEKA 80
  β2          αA                    αB

LQIANGIPNSAIVKTLNQSVIQQTVEISVMVEQLKKIIQE 120
              β3                αC

VLGLVINSTSFWNSVEATIKGTFTNLDTQIDEAWIFWHSL 160
            αD                  β4

SAHNTSYYYNILFSIQNEDTGAVMAVLPLAFEVSVDVEKQ 200
      β5              β6              αE

KVLFFTIKDSARYEVKMKALTLVQALHSSNAPIVDIFNVN 240
              β7                αF

NYNLYHSNHKIIQNLNLSN                       259
```

(B)

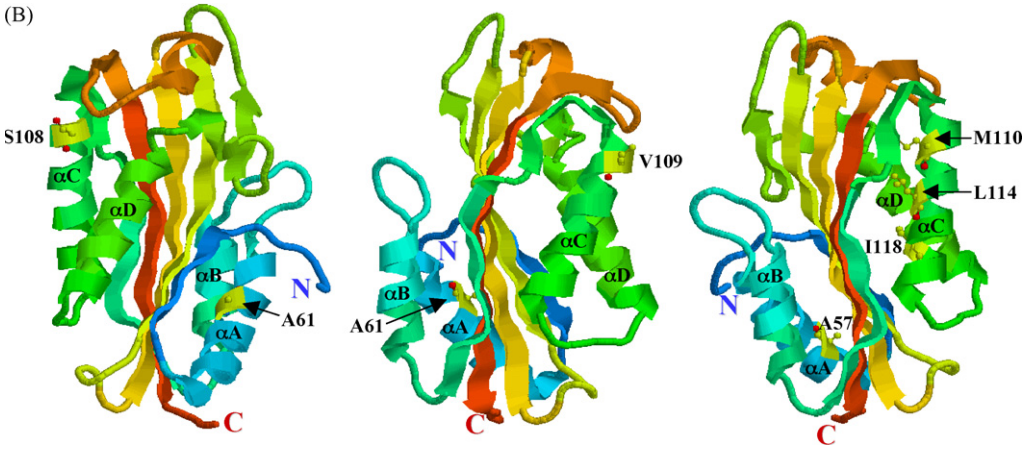

Fig. 1. Positions of the mutated residues in primary sequence (A) and on 3D models of Cyt2Aa2 (B). Selected positions for amino acid substitutions in αA and αC are shown in bold. Cleavage sites to produce the active toxin are indicated by arrows. The 3D models showing different views of Cyt2Aa2 are generated based on structure of Cyt2Aa1 (Li et al., 1996).

Table 2
Mosquito-larvicidal and hemolytic activities of the mutant toxins

Toxin	Hemolytic end-point (μg ml^{-1})	Mosquito-larvicidal LC_{50} (μg ml^{-1})	
Cyt2Aa2		*C. quinquefasciatus*	*A. aegypti*
Wild type	0.25–0.50	0.26 (0.21–0.32)	0.37 (0.26–0.47)
A57L	ND	57.11 (40.56–93.61)	Not toxic
A61C	4.00–8.00	0.29 (0.24–0.36)	0.43 (0.38–0.48)
S108A	4.00–8.00	14.02 (10.71–19.79)	1.56 (1.18–2.00)
V109A	0.13–0.25	46.88 (26.93–138.99)	1.35 (0.97–1.78)
M110A	ND	Not toxic	Not toxic
L114A	ND	24.07 (19.12–31.64)	Not toxic
I118A	ND	28.16 (16.59–71.39)	Not toxic

Data was from 3 independent experiments. ND means not determine because there was no activated toxin available. Not toxic means no mortality was observed when used the toxin at very high dose up to 250 μg ml^{-1}. LC_{50} was calculated from 6–8 different toxin concentrations and the fidulcial limits are shown in parenthesis.

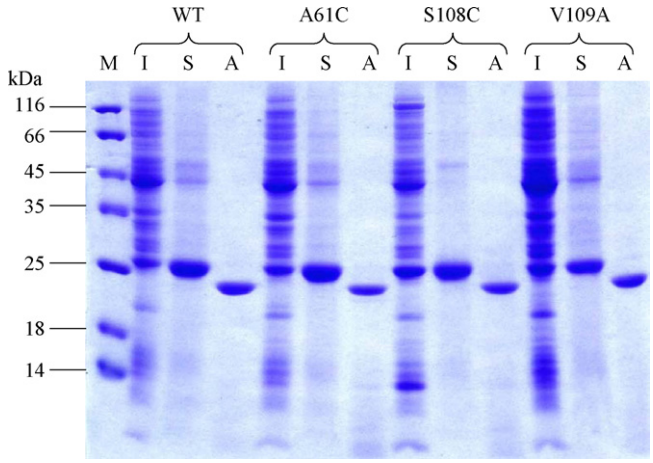

Fig. 2. Solubilization and activation of the mutant proteins. Toxin inclusions (I) were solubilized in 50 mM Na_2CO_3 pH 10.5 at 37 °C for 1 h. The samples were then centrifuged at 12,000 × *g* for 5 min. Supernatant containing soluble toxin (S) was removed and activated (A) with 1% proteinase K at 37 °C for 1 h. All fractions were analyzed on SDS-PAGE. WT represents the wild type toxin. Protein molecular weight markers (M) are shown alongside in kDa.

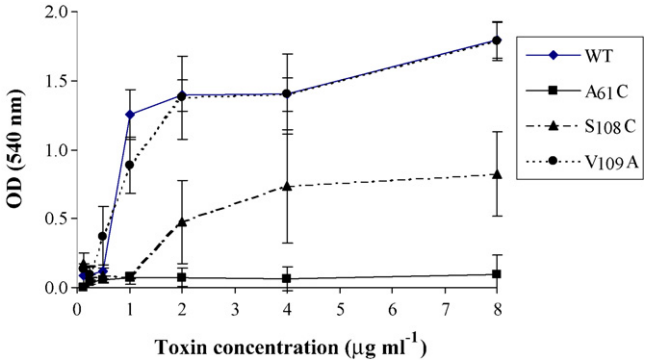

Fig. 3. Hemolytic activity of mutant proteins comparing to the wild type. Sheep red blood cells (1% in PBS pH 7.4) were incubated with different concentrations of activated toxins (0.125, 0.25, 0.5, 1.0, 2.0, 4.0 and 8.0 μg ml^{-1}) at room temperature for 1 h. Hemoglobin release was followed by measuring the absorbance (OD) at 540 nm. Data was the average from 4 independent experiments and vertical bars represent S.E.M.

Mosquito-larvicidal activity of insecticidal crystal proteins is normally tested by feeding the larvae with toxin inclusions (Schnepf et al., 1998). It was found that Cyt2Aa2 inclusion is highly toxic to both *C. quinquefasciatus* and *A. aegypti* larvae (Promdonkoy et al., 2003, 2005) similar to the closely related toxins, Cyt2Aa1 and Cyt1Aa1 (Koni and Ellar, 1993, 1994). The protease activated form of these toxins exhibited comparable hemolytic activity to each other. This is not unexpected because all Cyt toxins share high amino acid sequence homology (Guerchicoff et al., 2001) and they should have similar 3D structure (Li et al., 1996). Replacement at some positions such as A57L, M110A, L114A and I118A of Cyt2Aa2 yielded the toxin inclusions that are less soluble or insoluble in carbonate buffer. Hemolytic activity of these mutants could not be accessed because no activated toxin was available. These mutants exhibited very low larvicidal activity (Table 2). The mutants L114A and I118A showed higher activity comparing to other insoluble mutants indicated that the soluble fraction, even small amount, could retain some activity. It should be noted that these mutants exhibited higher toxicity to *C. quinquefasciatus* than *A. aegypti*. It is possible that solubility of the mutant inclusions in the larval gut may not be the same for both larvae.

Mutant inclusions that are readily solubilized in carbonate buffer showed different toxicity to *C. quinquefasciatus* and *A. aegypti* larvae (Table 2). Mutant A61C showed low hemolytic activity but high mosquito-larvicidal activity. In contrast the mutant V109A exhibited high hemolytic activity but showed very low toxicity against *C. quinquefasciatus* larvae and moderate activity to *A. aegypti*. The highly conserved mutant S108C yielded low hemolytic activity and low toxicity to *C. quinquefasciatus* but moderate toxicity against *A. aegypti*. Hemoglobin release assay (Fig. 3) demonstrated that S108C could not completely break RBC even when use at high concentration. It is therefore possible that this mutant affects oligomerization or pore stability. The mutant A61C showed very low hemolytic activity against sheep RBC. Less than 10% of hemoglobin release was detected after incubation of the activated toxin (8 μg ml^{-1}) with RBC for 1 h and the hemoglobin release increased to approximately 20% after incubation for 24 h. The mutant A61C could interfere membrane binding and oligomerization. Therefore, it needs more time for the toxin molecules to randomly accumulate until it reaches a certain number required to break the cell. The mutant V109A exhibited comparable hemolytic activity to the wild type (Fig. 3). However, at low concentrations (0.125–0.250 μg ml^{-1}), V109A mutant caused more hemoglobin release than that of the wild type. This observation was consistent with the hemolysis assay in microtitre plate (Table 2). Replacement by alanine at this position might be able to promote membrane binding and oligomerization of the toxin. Binding assay with liposomes (Fig. 4) demonstrated that membrane binding and oligomerization of the mutants A61C and S108C to liposomes were significantly reduced whereas the mutant V109A showed similar binding and oligomerization to that of the wild type. However, binding and oligomerization to red blood cell and mosquito larval cell membranes may not be the same as detected on liposomes because of the differences in membrane compositions. It could be possible that other membrane components such as glycoproteins and lipoproteins contribute in some ways to the binding of the toxin.

Our investigation discovered 3 positions that play important role for Cyt toxin activity. The first position Ala-61 in hydrophobic face of αA is important for hemolytic activity but not necessary for larvicidal activity. Substitution this position with cysteine could interfere hydrophobic patch of αA. This change may reduce binding to RBC membrane but promote binding to *C. quinquefasciatus* gut cell membrane. Second position Val-109 in hydrophilic side of αC (Fig. 1) is important for larvicidal activity. Replacement by a less hydrophobic residue (alanine) reduced hydrophobicity of this region. This change may decrease binding to the larval gut cell membrane but increase RBC binding. The next position Ser-108 is also in the hydrophilic side of αC. Replacement with a highly conserved

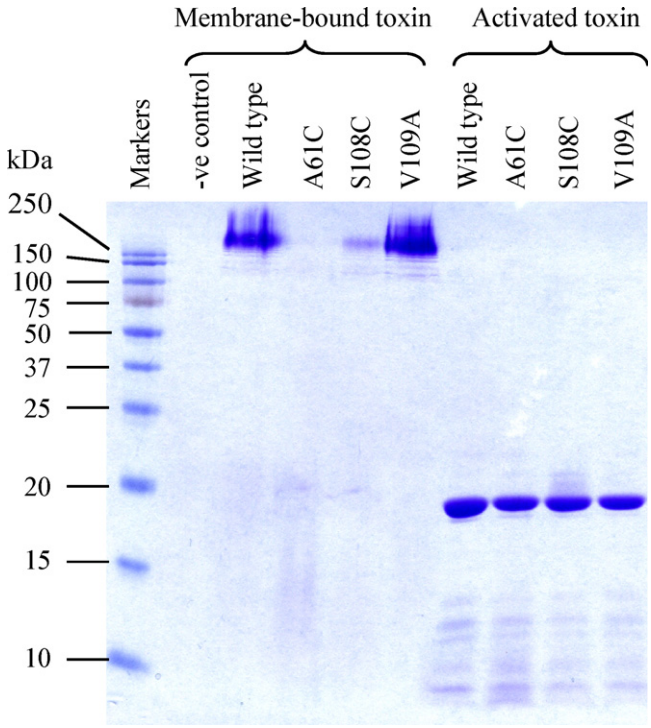

Fig. 4. Membrane binding activity and oligomerization of the mutant proteins. Activated toxins were incubated with liposomes at room temperature for 1 h. The membrane-bound toxins were washed twice with PBS and liposomes were mixed with protein loading buffer and loaded to SDS-PAGE without boiling. Liposomes incubated with buffer without toxin was used as negative control (−ve control). Proteins separated on SDS-PAGE were visualized by Coomassie blue stain. The activated toxins in solution without liposome existed as monomer. Protein molecular weight markers are shown alongside in kDa.

but slightly larger residue (cysteine) affected both hemolytic and larvicidal activities indicating that either side-chain volume or polarity is critical for this position. Results presented here clearly demonstrate that binding between Cyt toxin and cell membrane is specific. Amino acids in αA, and αC of the Cyt toxin may act as specificity determinant. These residues may interact with some components presented on the cell membrane either glycoproteins or lipoproteins. Changing amino acids in these regions could alter the target organism. This finding suggested that binding of the Cyt toxin to cell membrane could be made specific. Results reported here clearly demonstrated that we could improve mosquito-larvicidal activity and reduce hemolytic activity of the Cyt toxin. This is a very important and exciting discovery that could lead to improvement of the Cyt toxin to be more specific to the targeted insect larvae.

Acknowledgements

We would like to thank Chawewan Chimwai for supplying mosquito larvae. This work was supported by the National Center for Genetic Engineering and Biotechnology, National Science and Technology Development Agency, Thailand, the Thailand Research Fund, and the Commission on Higher Education, Thailand.

References

Bradford, M.M., 1976. A rapid and sensitive method for the quantitation of microgram quantities of protein utilizing the principle of protein-dye binding. Anal. Biochem. 72, 248–254.

Butko, P., 2003. Cytolytic toxin Cyt1A and its mechanism of membrane damage: data and hypothesises. Appl. Environ. Microbiol. 69, 2415–2422.

Cheong, H., Gill, S.S., 1997. Cloning and characterization of a cytolytic and mosquitocidal δ-endotoxin from *Bacillus thuringiensis* subsp. *jegathesan*. Appl. Environ. Microbiol. 63, 3254–3260.

Chow, E., Singh, F.J.P., Gill, S.S., 1989. Binding and aggregation of the 25 kilodalton toxin of *Bacillus thuringiensis* subsp. *israelensis* to insect cell membranes and alteration by monoclonal antibodies and amino acid modifiers. Appl. Environ. Microbiol. 55, 2779–2788.

Drobniewski, F.A., Ellar, D.J., 1988. Investigation of the membrane lesion induced *in vitro* by two mosquitocidal δ-endotoxins of *Bacillus thuringiensis*. Curr. Microbiol. 16, 195–199.

Drobniewski, F.A., Ellar, D.J., 1989. Purification and properties of a 28-kilodalton hemolytic and mosquitocidal protein toxin of *Bacillus thuringiensis* subsp. *darmstadiensis* 73-E10-2. J. Bacteriol. 171, 3060–3067.

Du, J., Knowles, B.H., Li, J., Ellar, D.J., 1999. Biochemical characterization of *Bacillus thuringiensis* cytolytic toxins in association with a phospholipid bilayer. Biochem. J. 338, 185–193.

Finney, D., 1971. Probit Analysis, 3rd ed. Cambridge University Press, London.

Gazit, E., Burshtein, N., Ellar, D.J., Sawyer, T., Shai, Y., 1997. *Bacillus thuringiensis* cytolytic toxin associates specifically with its synthetic helices A and C in the membrane bound state: implications for the assembly of oligomeric transmembrane pores. Biochemistry 36, 15546–15554.

Guerchicoff, A., Delecluse, A., Rubinstein, C.P., 2001. The *Bacillus thuringiensis cyt* genes for hemolytic endotoxins constitute a gene family. Appl. Environ. Microbiol. 67, 1090–1096.

Juarez-Perez, V., Guerchicoff, A., Rubinstein, C., Delecluse, A., 2002. Characterization of Cyt2Bc toxin from *Bacillus thuringiensis* subsp. *medellin*. Appl. Environ. Microbiol. 68, 1228–1231.

Knowles, B.H., White, P.J., Nicholls, C.N., Ellar, D.J., 1992. A broad spectrum cytolytic toxin from *Bacillus thuringiensis* var. *kyushuensis*. Proc. R. Soc. Lond. 248, 1–7.

Koni, P.A., Ellar, D.J., 1993. Cloning and characterization of a novel *Bacillus thuringiensis* cytolytic delta-Endotoxin. J. Mol. Biol. 229, 319–327.

Koni, P.A., Ellar, D.J., 1994. Biochemical characterization of *Bacillus thuringiensis* Cytolytic δ-endotoxins. Microbiology 140, 1869–1880.

Li, J., Derbyshire, D.J., Promdonkoy, B., Ellar, D.J., 2001. Structural implications for the transformation of the *Bacillus thuringiensis* delta-endotoxins from water-soluble to membrane-inserted forms. Biochem. Soc. Trans. 29, 571–577.

Li, J., Koni, P.A., Ellar, D.J., 1996. Structure of the mosquitocidal δ-endotoxin CytB from *Bacillus thuringiensis* sp. *kyushuensis* and implications for membrane pore formation. J. Mol. Biol. 257, 129–152.

Maddrell, S.H.P., Overton, J.A., Ellar, D.J., Knowles, B.H., 1989. Action of activated 27000 M_r toxin from *Bacillus thuringiensis* var. *israelensis* on malpighian tubules of the insect, *Rhodnius prolixus*. J. Cell Sci. 94, 601–608.

Manceva, S.D., Pusztai-Carey, M., Russo, P.S., Butko, P., 2005. A detergent-like mechanism of action of the cytolytic toxin Cyt1A from *Bacillus thuringiensis* var. *israelensis*. Biochemistry 44, 589–597.

Promdonkoy, B., Chewawiwat, N., Tanapongpipat, S., Luxananil, P., Panyim, S., 2003. Cloning and characterization of a cytolytic and mosquito larvicidal δ-endotoxin from *Bacillus thuringiensis* subsp. *darmstadiensis*. Curr. Microbiol. 46, 94–98.

Promdonkoy, B., Ellar, D.J., 2000. Membrane pore architecture of a cytolytic toxin from *Bacillus thuringiensis*. Biochem. J. 350, 275–282.

Promdonkoy, B., Ellar, D.J., 2003. Investigation of the pore forming mechanism of a cytolytic delta-endotoxin from *Bacillus thuringiensis*. Biochem. J. 374, 255–259.

Promdonkoy, B., Ellar, D.J., 2005. Structure–function relationships of a membrane pore forming toxin revealed by reversion mutagenesis. Mol. Membr. Biol. 22, 227–237.

Promdonkoy, B., Pathaichindachote, W., Krittanai, C., Audtho, M., Chewawiwat, N., Panyim, S., 2004. Trp132, Trp154 and Trp157 are essential for folding and activity of a Cyt toxin from Bacillus thuringiensis. Biochem. Biophys. Res. Commun. 317, 744–748.

Promdonkoy, B., Promdonkoy, P., Panyim, S., 2005. Co-expression of *Bacillus thuringiensis* Cry4Ba and Cyt2Aa2 in *Escherichia coli* revealed high synergism against *Aedes aegypti* and *Culex quinquefasciatus* larvae. FEMS Microbiol. Lett. 252, 121–126.

Schnepf, E., Crickmore, N., Van Rie, J., Lereclus, D., Baum, J., Feitelson, J., Zeigler, D.R., Dean, D.H., 1998. *Bacillus thuringiensis* and its pesticidal crystal proteins. Microbiol. Mol. Biol. Rev. 62, 775–801.

Song, L., Hobaugh, M.R., Shustak, C., Cheley, S., Bayley, H., Gouaux, J.E., 1996. Structure of Staphylococcal α-hemolysin, a heptameric transmembrane pore. Science 274, 1859–1866.

Thomas, W.E., Ellar, D.J., 1983. *Bacillus thuringiensis* var. *israelensis* crystal δ-endotoxin: effects on insect and mammalian cells *in vitro* and *in vivo*. J. Cell Sci. 60, 179–181.

DOI 10.1002/pmic.200700281

RESEARCH ARTICLE

Proteomic analysis of differentially expressed proteins in *Penaeus vannamei* hemocytes upon Taura syndrome virus infection

Phattara-orn Chongsatja[1], Apichai Bourchookarn[1], Chu Fang Lo[2], Visith Thongboonkerd[3] and Chartchai Krittanai[1]

[1] Institute of Molecular Biology and Genetics, Mahidol University, Salaya Campus, Nakhonpathom, Thailand
[2] Institute of Zoology, National Taiwan University, Taipei, Taiwan, ROC
[3] Medical Molecular Biology Unit, Office for Research and Development, Faculty of Medicine, Siriraj Hospital, Mahidol University, Bangkok, Thailand

Received: March 29, 2007
Revised: June 8, 2007
Accepted: June 29, 2007

To understand molecular responses of crustacean hemocytes to virus infection, we applied 2-DE proteomics approach to investigate altered proteins in hemocytes of *Penaeus vannamei* during Taura syndrome virus (TSV) infection. At 24 h postinfection, quantitative intensity analysis and nano-LC-ESI-MS/MS revealed 11 forms of 8 proteins that were significantly up-regulated, whereas 9 forms of 5 proteins were significantly down-regulated in the infected shrimps. These altered proteins play important roles in host defense (hemocyanin, catalase, carboxylesterase, transglutaminase, and glutathione transferase), signal transduction (14-3-3 zeta), carbohydrate metabolism (acetylglucosamine pyrophosphorylase), cellular structure and integrity (beta-tubulin, beta-actin, tropomyosin, and myosin), and ER-stress response (protein disulfide isomerase). Semiquantitative RT-PCR and Western blot analysis confirmed the upregulation of 14-3-3 at both mRNA and protein levels. Interestingly, several altered protein spots were identified as fragments of hemocyanin. Mass spectrometric analysis showed that the hemocyanin spots at acidic and basic regions represented the C- and N-terminal hemocyanin fragments, respectively. As three-quarters of C-terminal fragments were up-regulated, whereas two-thirds of N-terminal hemocyanin fragments were down-regulated, we therefore hypothesize that C- and N-terminal hemocyanin fragments may have differential roles in hemocytes. Further investigation of these data may lead to better understanding of the molecular responses of crustacean hemocytes to TSV infection.

Keywords:
Hemocytes / *Penaeus vannamei* / Shrimp / Taura syndrome virus

Correspondence: Dr. Chartchai Krittanai, Institute of Molecular Biology and Genetics, Mahidol University, Salaya Campus, Nakhonpathom 73170, Thailand
E-mail: stckt@mahidol.ac.th
Fax: +66-2-441-9906

Abbreviations: hpi, hours postinfection; **PDI,** protein disulfide isomerase; **TM,** tropomyosin; **TSV,** Taura syndrome virus

1 Introduction

Penaeid shrimp culture is an important aquaculture industry worldwide. The Pacific white shrimp, *Penaeus vannamei*, is one of the predominant shrimp species produced in the areas where water temperatures are greater than 20°C throughout the year [1, 2]. Stress factors such as overcrowding, abnormal temperature and low dissolved oxygen

can cause several diseases, particularly those of viral origin [3, 4]. Viral infection can lead to a serious problem of production shortage as a result from high mortality and slow growth rate. Economic loss due to viral infection in shrimps has made it necessary to improve the knowledge on the pathogenic mechanisms and invertebrate immunity [5]. While responses of the shrimp immune system to bacterial and fungal pathogens have been extensively studied, little is known about its responses to viruses. Currently, there are no effective methods to prevent viral diseases in shrimp culture. Therefore, molecular elucidation of shrimp immune responses to viral infection would be a great benefit for the disease prevention and control.

Shrimp innate immunity consists of cellular and humoral responses. Hemocytes in the hemolymph are the primary target of cellular immune responses in crustaceans. Hemocytes are involved in phagocytosis of small microbes, encapsulation of parasite [6], nonself recognition [7], and elimination of reactive oxygen intermediates [8]. Humoral immune responses include hemolymph coagulation, proteolytic cascades leading to opsonization and melanization [9], and production of antimicrobial peptides [10]. When the shrimps are infected, the virus can spread throughout the whole body within a few minutes *via* the circulating hemocytes, which are significantly increased after infectious stimulation [11].

Taura syndrome virus (TSV) is one of the most important pathogens in shrimps. It causes a highly virulent disease in penaeid shrimp, especially *P. vannamei*. The accumulative mortality of TSV-infected shrimps varies from 5% to more than 95%. This virus is normally found in the cytoplasm of the infected epithelial cells of shrimp cuticle. TSV was originally classified to be closely related to the Picornaviridae family [12], based on its morphology, virion size, and cytoplasmic location. Recently, it has been regrouped into the new genus of "Cricket paralysis-like viruses" (CrPV), based on the nucleotide sequences [13]. Physically, TSV is a nonenveloped virus with icosahedral shape of approximately 31–32 nm in diameter. The genome contains a single-stranded RNA of approximately 10 kb as a positive sense and two distinct ORFs. ORF1 and ORF2 encode for the nonstructural and structural proteins, respectively. Analysis of the TSV structural proteins by SDS-PAGE normally provides three major bands with molecular masses of 24, 40, and 55 kDa, and one minor band at 58 kDa.

Although there are a number of reports on crustacean immunity through genetic studies, host responses of virus-infected shrimp at the molecular level remain poorly understood. Additionally, alterations in protein expression and function in TSV-infected shrimp remain unknown. Our present study was aimed to identify differentially expressed proteins in the hemocytes of *P. vannamei* during TSV infection using a gel-based proteomics approach. A number of up-regulated or down-regulated proteins were successfully identified by nano-LC-ESI-MS/MS. Change in expression level of a selected protein (14-3-3) was confirmed and monitored at various time-points using Western blot analysis. In addition, semiquantitative RT-PCR was also applied to confirm change in 14-3-3 expression at the mRNA level.

2 Materials and methods

2.1 TSV stock and proliferation

TSV was obtained from the Center of Excellence for Shrimp Molecular Biology and Biotechnology (Centex Shrimp), Mahidol University, Bangkok, Thailand. Virus proliferation was performed by intramuscular injection of TSV into *P. vannamei*. When the infected shrimps became moribund, the hemolymph was withdrawn, mixed with NTE buffer (containing 200 mM NaCl, 20 mM Tris-HCl, and 20 mM EDTA; pH 7.4) and then centrifuged at $5000 \times g$ and 4°C for 15 min. The collected supernatant was then centrifuged at $89\,000 \times g$ and 4°C using swing rotor SW40 Ti on Beckman ultracentrifuge (Beckman, Fullerton, CA, USA.) for 1 h. The virus pellet was resuspended in NTE buffer at 4°C overnight, and the suspension was overlaid on top of a linear ficoll gradient (10–30% w/v in NTE) and centrifuged at $89\,000 \times g$ and 4°C for 1 h. After ultracentrifugation, the viral band was visualized, collected, diluted with ten volumes of NTE buffer, and centrifuged again at $89\,000 \times g$ for 1 h. The pellet was then resuspended in NTE buffer and stored at −80°C until used. The purity of the TSV stock was verified using 12.5% SDS-PAGE.

2.2 Shrimp preparation

The specific-pathogen-free Pacific white shrimps, *P. vannamei*, were obtained from a local farm in Trang province, Thailand. The shrimp was reared in aerated artificial seawater with 25 part-*per*-thousand salinity at 25°C. Twelve to fifteen shrimps were cultured in each 40×60 cm^2 tank. The artificial seawater was changed once daily. The healthy shrimps with average size of 10–14 cm in length and 17–20 g by weight were divided into control and TSV-infected groups.

2.3 TSV infection

For the infected group, 100 μL of partially purified TSV was diluted (1:250) in NTE buffer and intramuscularly injected into the healthy shrimps through the lateral surface of the fourth abdominal segment. For the control group, NTE buffer was used for injection instead of the partially purified TSV. After the injection, the inoculated shrimps were kept and observed for signs of the Taura syndrome disease. The hemolymph was collected from 12 shrimps in each experimental condition at 2, 4, 6, 12, 24, and 48 h postinfection (hpi; totally 144 shrimps were examined in the present study).

2.4 Isolation of hemocytes

Approximately 2 mL of hemolymph was drawn from shrimp abdominal hemocoel using 18 G needle. The sample was mixed with an equal volume of anticoagulant AC I solution (containing 27 mM sodium citrate, 450 mM NaCl, 115 mM glucose and 10 mM EDTA; pH 7.0) and immediately kept on ice. Hemocytes were harvested by centrifugation at $830 \times g$ and 4°C for 15 min. After discarding the plasma, the packed hemocytes were washed twice with AC I solution and stored at −20°C until used.

2.5 Extraction of hemocytic proteins

Protein extraction was performed using a lysis buffer containing 8 M urea, 2 M thiourea, 0.2% v/v Triton-X, 50 mM DTT, 1 mM PMSF, and 1 mM benzamidine. The cell lysate was then centrifuged at 12 000 rpm and 4°C for 15 min and the supernatant was kept at −20°C until used. Protein concentration was determined by a Bio-Rad protein assay, based on method described by Bradford [14]. BSA was used as the protein standard for quantitation.

2.6 2-DE

The first dimension of 2-DE was performed in IPGphor IEF system (Amersham Biosciences, Uppsala, Sweden). A total of 400 μg of proteins derived from three individual shrimps was loaded onto each IPG strip (nonlinear pH 4–7; 13-cm long) (Amersham Biosciences). Four IPG strips, representing 12 individual shrimps, were analyzed for each condition. Rehydration was done at 50 μA *per* strip in the presence of 8 M urea, 2 M thiourea, 4% v/v CHAPS, 50 mM DTT, 1 mM PMSF, and 1 mM benzamidine for 12 h. The IEF was performed at 20°C using a continuous increase in voltage (up to 8000 V) to reach 50 000 Vh. Prior to the second dimension, the focused IPG strip was incubated for 15 min in an equilibration buffer containing 30% w/v glycerol, 20% w/v sucrose, 2% w/v SDS, 50 mM Tris-HCl (pH 8.8), 100 mM DTT, and 0.002% w/v bromophenol blue. The strip was then further equilibrated for 15 min in a similar buffer, which replaced 100 mM DTT with 250 mM of iodoacetamide. The IPG strip was placed onto the top of 12.5% SDS-PAGE gel and sealed with hot agarose (1% w/v). After SDS-PAGE, the gel was fixed in a fixative solution containing 50% v/v ethanol and 2% v/v phosphoric acid, and stained with CBB-G250 stain, containing 10% w/v ammonium sulfate, 2% v/v phosphoric acid, and 0.001% w/v of Brilliant Blue G (USB, Cleveland, OH, USA).

2.7 Image analysis

The 2-D gel images were analyzed with MELANIE software version 5.0 (GeneBio, Geneva, Switzerland). Comparative analysis of protein spots was performed by matching corresponding spots across different gels. Each of the matched protein spots was rechecked manually. Intensity volumes of individual spots were normalized with total intensity volume of all spots present in each gel and were subjected to statistical analysis to compare the normalized intensity volumes of individual spots of the control group to those of the infected group. Only differentially expressed proteins were excised and subjected to subsequent identification by MS.

2.8 In-gel tryptic digestion

Differentially expressed protein spots were excised from 2-D gels with sterile scalpel. The gel pieces were washed with 50% v/v ACN in 25 mM ammonium bicarbonate (pH 8.5) for 15 min twice to remove Coomassie dye. After dehydration with 100% v/v ACN for 10 min at room temperature, the gel pieces were vacuum-dried and rehydrated with sequencing-grade modified trypsin (Promega, Madison, WI, USA.) in 25 mM ammonium bicarbonate (pH 8.5) at 37°C overnight. The in-gel tryptic digested samples were then subjected to nano-LC coupled to ESI MS/MS (nano-LC-ESI-MS/MS).

2.9 Nano-LC-ESI-MS/MS

Nano-LC-ESI-MS/MS was performed at the Proteomic Core Facility, Academia Sinica, Taiwan, as described previously [15]. Briefly, the in-gel tryptic digested samples were injected into an integrated a nano-LC-ESI-MS/MS system (Quadrupole/TOF Ultima API, Micromass, Manchester, UK). The injected samples were first trapped and desalted isocratically on an LC-Packings PepMap C_{18} μ-Precolumn cartridge (Dionex, Sunnyvale, CA, USA). After dissolving with 0.1% formic acid, the samples were loaded into an analytical C_{18} capillary column connected online to the mass spectrometer. Instrumental operation, data acquisition, and analysis were performed under the full control of MassLynx 4.0 (Micromass). The 1-s survey scans were run over the mass range of m/z from 400 to 2000. A maximum of three concurrent MS/MS acquisitions were triggered for 2^+, 3^+, and 4^+ charged precursor detection at an intensity above the predefined threshold.

The acquired peptide ions obtained from nano-LC-ESI-MS/MS were analyzed with the MASCOT search tool (www.matrixscience.com) using both NCBInr and EST databases. Parameters for the MASCOT search were peptide mass tolerance of 1 Da; MS/MS ion mass tolerance of 1 Da, maximally one missed cleavage; and tryptic digestion. Variable modifications included methionine oxidation and cysteine carbamidomethylation. Only proteins with the significant ions scores (>40) were reported.

2.10 Western blot analysis

Western blotting was performed by an electroblot transfer of proteins from SDS-PAGE or 2-D gels onto PVDF membranes using a Mini Trans-Blot electrophoresis transfer cell

(Bio-Rad, Richmond, CA, USA.). This semidry blotting was performed for 1 h at a constant voltage of 200 V. Membrane was presoaked in absolute methanol and equilibrated in Tris-glycine transfer buffer (39 mM glycine, 0.04% SDS, 10% methanol, and 48 mM Tris-HCl). After protein transfer, the membrane was blocked with 5% skim milk in 0.5% TTBS buffer (0.5% Tween, 20 mM Tris-HCl, and 150 mM NaCl; pH 7.4) to prevent nonspecific binding. Rabbit polyclonal anti-14-3-3 and antiphosphopyruvate hydratase (provided by Professor Lo, National Taiwan University) were used as the primary antibodies. The membrane was incubated with a primary antibody in 2.5% skim milk/0.5% TTBS at room temperature for 1 h with dilution factors of 1:10 000 for both anti-14-3-3 and antiphosphopyruvate hydratase. After three times of washing with 0.5% TTBS, the membrane was incubated at room temperature for 1 h with antirabbit IgG conjugated with HRP (KPL, Gaitherburg, MD, USA.) 1:10 000 in 2.5% skim milk/0.5% TTBS. After three washes, immunoreactive protein bands or spots were visualized with a chemiluminescence substrate using the ECL Plus Western Blot Detection System (Amersham Biosciences). The immunoreactive proteins were then quantitated using Image Master 2D Platinum software (Amersham Biosciences).

2.11 Semiquantitative RT-PCR

Total RNA was extracted from a pool of hemocyte pellets using TRI reagent (Sigma, St. Louis, MO, USA.). The first-strand cDNA was prepared from total RNA with PRT primer [16]. Briefly, the total RNA (1–5 μg) was mixed with 0.5 μg of PRT primer. RNase-free water was used to make a final volume of 5 μL. The mixture was heated at 70°C for 5 min and then cooled immediately on ice. Thereafter, the volume was adjusted to 20μL using 1 × reaction buffer containing 3 mM $MgCl_2$, 0.5 mM dNTPs, 3 U ImPromII reverse transcriptase (Promega) and RNase-free water. The first-strand cDNA was then used as the template for PCR amplification with the appropriate primers designed by the MASCOT analysis (www.matrixscience.com) of ESTs (Table1). Semiquantitative RT-PCR analysis was performed on total RNA isolated from control and infected hemocyte at various time-points. RT-PCR of elongation factor-1 was performed and used for normalization of total RNA variation. RNA expression levels were quantitatively analyzed using Image Master 2D Platinum software (Amersham Biosciences).

3 Results

3.1 TSV infection in *P. vannamei*

The healthy specific-pathogen-free *P. vannamei* was injected with partially purified TSV. Signs of TSV infection were observed in the TSV-injected *P. vannamei,* including soft shell and expansion of red chromatophores in all appendages, especially on the uropod, pleopod, and body surface. The infected shrimps became lethal within 4–5 days of infection. RT-PCR showed an mRNA band, corresponding to VP1 of TSV, in the infected hemocytes, as early as 4 hpi. The amplification of viral gene, *VP1,* provided the expected band at a size of 657 bp. Moreover, the PCR data also suggested that the intensity (quantity) of the 657-bp band was increased by time after infection, indicating propagation and accumulation of this virus in shrimps at the longer time-points (Fig. 1).

Table 1. Primer used in semiquantitative RT-PCR analysis

Target gene	Primer name	Primer sequence (5′–3′)
14-3-3 Zeta protein (*Penaeus monodon*)	14-3-3-F	CAGCCCACCCACCCCATC
	14-3-3-R	GTTTTGGTCGCCCTCGTTAGC
Elongation factor-1	EF-1-F	CATCTCATCTACAAATGCG
	EF-1-R	ATGAAATCACGATGGCCTG
Viral protein 1 (TSV)	VP1-F	TTACCTGGTAAGGGCTTCAC
	VP1-R	ATTGCTCCAATTCACCCAAG

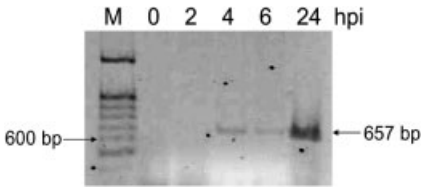

Figure 1. Time-course detection of TSV in the infected hemocytes. Using RT-PCR amplification, the 657 bp PCR product of VP1 was observed at 4 h postinfection (4 hpi) and was increased at the later time-points, particularly at 24 hpi.

3.2 Differentially expressed proteins in TSV-infected hemocytes

Proteins resolved in each gel were derived from a pooled sample of three individual shrimps and four replicated gels were analyzed for each condition. Thus, the data of each condition represented the information for a total of 12 shrimps. A pH gradient of 4–7 was found suitable for the separation of hemocytic proteins, as most of these proteins had p*I*s within the range of 4–7. Approximately 320–400 protein spots were visualized in each gel. At first, we investigated the modulation of proteins at 2 and 4 hpi aiming to obtain the data that may explain immune response mechanisms at an early phase of infection. Unfortunately, image analysis revealed no significant differences between the control and infected groups during these two early time-points, at 2 and 4 hpi.

Comparative analysis of the control and infected hemocytic proteome at 24 hpi was then performed and revealed a total of 32 protein spots to be differentially expressed in the

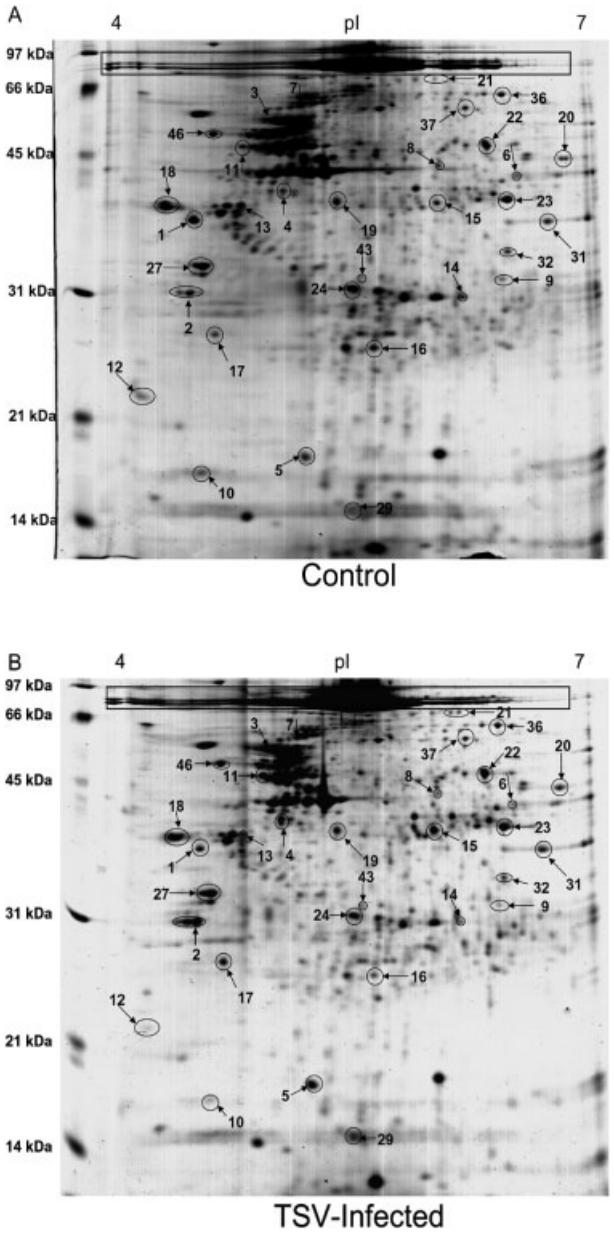

Figure 2. The representative 2-D gel image of shrimp hemocytes at 24 hpi. (A) Control hemocytes; and (B) TSV-infected hemocytes. Hemocyanin full-length, which is the most abundant protein in hemocytes, is shown in the rectangle. Differentially expressed proteins are labeled with numbers, which correspond to the numbers present in Table 2.

TSV-infected samples (Fig. 2). Using nano-LC-ESI-MS/MS, most of these altered proteins were successfully identified (except only for spot # 20, which remains unidentified) (Table 2). We then divided these altered protein spots into three groups. Group I: significant up-regulated proteins, which showed significantly increased expression levels (>1.5-fold compared to the control); Group II: significant down-regulated proteins, which showed significantly decreased expression levels (<0.67-fold compared to the control); and Group III: subtle altered proteins, which had subtle changes (0.68–1.49-fold changes). Based on these criteria, 11 forms of 8 identified proteins were significantly up-regulated, whereas 9 forms of 5 identified proteins were significantly down-regulated by TSV infection (Fig. 2 and Table 2).

Among these altered proteins, most of the down-regulated proteins (*i.e.*, hemocyanin, transglutaminase, and glutathione transferase) had functional roles in defensive mechanisms of shrimps. Whereas the down-regulated proteins had physiological significance in self defense, the up-regulated proteins played important roles in (i) signal transduction (*i.e.*, 14-3-3 zeta); (ii) carbohydrate metabolism (*i.e.*, acetylglucosamine pyrophosphorylase); (iii) detoxification (*i.e.*, catalase and carboxylesterase); (iv) cellular structure and integrity (*i.e.*, beta-tubulin and beta-actin); and (iv) ER-stress response (*i.e.*, protein disulfide isomerase; PDI).

3.3 Confirmation of the proteomic data by Western blot analysis and RT-PCR

The increased 14-3-3 zeta protein (spot #2) was found interesting since it showed a marked increase of approximately 1.89-fold on 2-D gels of the TSV-infected hemocytes at 24 hpi (Fig. 2). However, the increased expression of this protein was not observed at 2 and 4 hpi. We therefore performed additional experiments, using both RT-PCR and Western blotting, to confirm the proteomic data. Western blot analysis, using phosphopyruvate hydratase as an internal control for

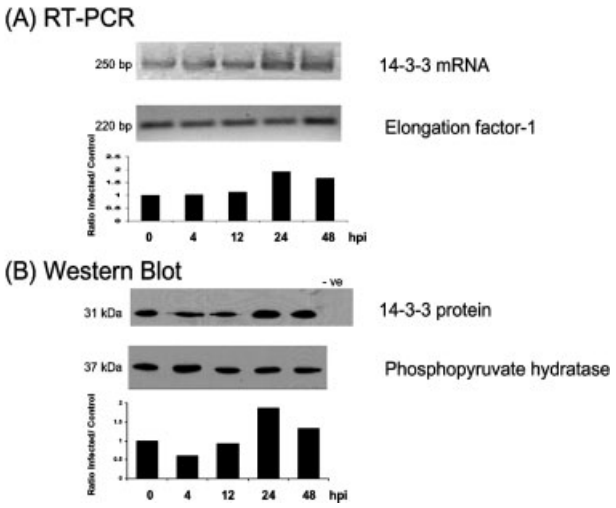

Figure 3. Time-course analysis of 14-3-3 mRNA and protein expression in TSV-infected hemocytes. (A) Semiquantitative RT-PCR of 14-3-3 mRNA at various time-points (0, 4, 12, 24, and 48 hpi) using elongation factor-1 as an internal control. (B) Western blot analysis of 14-3-3 protein with at various time-points using phosphopyruvate hydratase as an internal control to normalize the quantitative data.

Table 2. Differentially expressed hemocytic proteins in TSV-infected shrimp (*P. vannamei*) identified by nano-LC-ESI-MS/MS

Spot no.	Protein (organism)	Accession number	Predicted MW (kDa)/p*I*	Observed MW (kDa)/p*I*	Ions scores/% Coverage		Ratio infected/ control
					NCBI	EST	
Significantly up-regulated proteins (expression levels were>1.5-fold of controls)							
2	14-3-3 Zeta protein (*P. monodon*)	DQ311235.1	28/4.90	31/4.50	298/25%	585/ 36%	1.89 ± 0.53
3	Tubulin beta-2 chain (*Homarus americanus*)	Q94571	50/4.85	55/5.00	706/31%	586/36%	1.66 ± 0.18
4	Beta-actin (*Culex pipiens*)	ABD48797	41/5.30	40/4.85	212/11%	192/14%	2.36 ± 0.63
5	Acetylglucosamine pyrophosphorylase (*Aedes aegypti*)	AAU25808	54/5.40	17/5.10	42/6%	NA	1.80 ± 0.49
7	Hemocyanin (*P. vannamei*)	CAA57880	74/5.27	62/5.10	334/13%	146/33%	1.92 ± 0.69
11	Hemocyanin (*P. vannamei*)	CAA57880	74/5.27	48/4.90	186/5%	208/19%	2.05 ± 0.34
15	Hemocyanin (*P. vannamei*)	CAA57880	74/5.27	38/5.90	223/6%	132/17%	2.25 ± 0.26
17	Hemocyanin (*P. vannamei*)	CAA57880	74/5.27	26/4.60	74/2%	NA	1.50 ± 0.15
18	Protein disulfide isomerase precursor (*Tribolium castaneum*)	XP_789669	89/5.39	39/4.40	NA	117/13%	1.56 ± 0.20
19	Catalase (*A. aegypti*)	ABF18150	48/7.28	39/5.20	NA	82/4%	1.53 ± 0.03
20	Unknown protein			45/6.60	NA	NA	1.60 ± 0.41
21	Carboxylesterase (*Spodoptera litura*)	ABE01157	60/5.69	70/6.00	NA	173/30%	2.65 ± 0.47
Significantly down-regulated proteins (Expression levels were <0.67-fold of controls)							
1	TM (*Farfantepenaeus aztecus*)	Q25456	31 /4.60	38/4.45	934/45%	1641/76%	0.25 ± 0.08
6	Transglutaminase (*P. monodon*)	AAL78166	84/5.51	40/6.40	137/5%	149/10%	0.62 ± 0.17
8	Transglutaminase (*P. monodon*)	AAL78166	84/5.51	44/6.00	240/8%	269/29%	0.54 ± 0.19
9	Transglutaminase (*P. monodon*)	AAL78166	84/5.51	44/6.00	260/8%	250/18%	0.48 ± 0.12
10	Myosin light chain (*Lonomia obliqua*)	AAV91413	16/4.57	16/4.60	NA	461/28%	0.23 ± 0.05
12	Glutathione transferase (*Schistosoma japonicum*)	A26484	25/6.30	22/4.10	146/11%	NA	0.09 ± 0.06
13	Hemocyanin (*P. vannamei*)	CAA57880	74/5.27	39/4.70	169/7%	135/12%	0.37 ± 0.19
14	Hemocyanin (*P. vannamei*)	CAA57880	74/5.27	30/6.00	107/4%	183/28%	0.42 ± 0.12
16	Hemocyanin (*P. vannamei*)	CAA57880	74/5.27	25/5.50	302/8%	149/8%	0.53 ± 0.11
Proteins with subtle changes (Expression levels were 0.68–1.49-fold of controls)							
22	Phosphopyruvate hydratase (*P. monodon*)	AAC78141	47/6.18	47/6.10	919/34%	393/22%	0.80 ± 0.24
23	Arginine kinase (*P. monodon*)	AAO15713	40/6.05	39/6.30	954/38%	732/57%	0.81 ± 0.20
24	Proteasome subunit (*A. aegypti*)	EAT38162	27/6.80	31/5.20	NA	382/31%	1.14 ± 0.06
27	TM (*H. americanus*, Lobster)	P31816	32/4.70	33/4.20	434/16%	434/17%	0.95 ± 0.18
29	Profilin (*Branchiostoma belcheri*)	AAL75808	13/5.61	<10/5.40	NA	298/ 37%	1.07 ± 0.33
31	Glyceraldehyde-3-phosphate dehydrogenase (*H. americanus*)	AB094145	35/6.25	36/6.80	440/ 27%	366/21%	1.07 ± 0.44
32	Similar to annexin 11a isoform (*Danio rerio*)	XP_683620	20/5.38	34/6.40	NA	268/27%	0.96 ± 0.45
36	Transketolase (*A. aegypti*)	EAT44192	67/6.54	62/6.20	103/3%	456/20%	0.83 ± 0.16
37	Fascin (*A. aegypti*)	EAT33922	19/8.34	58/5.90	NA	359/34%	0.83 ± 0.02
43	Cytosolic MnSOD (*P. vannamei*)	AAY57407	31/5.62	31/5.20	294/27%	109/6%	1.46 ± 0.60
46	ATP synthase beta subunit (*Leucosolenia sp.*)	AAZ30666	43/4.89	53/4.60	607/27%	631/54%	1.15 ± 0.13

NA = not applicable (not available).

normalization, clearly confirmed the significant increase in expression of 14-3-3 protein at 24 hpi (approximately 1.87-fold increase) and also at a longer time-point at 48 hpi (with a lesser degree of increase, approximately 1.45-fold) (Fig. 3B). RT-PCR, using elongation factor-1 as a PCR internal control, also showed the significant increase in expression of 14-3-3 at the mRNA level (approximately 1.76-fold increase at 24 hpi and 1.35-fold increase at 48 hpi) (Fig. 3A).

3.4 Calculation of theoretical p*I* and MW of C-terminal and N-terminal hemocyanin fragments

Hemocyanin is the most abundant protein in hemolymph and is a copper-containing respiratory pigment. Expression level of the most prominent protein spot at an MW of approximately 75 kDa (located inside a rectangle in Fig. 2) was unchanged during TSV infection. This major abundant

protein was subsequently identified by nano-LC-ESI-MS/MS as hemocyanin. While expression level of the most abundant full-length hemocyanin remained unchanged, a number of differentially expressed protein spots (both up-regulated and down-regulated ones) in TSV-infected hemocytes were identified by nano-LC-ESI-MS/MS as hemocyanin fragments. They were found to be widely distributed in the 2-D gel, with various p*I*s and MWs. Interestingly, mass spectrometric analysis of hemocyanin spots present at the more acidic region identified peptides covering amino acid residues only at the C-terminus of hemocyanin (Fig. 4). In contrast, the hemocyanin spots present at the less acidic area had sequence coverage only at the N-terminus of hemocyanin.

We performed a bioinformatic analysis to address whether this difference in p*I*s of C-terminal and N-terminal hemocyanin fragments was due to a greater proportion of negatively charged residues in the C-terminus as compared to the N-terminus of hemocyanin. ProtParam tool (http://expasy.org/tools/protparam.html) was employed for this bioinformatic search. Figure 4 clearly confirmed that theoretical p*I* of a C-terminal hemocyanin fragment (spot # 7) was more acidic (p*I* = 4.81) than that of an N-terminal hemocyanin fragment (spot #15; p*I* = 5.64). The data also confirmed that the more acidic p*I* of the C-terminal fragments was due to the greater proportion of negatively charged residues in the C-terminus of hemocyanin. As only the hemocyanin fragments (either C-terminal or N-terminal ones), not its full-length, were significantly altered during TSV infection, we hypothesize that these fragments should have functional significance in molecular responses of shrimp hemocytes during TSV infection, and that C-terminal and N-terminal hemocyanin fragments may have differential roles in hemocytes. Further investigation is required to address our hypothesis.

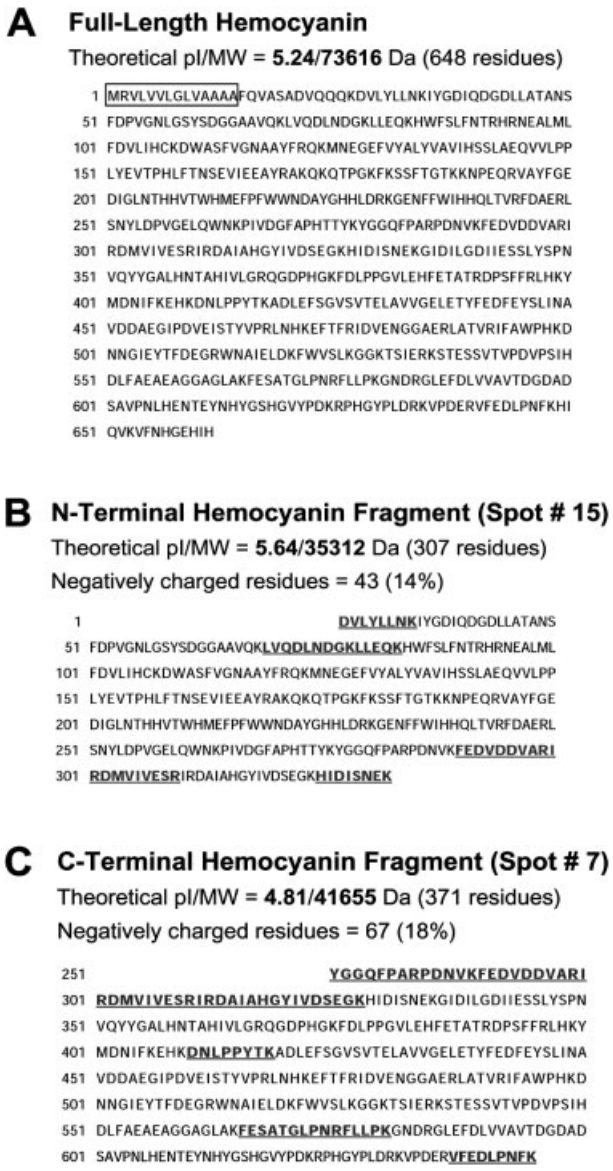

Figure 4. Alignment and bioinformatic analysis of full-length (A), N-terminal (B), and C-terminal (C) hemocyanin. ProtParam was used for calculation of theoretical p*I* and MW. Number and proportion of the negatively charged amino acid residues of N- and C-termini were also compared. Bold and underlined residues represent peptide sequences identified by nano-LC-ESI-MS/MS. Note that the first 14 residues (boxed) were not used for the calculation of the full-length hemocyanin in (A) as they are the components of signal peptide. However, when these residues were included the results remained almost the same (p*I*/MW = 5.27:74 980).

4 Discussion

To date, the knowledge on shrimp immune responses, particularly at the molecular level, to a virus infection is still limited. In the present study, we applied a gel-based proteomics approach to explore the molecular responses of *P. vannamei* during TSV infection. Our results revealed 21 out of the average of 281 protein spots in each gel of shrimp hemocytes that had significant alterations in their expression levels upon TSV infection. Peptide sequencing by nano-LC-ESI-MS/MS allowed reliable identification of 20 among these 21 differentially expressed proteins.

We observed a significant increase in 14-3-3 expression at both protein and mRNA levels, at 24 and 48 hpi. The functional role of this protein has been elucidated and reported for eukaryotic cells [17–19]. In mammalians, 14-3-3 proteins are crucial for cell signaling and survival. However, its role in invertebrates, particularly crustaceans, is not well understood although there is recent evidence demonstrating an increase in this protein in shrimp lymphoid organ and stomach cells after white spot syndrome virus (WSSV) infection [20].

The up-regulated cytoskeletal proteins, including beta-actin and beta-tubulin, have been suggested to play an important role during viral infection. Actin has been shown

to play an active role in gene expression and maturation of several viruses [21]. In addition, the virus can use actin polymerization to facilitate its migration to neighboring cells [21]. For tubulin, there are several reports showing that viruses may require microtubule components for RNA synthesis [22, 23].

Upregulations of proteins involved in cytoskeletal arrangements, cell signaling, and proliferation are cellular response reactions. An upregulation of ER-stress response protein (PDI) was also observed in our present study. It is an enzyme involved in protein modification and folding. The up-regulated PDI might be related to an increase in protein synthesis or to a mechanism to refold/renature the misfolded/denatured proteins, which were the results of oxidative and cellular stresses [24].

Another group of the altered proteins was the antioxidant enzymes, including catalase, carboxylesterase, and glutathione transferase. Virus-induced oxidative stress is associated with the activation of phagocytsis and the release of ROS that can damage lipids, proteins, carbohydrates, and nucleotides [25–28]. Catalase is a primary defense component that plays an important role not only in the protection of cells from the toxic effects by breaking down hydrogen peroxide, but also in the detoxification pathway [29]. Therefore, an upregulation of catalase is essential for shrimp survival as it can catalyze the conversion of hydrogen peroxide into water and oxygen. Another protein with a significant upregulation is carboxylesterase. It is one of most important detoxification enzymes involved in the hydrolysis of ester and amide bonds of xenobiotics [30]. This enzyme has been reported to be upregulated in tumor cells and be involved in cell turnover rates [31]. The hemocytic level of glutathione transferase was markedly decreased in TSV-infected shrimp. Our data were consistent with a recent report of WSSV-infected animals that showed reduced activities of several antioxidant enzymes, such as superoxide dismutase and glutathione-associated enzymes [32]. While catalase and carboxylesterase were up-regulated, glutathione transferase was markedly down-regulated in TSV-infected hemocytes. The reason of the disparate results of alterations in these antioxidant enzymes remains unclear and deserves further investigation.

Three distinctive spots with reduced expression levels in TSV-infected hemocytes were identified as transglutaminase. Transglutaminase in shrimp hemocytes is generally known to play critical roles in blood coagulation and fibrin crosslinking. Some of transglutaminase isoforms, such as mammalian Type II transglutaminase, have a diverse function, including cell attachment [33], signal transduction, and programmed cell death [34–36]. The study in *P. monodon* has shown that transglutaminase is expressed at the highest levels in hemocytes and muscles [37]. As a part of the innate immune response of crustaceans, transglutaminase participates in coagulation of hemolymph. It prevents leakage of hemolymph from the injected sites and also protects dissemination of the invaders, such as bacteria, throughout the body.

In addition to transglutaminase, significant reduction of tropomyosin (TM) is also observed. TM is a protein within the troponin complex, which is associated with actin and is responsible for mediating calcium in the contraction-generating interaction of actin and myosin [38, 39]. Down-regulation of TM may destabilize microfilament architecture and contribute to changes in cell shape and mobility that usually accompany virus infection [40].

There are a number of protein spots identified as hemocyanin. Their appearance as multiple spots in a 2-D gel may be a result from its heterogeneity. In addition to the main function as an oxygen transporter, hemocyanin has been identified as a multifunctional protein involved in several physiological processes including phenoloxidase activation [41], antimicrobial mechanisms [42–44], and acting as lectin in specific agglutination [45, 46]. We have identified upregulation of several C-terminal hemocyanin fragments in shrimp hemocytes during TSV infection. It has been demonstrated that the peptides with antibacterial and antifungal properties isolated from shrimps are originated from the C-terminal part of hemocyanin [42, 43]. The increased abundance of the C-terminal hemocyanin fragments may be a result from hemocyanin-processing system, which is crucial for antiviral activity.

Interestingly, mass spectrometric analysis of hemocyanin spots present at the more acidic region identified peptides covering amino acid residues only at the C-terminus of hemocyanin. In contrast, the hemocyanin spots present at the less acidic area had sequence coverage only at the N-terminus of hemocyanin. Bioinformatic calculation clearly confirmed that theoretical p*I* of a C-terminal hemocyanin fragment (spot #7) was more acidic (p*I* = 4.81) than that of an N-terminal hemocyanin fragment (spot #15; p*I* = 5.64) (Fig. 4). Because three-fourth of the C-terminal fragments were up-regulated, whereas two-third of the N-terminal hemocyanin fragments were down-regulated, we therefore hypothesize that the C-terminal and the N-terminal hemocyanin fragments may have differential roles in hemocytes.

In summary, we have identified several proteins in hemocytes that were modulated during TSV infection. While roles of some of these alterations could be related to host responses during a viral infection, functional significance of other altered proteins remains unclear. Further investigation of these data may lead to better understanding of the molecular responses of crustacean hemocytes to TSV infection and ultimately to a better control of virus infection in shrimp culture.

We would like to thanks Dr. Kallaya Sritunyalucksana at the Center of Excellence for Shrimp Molecular Biology and Biotechnology, Mahidol University for providing TSV. This work was supported by The Thailand Research Fund (TRF) under the Royal Golden Jubilee Ph.D. program, and Mahidol University.

5 References

[1] Wyban, J. A., Sweeney, J. N., *Intensive Shrimp Production Technology*, High Health Aquaculture Inc., Hawaii 1991.

[2] Rosenberry, B., *World Shrimp Farming*, Shrimp News International, San Diego 2002.

[3] Brock, J. A., Main, K. L., *A Guide to Common Problems and Diseases of Cultured Penaeus vannamei*, World Aquaculture Society, Louisiana 1994.

[4] Fulks, W., Main, K. L., *Diseases of Cultured Penaeid Shrimp in Asia and the United States*, High Health Aquaculture Inc., Hawaii 1992.

[5] Hoffmann, J. A., Kafatos, F. C., Janeway, C. A., Ezekowitz, R. A. B., *Phylogenetic perspectives in innate immunity. Science* 1999, *284*, 1313–1318.

[6] Martin, G. G., Poole, D., Poole, C., Hose, J. E. *et al.*, Clearance of bacteria infected into the hemolymph of the penaeid shrimp, *Sicyonia ingentis*. *J. Inventebr. Pathol.* 1993, *62*, 308–315.

[7] Vazquez, L., Maldonado, G., Aqundis, C., Perez, A. *et al.*, Participation of a sialic acid-specific lectin from freshwater prawn *Macrobrachium rosenbergii* hemocytes in the recognition of nonself cells. *J. Exp. Zool.* 1997, *279*, 265–272.

[8] Munoz, M., Cedeno, R., Rodriguez, J., van der Knoop, W. P. W. *et al.*, Measurement of reactive oxygen intermediate production in haemocytes of the penaeid shrimp, *Penaeus vannamei*. *Aquaculture* 2000, *191*, 89–107.

[9] Soderhall, K., Cerenius, L., Role of the prophenoloxidase-activating system in invertebrate immunity. *Curr. Opin. Immunol.* 1998, *10*, 23–28.

[10] Dimarq, J. L., Imler, J. L., Lanot, J., Ezekowitz, R. *et al.*, Treatment of 1 (2) mbn Drosophila tumours blood cells with the steroid hormone ecdysone amplifies the inducibility of anti-microbial peptide gene expression. *Insect. Biochem. Mol. Biol.* 1997, *27*, 877–886.

[11] Song, Y. L., Yu, C. I., Lien, T. W., Huang, C. C. *et al.*, Haemolymph parameters of Pacific white shrimp (*Litopenaeus vannamei*) infected with Taura syndrome virus. *Fish. Shellfish. Immun.* 2003, *14*, 317–331.

[12] Bonami, J. R., Hasson, K. W., Mari, J., Poulos, B. T. *et al.*, Taura syndrome of marine penaeid shrimp: Characterization of the viral agent. *J. Gen. Virol.* 1997, *78*, 313–319.

[13] Mari, J., Poulos, B. T., Lightner, D. V., Bonami, J. R., Shrimp Taura syndrome virus, genomic characterization and similarity with member of the genus Cricket paralysis-like viruses. *J. Gen. Virol.* 2002, *83*, 915–926.

[14] Bradford, M. M., A rapid and sensitive method for the quantitation of microgram quantities of protein utilizing the principle of protein-dye binding. *Anal. Biochem.* 1976, *72*, 248–254.

[15] Tsai, J. M., Wang, H. C., Leu, J. H., Hsiao, H. N. *et al.*, Genomic and proteomic analysis of thirty-nine structural proteins of shrimp white spot syndrome virus. *J. Virol.* 2004, *78*, 11360–11370.

[16] Udomkit, A., Chooluck, S., Sonthayanon, B., Panyim, S., Molecular cloning of cDNA encoding a member of CHH/MIH/GIH family from *Penaeus monodon* and analysis of its gene structure. *J. Exp. Mar. Biol. Ecol.* 2000, *244*, 145–156.

[17] Aitken, A., Jones, D., Soneji, Y., Howell, S., 14-3-3 protein: Biological function and domain structure. *Biochem. Soc. T.* 1995, *23*, 605–611.

[18] Muslin, A. J., Tanner, J. W., Allen, P. M., Shaw, A. S., Interaction of 14-3-3 with signaling proteins is mediated by the recognition of phosphoserine. *Cell* 1996, *84*, 889–897.

[19] Yaffe, M. B., Rittinger, K., Volinia, S., Caron, P. R. *et al.*, The structural basis for 14-3-3: Phosphopeptide binding specificity. *Cell* 1997, *91*, 961–971.

[20] Wang, H. C., Wang, H. C., Leu, J. H., Kou, G. H. *et al.*, Protein expression profiling of the shrimp cellular response to white spot syndrome virus infection. *Dev. Comp. Immunol.* 2007, *31*, 672–686.

[21] Cudmore, S., Cossart, P., Griffiths, G., Way, M., Actin-based motility of vaccinia virus. *Nature* 1995, *378*, 636–638.

[22] Hill, V. M., Summers, D. F., A minor microtubule-associated protein is responsible for the stimulation of vesicular stomatitis virus transcription *in vitro*. *J. Gen. Virol.* 1990, *71*, 289–298.

[23] Moyer, S. A., Baker, S. C., Lessard, J. L., Tubulin: A factor necessary for the synthesis of both Sendai virus and vesicular stomatitis virus RNAs. *Proc. Natl. Acad. Sci. USA* 1986, *83*, 5405–5409.

[24] Harvie, M., Jordan, T. W., Flamme, A. C., Differential liver protein expression during schistosomiasis. *Infect. Immun.* 2007, *75*, 736–744.

[25] Orr, W. C., Orr, E. C., Legan, S. K., Sohal, R. S., Molecular analysis of the Drosophila catalase gene. *Arch. Biochem. Biophys.* 1996, *330*, 251–258.

[26] Vaughan, M., Oxidative modification of macromolecules. *J. Biol. Chem.* 1997, *272*, 18513.

[27] Schwarz, K. B., Oxidative stress during viral infection: A review. *Free Radic. Biol. Med.* 1996, *21*, 641–649.

[28] Yu, B. P., Cellular defenses against damage from reactive oxygen species. *Physiol. Rev.* 1994, *74*, 139–162.

[29] Arun, S., Subramanian, P., Antioxidant enzymes in freshwater prawn *Macrobrachium malcolmsonii* during embryonic and larval development. *Comp. Biochem. Phy.* 1998, *121*, 273–277.

[30] Jokanovic, M., Biotransformation of organophosphorus compounds. *Toxicology* 2001, *166*, 139–160.

[31] Satoh, T., Hosokawa, M., Structure, function and regulation of carboxylesterases. *Chem. Biol. Interact.* 2006, *162*, 195–211.

[32] Mohankumar, K., Ramasamy, P., White spot syndrome virus infection decreases the activity of antioxidant enzymes in *Fenneropenaeus indicus*. *Virus Res.* 2006, *115*, 69–75.

[33] Tyrrell, D. J., Sale, W. S., Slife, C. W., Organization and evolution of the human epidermal keratinocyte transglutaminase I gene. *J. Biol. Chem.* 1998, *263*, 1946–1951.

[34] Fesus, L., Thomazy, V., Falus, A., Calcium glucarate prevents tumor formation in Mouse Skin. *FEBS Lett.* 1987, *224*, 104–108.

[35] Lorand, L., Graham, R. M., Transglutaminase, cross-linking enzymes with pleiotropic functions. *Nat. Rev. Mol. Cell Biol.* 2003, *4*, 140–156.

[36] Melino, G., Piacentini, M., Tissue transglutaminase in cell death: A downstream or a multifunctional upstream effector. *FEBS Lett.* 1998, *430*, 59–63.

[37] Yeh, M. S., Kao, L. R., Huang, C. J., Tsai, I. H., Biochemical characterization and cloning of transglutaminases responsible for hemolymph clotting in *Penaeus monodon* and *Marsupenaeus japonicus*. *Biochim. Biophys. Acta.* 2006, *1764*, 1167–1178.

[38] Ebashi, S., Endo, M., Ohtsuki, I., Control of muscle contractions. *Q. Rev. Biophys.* 1969, *2*, 351–384.

[39] Hanson, J., Lowry, J., The structure of F-actin and actin filaments isolated from muscle. *J. Mol. Biol.* 1963, *6*, 46–60.

[40] Hendricks, M., Weintraub, H., Multiple tropomyosin polypeptides in chicken embryo fibroblasts: Differential repression of transcription by rous sarcoma virus transformation. *Mol. Cell. Biol.* 1984, *4*, 1823–1833.

[41] Decker, H., Rimke, T., Tarantula hemocyanin shows phenoloxidase activity. *J. Biol. Chem.* 1998, *273*, 25889–25892.

[42] Destoumieux, D., Saulnier, D., Garnier, J., Jouffrey, C. *et al.*, Crustacean immunity: Antifungal peptides are generated from the C terminus of shrimp hemocyanin in response to microbial challenge. *J. Biol. Chem.* 2001, *276*, 47070–47077.

[43] Destoumieux, D., Bulet, P., Loew, D., Dorsselaer, A. V. *et al.*, Penaeidins, a new family of antimicrobial peptides isolated from the shrimp *Penaeus vannamei* (Decapoda). *J. Biol. Chem.* 1997, *272*, 28398–28406.

[44] Zhang, X., Huang, C., Qin, Q., Antiviral properties of hemocyanin isolated from shrimp *Penaeus monodon*. *Antiviral. Res.* 2004, *61*, 93–99.

[45] Alpuche, J., Pereyra, A., Agundis, C., Rosas, C. *et al.*, Purification and characterization of a lectin from the white shrimp *Litopenaeus setiferus* (*Crustacea decapoda*) hemolymph. *Biochim. Biophys. Acta* 2005, *1724*, 86–93.

[46] Zhang, Y., Wang, S., Xu, A., Chen, J. *et al.*, Affinity proteomic approach for identification of an IgA-like protein in *Litopenaeus vannamei* and study on its agglutination characterization. *J. Proteome Res.* 2006, *5*, 815–821.

Available online at www.sciencedirect.com
ScienceDirect
Biochimica et Biophysica Acta 1784 (2008) 504–511
Biochimica et Biophysica Acta BBA
www.elsevier.com/locate/bbapap

Proteomic analysis of altered proteins in lymphoid organ of yellow head virus infected *Penaeus monodon*

Apichai Bourchookarn [a], Phattara-Orn Havanapan [a], Visith Thongboonkerd [b], Chartchai Krittanai [a,*]

[a] *Institute of Molecular Biology and Genetics (IMBG), Mahidol University, Salaya Campus, Nakhonpathom, Thailand*
[b] *Medical Molecular Biology Unit, Office for Research and Development, Faculty of Medicine Siriraj Hospital, Mahidol University, Bangkok, Thailand*

Received 9 September 2007; received in revised form 16 November 2007; accepted 7 December 2007
Available online 16 January 2008

Abstract

A comparative proteomic analysis was employed to identify altered proteins in the yellow head virus (YHV) infected lymphoid organ (LO) of *Penaeus monodon*. At 24 h post-infection, the infected shrimps showed obvious signs of infection, while the control shrimps remained healthy. Two-dimensional electrophoresis of proteins extracted from the LO revealed significant alterations in abundance of several proteins in the infected group. Protein identification by MALDI–TOF MS and nanoLC–ESI–MS/MS revealed significant increase of transglutaminase, protein disulfide isomerase, ATP synthase beta subunit, V-ATPase subunit A, and hemocyanin fragments. A significant decrease was also identified for Rab GDP-dissociation inhibitor, 6-phosphogluconate dehydrogenase, actin, fast tropomyosin isoform, and hemolymph clottable protein. Some of these altered proteins were further investigated at the mRNA level using real-time RT-PCR, which confirmed the proteomic data. Identification of these altered proteins in the YHV-infected shrimps may provide novel insights into the molecular responses of *P. monodon* to YHV infection.

Keywords: *Penaeus monodon*; Proteomics; Lymphoid organ; Yellow head virus

1. Introduction

Yellow head virus (YHV) is an enveloped viral particle, causing a significantly high mortality rate for the penaeid shrimps. The YHV genome is a single-stranded RNA containing 3 major structural proteins: gp116, gp64 and p20 [1,2]. The YHV-infected shrimps usually exhibit a yellow color on cephalothorax and gills, which are the clinical sign of yellow head disease (YHD) [3]. A widespread of necrosis in lymphoid organ (LO), gills, connective tissues, hemocytes, and hematopoietic organs can lead to death within a few days after infection [4]. Hence, this viral disease can cause rapid and massive loss of shrimp production. At present, there is no effective treatment for the YHD.

The LO in penaeid shrimp is localized at an anterodorsal surface of hepatopancreas. The structure is composed of folded tubules with a central haemal lumen and cellular wall [5]. From histopathological studies and a recent detection of YHV receptor, the LO is likely to be a primary target of YHV and involved in the defense mechanisms [6–8].

To gain more insights, this present study aimed to identify altered proteins in the LO of YHV-infected *P. monodon*. LO proteins from the experimentally infected shrimps were extracted and analyzed by a proteomics workflow using 2-DE and mass spectrometry. Comparative analysis of the infected versus control samples revealed a set of altered proteins at 24 h post-infection (hpi). The alterations of selected proteins were then investigated further and confirmed at the transcriptional level using real-time RT-PCR. Potential roles of some altered proteins in response to YHV infection are discussed.

2. Materials and methods

2.1. Animal preparation and virus injection

The juvenile *P. monodon* (16–22 g) from local farm were acclimatized and reared in 10-ppt artificial seawater (Mariscience) at 25–28 °C. The air was continuously supplied using an electric pump. The YHV stock was purified and diluted (1:10,000)

Abbreviations: ER, endoplasmic reticulum; HCP, hemolymph clottable protein; hpi, hours post-infection; LO, lymphoid organ; PDI, protein disulfide isomerase; TGase, transglutaminase; YHV, yellow head virus

* Corresponding author. Tel.: +662 800 3624; fax: +66 2 441 9906.
E-mail address: stckt@mahidol.ac.th (C. Krittanai).

1570-9639/$ - see front matter © 2007 Elsevier B.V. All rights reserved.
doi:10.1016/j.bbapap.2007.12.006

in NTE buffer (200 mM NaCl, 20 mM Tris–HCl, and 20 mM EDTA; pH 7.4). Shrimps were injected with YHV (100 μl per 20 g of each shrimp) using 26G-gauge needle. The control shrimps were injected with an equal volume of NTE buffer.

2.2. Protein extraction and quantitation

At 24 hpi, shrimps were chilled on ice and dissected for LO from an opened carapace. After washing with cold anticoagulant (27 mM sodium citrate, 330 mM NaCl, 100 mM glucose, and 10 mM EDTA; pH 6.8), the tissue was homogenized in a lysis buffer (8 M urea, 2 M thiourea, 60 mM DTT, 0.2% Triton X-100, 2% CHAPS, 1 mM PMSF, and 1 mM benzamidine). Protein solution was collected after a 10 min centrifugation at 12,000 rpm, 4 °C. Protein concentration was determined by Bradford's assay using bovine serum albumin as the standard [9].

2.3. Two-dimensional gel electrophoresis (2-DE) and spot analysis

All materials used for 2-DE experiment were supplied by GE HealthCare (Uppsala, Sweden). A pool of LO samples isolated from 5 animals (within the same group) was used for resolving the LO proteins in a 2-DE gel. Three individual pools per group were used for comparative proteomic analysis of the YHV-infected versus control (uninfected) LO (with a sum of 15 animals per group; totally 30 animals were used in the present study). The IEF was performed at 20 °C on Ettan IPGphor II system (Amersham Biosciences). The 13-cm IPG strip (pH 4–7) was rehydrated for 12 h with 150-mg total protein in the lysis buffer added with 0.5% (v/v) IPG buffer. The strip was then equilibrated in an equilibration buffer [6 M urea, 2% SDS, 30% glycerol, 50 mM Tris–HCl (pH 8.8) and 0.002% (w/v) bromophenol blue] with 10 mg/ml DTT for 15 min and then with 25 mg/ml iodoacetamide for another 15 min. A 12.5% SDS-PAGE was performed using a SE600 Ruby electrophoresis set with a constant current of 10 mA/gel for 30 min, and then with a constant voltage of 100 V until the tracking dye reached the gel bottom. Gels were then stained with Colloidal Coomassie Brilliant Blue G250 and images were analyzed using ImageMaster 2D platinum software (Amersham Biosciences). In order to normalize the intensity data of individual protein spots present in each gel, intensity volumes of all protein spots were summed into a hundred percent. Then the percent intensity volume (%vol) of each individual spot (relative to the intensity volumes of all spots) was used for the comparative analysis with unpaired Student's *t*-test. *P* values less than 0.05 were considered statistically significant.

2.4. In-gel digestion, MALDI–TOF MS and nanoLC–ESI–MS/MS

Excised protein spots were chopped into pieces, and washed twice with water. In-gel tryptic digestion was performed using 2 ng/μl of sequencing-grade trypsin (Promega) in 100 mM ammonium bicarbonate buffer, pH 7.8, at 37 °C for 6 h. Peptides were extracted twice using ACN/water/formic acid (47.5/47.5/5%) solution. Peptide mass fingerprinting was obtained using a Proteome Works System M@LDI Reflectron mass spectrometer (Waters). Peptide solution was mixed with an equal volume of alpha-cyano-4-hydroxycinnamic acid matrix solution and applied on a target plate. After air drying and washing with water, mass spectra were collected over the m/z range of 800–3000. Peak lists obtained by Masslynx 4.0 software (Waters) were subjected to the database search via the Mascot tool (www.matrixscience.com).

MS/MS sequencing on a nanoLC Micromass Qtof2 quadrupole time-of-flight tandem mass spectrometer was performed under the control of MassLynx 4.0 Sp1 (Waters). MS/MS ion search was performed against the NCBInr and ESTothers databases using the Mascot tool. Only matched proteins with significant ions scores (>40; *p*-value < 0.05) were reported. Due to a limitation in shrimp protein database, some of the spots were *de novo* sequenced and searched using NCBI-BLAST or the Marine Genomics Project stand-alone BLAST (www.marinegenomics.org/sablast.php).

2.5. Analysis of mRNA levels by real-time RT-PCR

mRNA levels of the selected genes (Table 1) were analyzed at 0, 6, 12, 24 and 48 hpi. Total RNA was extracted from homogenized LO using 1 ml of TRI Reagent (Molecular Research Center) and precipitated in 0.5 ml of isopropanol. After washing with 1 ml of 75% ethanol, the pellet was dissolved in DEPC-treated water at 55 °C for 15 min. A microgram of total RNA was reverse transcribed with 5 U of ImProm-II reverse transcriptase (Promega) using 500 ng of Oligo-dT as the first strand primer in 20 μl reaction. The SYBR Green real-time RT-PCR was performed using ABI 7500 Real-Time PCR System (Applied Biosystems). Amplification was carried out in a 96-well plate; each 25 μl reaction volume contained 0.25 μM (each) forward and reverse primers, 1× QuantiTect SYBR Green PCR, and 1 μl cDNA. The final volume was then adjusted by PCR–water. The experimental cycling profile was set as recommended in the manufacturer's manual for QuantiTect SYBR Green PCR kit (QIAGEN) under the control of SDS 1.3.1 software. The cycling was as follows: PCR initial activation step (95 °C, 15 min), 40 repeated of 3-step cycling (94 °C for 15 s 55 °C for 30 s, and 72 °C for 40 s, respectively). The targeted gene was then analyzed in three individual pools per group (each pool was derived from 5 animals; totally 30 animals were used for PCR analysis) using *Ef1α* gene of *P. monodon* as an internal control. Normalization of the target gene with an endogenous standard was done via the reference gene expression, to compensate inter-PCR variations. Control expression levels were included in the calculation model to standardize each reaction run with respect to RNA integrity, RT efficiency and cDNA sample loading variations based on the method described by Pfaffl [10].

Table 1
List of primers used for relative quantification by SYBR Green real-time RT-PCR

Target gene (Accession number)	Primer name	Sequence (5′–3′)	Tm
Protein disulfide isomerase (PDI)	PmPDI_F	TGGCGAGTCGTTATGGTGTA	61.20
(gi|113366589, EE663080)	PmPDI_R	TGTCAGGATGGCATTGTCTG	59.50
Transglutaminase (TGase)	PmTran_F	ACGACGACTGGGACATAAGG	62.10
(gi|33694273, AY074924)	PmTran_R	CATACTCCTGGCGCATTTTT	58.80
Hemolymph clottable protein (HCP)	PmClot_F	CCTATGCCGTGTCCATCATC	61.30
(gi|6601497, AF089867)	PmClot_R	GCGTGCGACCAACAGTAAG	60.47
Fast tropomyosin isoform	PmTropo_F	TCTCTTCCTATGCCCTCAGC	59.53
(gi|125995156, AB270629)	PmTropo_R	TATGGCAGACTTCACCAACG	59.72
Elongation factor 1 alpha (Ef1α)	PmEf1a_F	CATCTCATCTACAAATGCG	59.35
(gi|11037863, AW600734)	PmEf1a_R	ATGAAATCACGATGGCCTG	60.10

3. Results

3.1. Clinical signs of the YHV-infected P. monodon

After injection with the purified YHV, the infected shrimps showed obvious signs of YHV infection. As early as 24 hpi, the infected shrimps had an irregular swimming pattern, fading of body and gills' colors, and no feeding. Some of the infected shrimps were found dead at 24–48 hpi, with a mortality rate of 80–100% at 48 hpi. The yellow color was found on the cephalothorax in some of the moribund shrimps, while the faint body color was found in other infected shrimps. In contrast, the control shrimps injected with the NTE buffer were all healthy with normal feeding and swimming activity.

3.2. 2-DE and identification of altered proteins in the infected LO

The proteomic profiles of LO from control and YHV-infected shrimps were analyzed at 24 hpi. Approximately 370–420 spots

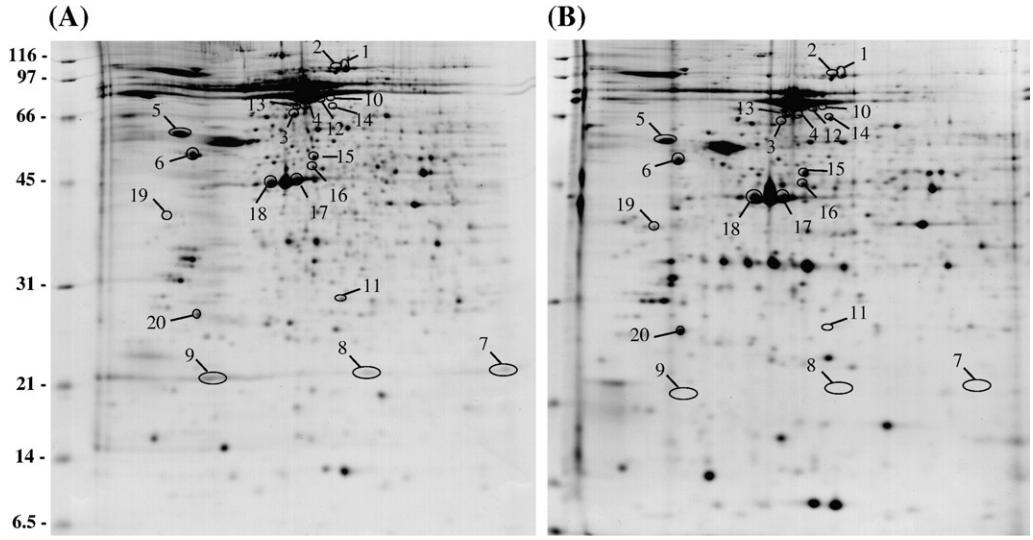

Fig. 1. Representative 2-D gels of lymphoid proteins for (A) YHV-infected and (B) control samples at 24 hpi. Spots numbers are labeled corresponding to Table 2.

were visualized on each gel. The "significant changes" in protein abundance was defined with the criteria that (i) p values must be <0.05, (ii) means of both groups using the unpaired Student's t-test; must be either >1.5-fold (significant increase) or <0.75-fold (significant decrease). We observed significant changes in abundance of totally 33 protein spots (Fig. 1). Of these, 20 were successfully identified by peptide mass fingerprinting, MS/MS ion search, and *de novo* sequencing (Table 2).

Among the annotated proteins, 8 forms of 5 unique proteins were found to have significantly increased levels upon the YHV infection. These proteins included transglutaminase (TGase) (spots #1 and 2), protein disulfide isomerase (PDI) (spots # 5), ATP synthase beta subunit (spot # 6), V-ATPase subunit A (spot #10), and hemocyanin fragments (spots #3, 4 and 11). In contrast, other 9 proteins showed significantly decreased levels during the infection. These included est_l_vannamei501 (spot #12), hemocyanin fragment (spot #13), est_l_vannamei1751 (spot #14), Rab GDP-dissociation inhibitor (spot #15), 6-phosphogluconate dehydrogenase (spot #16), beta-actin (spots #17), actin-2 (spot #18), fast tropomyosin isoform (spot #19), and hemolymph clottable protein (HCP) (spot #20). Convincingly, there were 3 altered protein spots (#7–9) observed only in the infected LO and were identified as the p20 nucleocapsid protein of YHV. This is indicating the successful infection of YHV in the LO of our experimental model (Fig. 1 and Table 2). Fig. 2 illustrates the zoom-in images, in all gels, of some of the altered protein spots with significantly increased (Fig. 2A and B) and decreased (Fig. 2C and D) levels. These spots were identified as PDI, TGase, HCP, and fast tropomyosin isoform, respectively.

3.3. Quantitative analysis of changes at the mRNA levels

The mRNA expressions levels of some selected genes were assessed by relative quantification using real-time RT-PCR. The primer set for the selected target genes are given in Table 1. These selected genes corresponded to two increased proteins (PDI and TGase), and two decreased proteins (HCP and fast tropomyosin isoform). *Ef1*α served as an internal control gene. Fig. 3 shows fold-changes of mRNA levels of these genes at various time-points in relation to the baseline levels of their respective transcripts at 0 hpi. The results demonstrated a substantial up-regulation of PDI transcript over time of the infection (Fig. 3A). TGase was also found to have a substantial increasing, although with a decline at 6 hpi (Fig. 3B). Focusing at 24 hpi, the results obtained from real-time RT-PCR were really consistent with the proteomic data, all of which showed up-regulations of these two gene products (Fig. 3A and B). In contrast, mRNA level of HCP was decreased from the baseline level till 48 hpi, with a maximal decline at 6 hpi (Fig. 3C). However, the mRNA level of fast tropomyosin isoform was declined only at 6 hpi, returned to the baseline level at 12 hpi, and finally increased (Fig. 3D).

4. Discussion

The YHV has been proven to be one of the most serious pathogens for shrimps. In this study, the YHV-infected *P. monodon* showed a mortality rate up to 80–100% within 48 hpi. The moribund shrimps clearly demonstrated the gross signs of YHD with yellow head and gills, fading of body colors, and defective activity in feeding and swimming. To investigate the molecular responses of YHV infection in the LO of *P. monodon*, a comparative analysis of proteomic profiles of control and infected LO at 24 hpi was performed. From the 2D gels, most of the protein spots were well defined which are likely to represent a single protein in each spot. Some of the spots were found as smears and might be suspected to contain a mixture of proteins. However the analysis results of their protein fingerprinting and MS/MS showed only one positive or significant hit in every spot without a possibility of having more than one proteins in these spots. Quantitative analyses of the comparative gels revealed a set of 33 protein spots with significant changes in their relative intensity volumes. However due to the lack of a genome database of penaeid shrimp species, very few proteins were successfully identified from peptide mass

Table 2
The altered proteins identified by peptide mass fingerprinting (PMF), MS/MS ion search, and *de novo* sequencing

ID	Protein	NCBI GenInfo	Method	Queries and peptides [a] matched	Score			Observed pI/MW (kDa)	Theoretical pI/MW (kDa)	Spot volume (%)		Ratio YHV/Ctrl	Function
					PMF	MS/MS	e-value/ %identity			Ctrl	YHV		
Up-regulated proteins													
1	Transglutaminase	gi|33694274	MS/MS	4	–	103	–	5.80/90	5.51/84.60	0.09±0.03	0.24±0.04	2.81±0.48	Catalyze Protein cross-linking
2	Transglutaminase	gi|33694274	*de novo*	LNQNVALASAQELK			0.00009/100	5.75/90	5.51/84.60	0.34±0.12	0.85±0.14	2.65±0.66	Catalyze Protein cross-linking
				PTVDALSDLANR			0.04500/91						
3	Hemocyanin	gi|16612121	PMF	8	92	–	0.00016 /–	5.45/66	5.10/51.12	0.12±0.01	0.35±0.05	3.03±0.24	Oxygen transport
4	Hemocyanin	gi|16612121	PMF	9	102	–	0.000016/–	5.50/66	5.10/51.12	0.06±0.02	0.21±0.02	3.13±0.76	Oxygen transport
5	Protein disulfide isomerase	gi|91753065	MS/MS	6	–	59	–	4.60/60	5.11/67.44	1.07±0.34	2.77±0.17	2.70±0.60	ER stress response, chaperone
6	ATP synthase beta subunit	gi|113204646	PMF	10	98	–	0.000043/–	4.65/50	5.31/55.80	0.65±0.18	2.08±0.52	3.18±0.32	Energy buffering
7	YHV-p20	gi|71040948	MS/MS	4	–	185	–	7.00/21	9.98/16.31	–	0.14±0.05	NA	YHV nucleocapsid protein
8	YHV-p20	gi|71040948	MS/MS	3	–	103	–	5.80/21	9.98/16.31	–	0.09±0.02	NA	YHV nucleocapsid protein
9	YHV-p20	gi|71040948	MS/MS	4	–	142	–	4.75/22	9.98/16.31	–	1.16±0.62	NA	YHV nucleocapsid protein
10	V-ATPase subunit A	gi|401323	MS/MS	2		48		5.20/68	5.14/68.00	0.011±0.002	0.038±0.010	3.46±0.65	H(+)-transporting ATPase
11	Hemocyanin	gi|854403	*de novo*	NQAGGAGLSEFESATAVPNR			0.00100/80	5.70/29	5.20/67.50	0.05±0.01	0.11±0.01	2.24±0.13	Oxygen transport
Down-regulated proteins													
12	Est_1_vannamei501 [b]	gi|40956394	MS/MS	3	–	96	–	5.14/68	–/–	0.11±0.02	0.05±0.01	0.51±0.03	Similar to V-ATPase subunit A
13	Hemocyanin	gi|16612121	MS/MS	6	–	88	–	5.45/66	5.10/51.12	0.14±0.01	0.06±0.01	0.45±0.10	Oxygen transport
14	Est_l_vannamei1751 [b]	gi|40957271	MS/MS	2	–	57	–	5.80/66	–/–	0.16±0.01	0.08±0.01	0.53±0.09	Unknown
15	Rab GDP-dissociation inhibitor	gi|108870669	MS/MS	4	–	81	–	5.60/50	5. 38/50.20	0.64±0.01	0.35±0.09	0.55±0.14	Required for Rab recycle
16	6-phosphogluconate dehydrogenase	gi|118783576	MS/MS	4	–	57	–	5.57/46	7.60/53.40	0.27±0.03	0.13±0.02	0.46±0.10	NADP binding, oxidoreductase
17	Beta actin	gi|10304437	PMF	9	114	–	0.000001/–	5.40/43	5.51/42.50	2.64±0.31	1.28±0.21	0.48±0.10	Cytoskeleton
18	Actin-2	gi|543767	PMF	10	82	–	0.000780/–	5.30/43	5.37/41.85	4.32±1.04	2.00±0.21	0.47±0.06	Cytoskeleton
19	Fast tropomyosin isoform	gi|2660868	MS/MS	5	–	142	–	4.50/38	4.70/32.80	0.21±0.08	0.03±0.01	0.16±0.05	Cytoskeleton
20	Hemolymph clottable protein	gi|46396031	MS/MS	2		51	–	4.65/29	5.27/189.70	0.40±0.10	0.15±0.02	0.37±0.05	Substrate for transglutaminase,
			de novo	LPVNLAEEVNVQR	–		0.00030/10						
				LNYGAVEETLVGR			0.00060/100						

[a] Peptide queries submitted for BLAST search. Underlined indicates identical residues to the obtained protein entry.
[b] Name obtained from ESTothers database.
NA = not applicable (divided by zero).

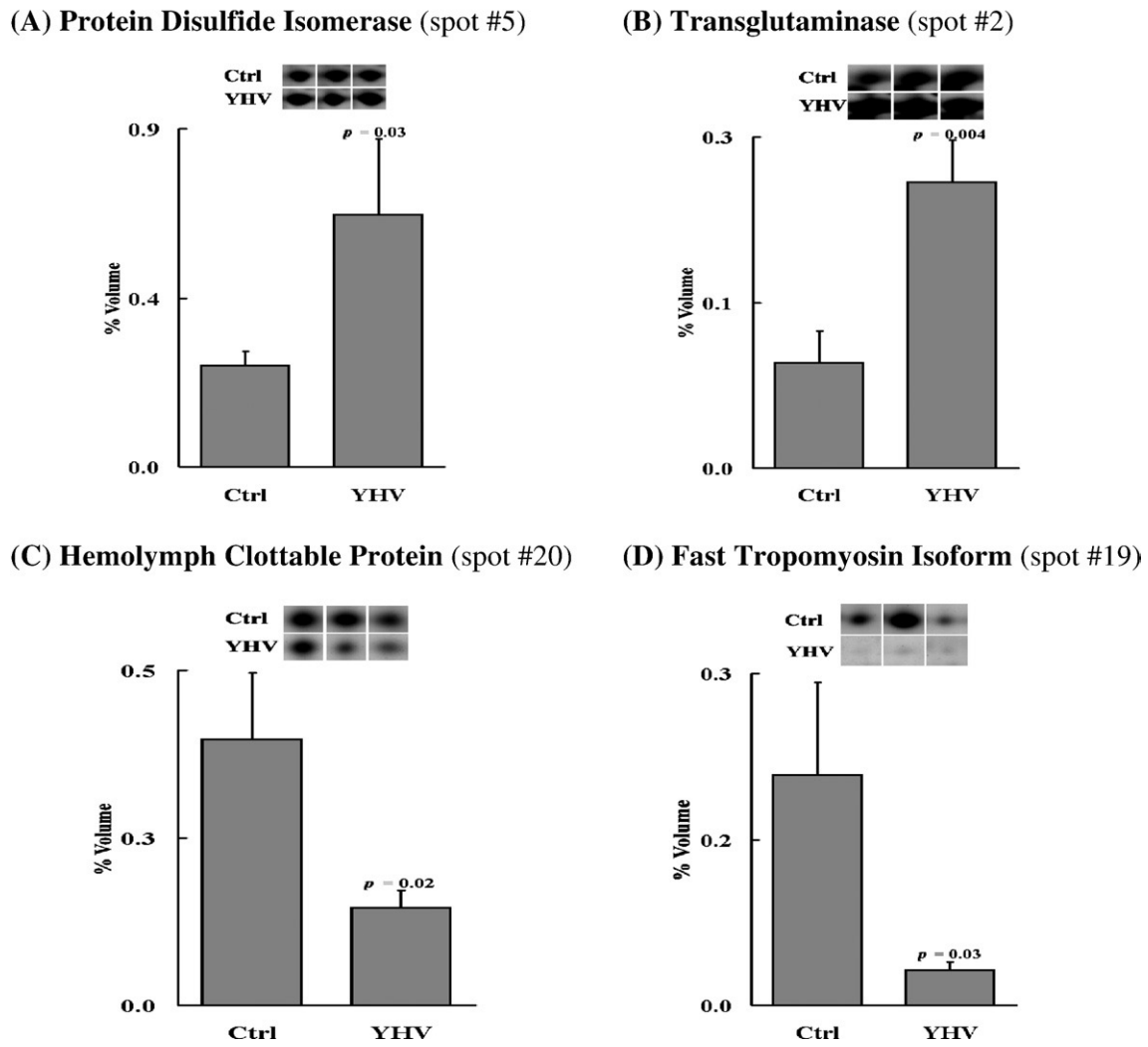

Fig. 2. Zoom-in images and quantitative intensity data of some altered proteins obtained from individual gels. (A) protein disulfide isomerase (PDI), (B) transglutaminase (TGase), (C) hemolymph clottable protein (HCP), and (D) fast tropomyosin isoform.

fingerprinting. MS/MS ion search and extended search on EST databases had significantly improved the identification and could add up a considerable number of identified proteins. A list of successfully identified proteins is compiled in Table 2, containing 20 forms of 13 unique proteins.

We have identified a marked increase of PDI upon YHV infection (Fig. 2A). PDI is normally localized in the lumen of endoplasmic reticulum (ER), catalyzing the formation and isomerization of disulfide bonds [11]. It has been also reported to involve in folding and assembly of viral proteins in the ER [12]. The YHV structural protein, gp116 and gp64, contain 26 and 24 cysteine residues, respectively, in their sequences. A possible role of PDI may be connected to the formation of inter-and intramolecular disulfide bonds during the folding of these viral proteins. Up-regulation of PDI at the transcriptional level was confirmed by real-time RT-PCR using *Ef1*α as a reference gene (Fig. 3A). The use of *Ef1*α was based on the report that confirmed a greater sensitivity, specificity and efficiency of amplification than a conventional actin gene in viral infected tissue of *P. monodon* [13]. It was found to have low sample to sample variation and used as a preference control for genetic studies in shrimp aquaculture. The increased level of PDI mRNA was correlated well with the protein expression. This could be associated with a progression of YHV infection and accumulation of viral proteins in the ER. PDI also functions as a co-receptor to promote disulfide bonds rearrangement of glycoprotein gp120 during the entry of HIV-1 into human $CD4^{+}$lymphoid [14]. Recently, the YHV gp116 has been found to bind to a 65-kDa surface receptor in the LO primary cell culture of *P. monodon* [15]. Perhaps, PDI might also play an important role as a co-receptor to promote gp116 mediated virus entry, the mechanism of which deserves further investigation [14].

We have identified alterations in the defense-related proteins, TGase and HCP. They are known to function in a clotting system, and involved in the defense mechanisms of crustacean [16]. In general, TGase, a Ca^{2+}-dependent enzyme, functions in an intermolecular cross-linking reaction among the clotting proteins to form a stable clot in hemolymph [17]. In this study, TGase was found up-regulated during the YHV infection. The analysis of its transcript showed a drop at 6 hpi, but the level was then

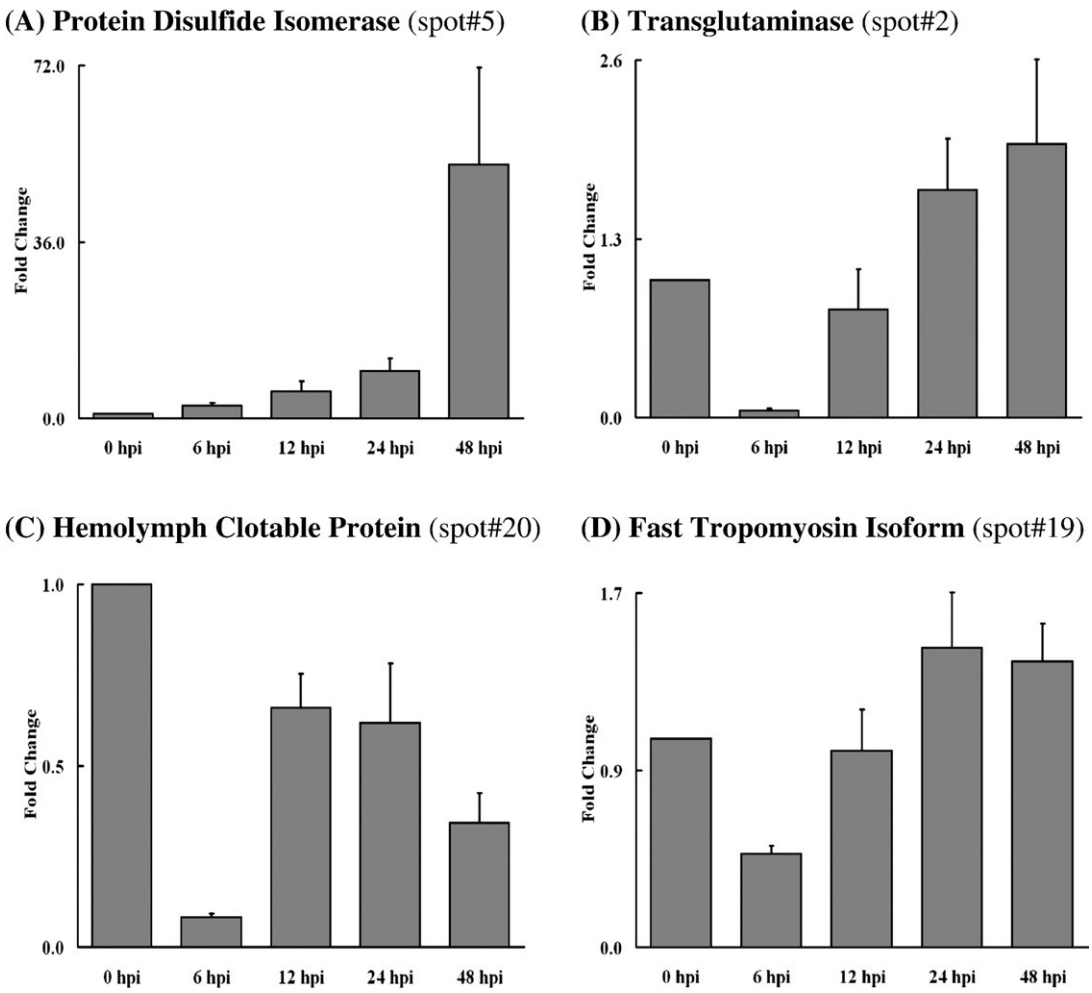

Fig. 3. Fold changes in mRNA levels of (A) protein disulfide isomerase (PDI), (B) transglutaminase (TGase), (C) hemolymph clottable protein (HCP), and (D) fast tropomyosin isoform.

progressively increased over time (Fig. 3B). This data suggested a transcriptional triggering of the clotting system upon the YHV infection. Another protein, HCP, was found down regulated. HCP identified in this work (spot #20) was presented at a much lower molecular mass than HCP reported in the database (Table 2). However, the peptide fragments from MS/MS sequencing gave a good alignment with the N-terminal fragment of HCP. HCP is a secreted protein in shrimp hemolymph that functions without a proteolytic activation. The synthesis of HCP transcript has been reported in heart, gills, and LO of *P. monodon* [18]. A significant decline of HCP suggested an involvement or usage of this protein upon YHV infection. The mRNA data from real-time RT-PCR also confirmed our proteomic data (Fig. 3C).

An alteration of vacuolar (H^+)-ATPase subunit A (V-ATPase-A) was clearly observed during the YHV infection (Table 2). This multimeric integral membrane enzyme catalyzes the ATP-hydrolysis and pumping activities. The resulting acidification of endosome can play role in a cell entry of pathogens and viruses [19,20]. The marked increase of V-ATPase-A and a possible association with the YHV entry should be further investigated. Substantial decreases of beta-actin (spots #17), actin-2 (spot #18) and fast tropomyosin (spot #19) were observed in the infected LO. The decline of tropomyosin, however, was inconsistent with its up-regulated mRNA (Fig. 2D and 3D). This was not surprising as changes in protein levels are not always correlated well with changes in mRNA levels, most likely due to post-translational modifications. Tropomyosin in a non-muscle cell is involved in stabilization of actin network by binding with actin filament and controls a dynamic regulation of actin polymer [21]. The decreased level of tropomyosin could affect the ability of actin polymer in maintaining the cellular structure. A decline of actin could be related to the polymerization network. In addition, it has been reported to bind and inhibit DNase I, a key enzyme in apoptosis cascade [22]. According to a reported apoptosis in the infected LO [23], a decrease of actin abundance may link to DNase I imbalance and progressive cell death.

6-phosphogluconate dehydrogenase is a metabolic enzyme of carbohydrate. The reduction of this protein could reflect the effect of YHV infection on energy production pathways. However, an up-regulation of ATP synthase beta subunit was possibly an attempt to balance the energy production in the infected cells.

Rab GDP-dissociation inhibitor is a 50-kDa protein that prevents the dissociation of GDP and Rab-binding complex during

the trafficking cycle [24]. Recently, it has been reported to block the export of proteins from the ER using vesicular stomatitis virus glycoprotein [25]. The decrease of this protein in the YHV-infected LO might reflect a disturbance of protein trafficking in the infected LO.

Among the altered proteins identified from 2-D gels, there were several spots identified as hemocyanin fragments. At least 3 spots of hemocyanin fragments were increased and one spot was decreased. These spots were found at various pI and molecular weights on 2-D gels. Interestingly, peptide mass fingerprinting and MS/MS sequencing revealed that the increased spots were likely to match to the C-terminal fragment of hemocyanin. The major role of hemocyanin is to serve as an oxygen transport protein. The additional function is related to the defense mechanisms via phenoloxidase activity [26] and antimicrobial activity through its C-terminal peptide [27]. The up-regulation of C-terminal hemocyanin observed in this work could also support the defensive role of hemocyanin in viral infection.

The appearance of YHV nucleocapsid protein (p20) was also clearly identified in the infected sample (spots # 7–9; Fig. 1). This finding implies the distinctive role of the LO either in immunity or in YHV propagation. This hypothesis is supported by the recent findings that YHV infectious particles can be produced from the LO primary cell culture of *P. monodon* [28]. The presence of YHV p20 and altered defense-related proteins identified in this work strengthened our hypothesis that the LO may be the target for YHV replication.

In conclusion, infection of YHV to the LO of *P. monodon* was associated with replication of viral particles in the LO. The nascent viral proteins might require host proteins for folding and modifications. On the other hand, defense mechanisms and physiological balance of host cells were triggered for viral eradication. We have successfully identified the proteomic changes in the YHV-infected LO. The proteins with increased levels during the YHV infection were likely to play important roles in the defense mechanisms, while the proteins with declined levels might be involved in arrangements of cytoskeleton assembly, metabolism, and trafficking pathways. These findings have provided a number of possible hypotheses, which deserve further investigations, and may lead to novel insights into the virus-host interactions, particularly host defense mechanisms, in the LO of *P. monodon* during YHV infection.

Acknowledgements

This work was supported by the Royal Golden Jubilee (RGJ) Ph.D. Program and the Thailand Research Fund (TRF). We are grateful to the EMBL Proteomic Core Facility for their support on protein mass spectrometry. We also thank Dr. Assvalarpsakul for providing YHV and Dr. Sritunyalucksana for TGase and HCP primers.

Appendix A. Supplementary data

Supplementary data associated with this article can be found, in the online version, at doi:10.1016/j.bbapap.2007.12.006.

References

[1] C. Wongteerasupaya, S. Sriurairatana, J.E. Vickers, V. Boonsaeng, S. Panyim, A. Tassanakajon, B. Withyachumnarnkul, T.W. Flegel, Yellow-head virus of *Penaeus monodon* is an RNA virus, Dis. Aquat. Org. 22 (1995) 45–50.
[2] Y.C. Wang, P.S. Chang, Yellow head virus infection in the giant tiger prawn *Penaeus monodon* cultured in Taiwan, Fish Pathol. 35 (2000) 1–10.
[3] C. Chantanachooklin, S. Boonyaratpalin, J. Kasornchandra, U. Ekpanithanpong, K. Supamataya, S. Sriurairatana, T.W. Flegel, Histology and ultrastructure reveal a new granulosis-like virus in *Penaeus monodon* affected by yellow-head disease, Dis. Aquat. Org. 17 (1993) 145–157.
[4] C.S. Wang, K.F.J. Tang, G.H. Kou, S.N. Chen, Yellow head disease-like virus infection in the Kuruma shrimp *Penaeus japonicus* cultured in Taiwan, Fish Pathol. 31 (1996) 177–182.
[5] C.B.T. van de Braak, M.H.A. Botterblom, N. Taverne, W.B. van Muiswinkel, J.H. Rombout, W.P. van der Knaap, The roles of haemocytes and the lymphoid organ in the clearance of injected *Vibrio* bacteria in *Penaeus monodon* shrimp, Fish & Shellfish Immunol. 13 (2002) 293–309.
[6] J.E. Burgents, L.E. Burnett, E.V. Stabb, K.G. Burnett, Localization and bacteriostasis of *Vibrio* introduced into the Pacific white shrimp, *Litopenaeus vannamei*, Develop. Comp. Immunol. 29 (2005) 681–691.
[7] Y. Lu, L.M. Tapay, P.C. Loh, J.A. Brock, R.B. Gose, Distribution of yellow-head virus in selected tissues and organs of penaeid shrimp *Penaeus vannamei*, Dis. Aquat. Org. 23 (1995) 67–70.
[8] W. Assavalapsakul, D.R. Smith, S. Panyim, Identification and characterization of a *Penaeus monodon* lymphoid cell-expressed receptor for the yellow head virus, J. Virol. 80 (2006) 262–269.
[9] M.M. Bradford, A rapid and sensitive method for the quantitation of microgram quantities of protein utilizing the principle of protein-dye binding, Anal Biochem. 72 (1976) 248–254.
[10] M.W. Pfaffl, A new mathematical model for relative quantification in real-time RT-PCR, Nucleic Acids Res. 29 (2001) 2002–2007.
[11] R. Noiva, W.J. Lennarz, Protein disulfide isomerase; A multifunctional protein resident in the lumen of the endoplasmic reticulum, J. Biol. Chem. 267 (1992) 3553–3556.
[12] R.W. Doms, R.A. Lamb, J.R. Rose, A. Helenius, Folding and assembly of viral membrane proteins, Virology. 193 (1993) 545–562.
[13] A.K. Dhar, M.M. Roux, K.R. Klimpel, Quantitative assay for measuring the Taura syndrome virus and yellow head virus load in shrimp by real-time RT-PCR using SYBR Green chemistry, J. Virol. Methods 104 (2002) 69–82.
[14] R. Barbouche, R. Miquelis, I.M. Jones, E. Fenouillet, Protein-disulfide isomerase-mediated reduction of two disulfide bonds of HIV envelope glycoprotein 120 occurs post-CXCR4 binding and is required for fusion, J. Biol. Chem. 278 (2003) 3131–3136.
[15] W. Assavalapsakul, W. Tirasophon, S. Panyim, Antiserum to the gp116 glycoprotein of yellow head virus neutralizes infectivity in primary lymphoid organ cells of *Penaeus monodon*, Dis. Aquat. Org. 63 (2005) 85–88.
[16] V.J. Smith, J.R.S. Chisholm, Non-cellular immunity in crustaceans, Fish & Shellfish Immunol. 2 (1992) 1–31.
[17] M.Y. Chen, K. Hub, C. Huanga, Y. Song, More than one type of transglutaminase in invertebrates? A second type of transglutaminase is involved in shrimp coagulation, Dev. Comp. Immunol. 29 (2005) 1003–1016.
[18] M.S. Yeh, C.J. Huang, J.H. Leu, Y.C. Lee, I.H. Tsai, Molecular cloning and characterization of a hemolymph clottable protein from tiger shrimp (*Penaeus monodon*), Eur. J. Biochem. 266 (1999) 624–633.
[19] G.H. Sun-Wada, Y. Wada, M. Futai, Diverse and essential roles of mammalian vacuolar-type proton pump ATPase: toward the physiological understanding of inside acidic compartments, Biochim. Biophys. Acta. 1658 (2004) 106–114.
[20] L. Perez, L. Carrasco, Involvement of the vacuolar H^+-ATPase in animal virus entry, J. Gen. Virol. 75 (1994) 2595–2606.
[21] K.K. Wen, B. Kuang, P.A. Rubenstein, Tropomyosin-dependent filament formation by a polymerization-defective mutant yeast actin (V266G, L267G), J. Biol. Chem. 275 (2000) 40594–40600.
[22] C. Kayakar, T. Örd, M.P. Testa, L. Zhong, D. Bredesen, Cleavage of actin by interleukin 1 beta-converting enzyme to reverse DNase I inhibition, Proc. Natl. Acad. Sci. 93 (1996) 2234–2238.

[23] K. Khanobdee, C. Soowannayan, T.W. Flegel, S. Ubol, B. Withyachumnarnkul, Evidence for apoptosis correlated with mortality in the giant black tiger shrimp *Penaeus monodon* infected with yellow head virus, Dis. Aquat. Org. 48 (2002) 79–90.

[24] H. Stenmark, V.M. Olkkonen, The Rab GTPase family, Genome Biol. 2 (2001) 3007.1–3007.7.

[25] F. Peter, C. Nuoffer, S.N. Pind, W.E. Balch, Guanine nucleotide dissociation inhibitor is essential for Rabl function in budding from the endoplasmic reticulum and transport through the Golgi stack, J. Cell Biol. 126 (1994) 1393–1406.

[26] S.Y. Lee, B.L. Lee, K. Söderhäll, Processing of crayfish hemocyanin subunits in to phenoloxidase, Biochem. Biophys. Res. Com. 322 (2004) 490–496.

[27] D. Destoumieux-Garzón, D. Saulnier, J. Garnier, C. Jouffrey, P. Bulet, E. Bachère, Antifungal peptides are generated from the C terminus of shrimp hemocyanin in response to microbial challenge, J. Biol. Chem. 276 (2001) 47070–47077.

[28] W. Assavalapsakul, D.R. Smith, S. Panyim, Propagation of infectious yellow head virus particles prior to cytopathic effect in primary lymphoid cell cultures of *Penaeus monodon*, Dis. Aquat. Org. 55 (2003) 253–258.

VERSITA

Biologia **64**/1: 27—42, 2009
Section Cellular and Molecular Biology
DOI: 10.2478/s11756-009-0013-y

Quantitative analysis of time-series fluorescence microscopy using a spot tracking method: application to Min protein dynamics

Somrit Unai[1]*, Paisan Kanthang[1]*, Udorn Junthon[1], Waipot Ngamsaad[1], Wannapong Triampo[1,2,3]**, Charin Modchang[1] & Chartchai Krittanai[4]

[1] *R&D Group of Biological and Environmental Physics, Department of Physics, Faculty of Science, Mahidol University, Rama 6 Rd., Ratchatewee, Bangkok 10400, Thailand; e-mails: scwtr@mahidol.ac.th or wtriampo@gmail.com*
[2] *Center of Excellence for Vector and Vector-Borne Diseases, Faculty of Science, Mahidol University, Nakhonpathom, Thailand*
[3] *Institute for Innovation and Development of Learning Process, Mahidol University, Bangkok, Thailand*
[4] *Institute of Molecular Biology. and Genetics, Mahidol University, Nakhonpathom, Thailand*

Abstract: The dynamics of MinD protein has been recognized as playing an important role in the accurate positioning of the septum during cell division. In this work, spot tracking technique (STT) was applied to track the motion and quantitatively characterize the dynamic behavior of green fluorescent protein-labeled MinD (GFP-MinD) in an *Escherichia coli* system. We investigated MinD dynamics on the level of particle ensemble or cluster focusing on the position and motion of the maximum in the spatial distribution of MinD proteins. The main results are twofold: (i) a demonstration of how STT could be an acceptable tool for MinD dynamics studies; and (ii) quantitative findings with parametric and non-parametric analyses. Specifically, experimental data monitored from the dividing *E. coli* cells (typically 4.98 ± 0.75 μm in length) has demonstrated a fast oscillation of the MinD protein between the two poles, with an average period of 54.6 ± 8.6 s. Observations of the oscillating trajectory and velocity show a trapping or localized behavior of MinD around the polar zone, with average localization velocity of 0.29 ± 0.06 μm/s; and flight switching was observed at the pole-to-pole leading edge, with an average switching velocity of 2.95 ± 0.31 μm/s. Subdiffusive motion of MinD proteins at the polar zone was found and investigated with the dynamic exponent, α of 0.34 ± 0.16. To compare with the Gaussian-based analysis, non-parametric statistical analysis and noise consideration were also performed.

Key words: spot tracking; *E. coli*; cell division; Min proteins; MinD; protein oscillation.

Abbreviations: GFP-MinD, green fluorescent protein-labeled MinD protein; MTS, membrane-targeting sequence; MSD, mean squared displacement; PSD, power spectrum density; ROI, region of interest; SPT, single particle tracking; STT, spot tracking technique; Z-ring, equatorial ring.

Introduction

In *Escherichia coli* and other rod-shaped bacteria, cell division depends on the precise placement of a division septum in the middle of the cell, a process initiated by the assembly of an equatorial ring (Z-ring) of the tubulin-like FtsZ GTPase on the cytoplasmic membrane (Lutkenhaus & Addinall 1997; Rothfield et al. 1999). The Z-ring assembly is spatially restricted to midcell by nucleoid occlusion (Woldringh et al. 1991; Yu & Margolin 1999) and by the dynamics of the Min system (de Boer et al. 1989; Rothfield et al. 2001). Nucleoid-free zones provide for the possible placement of the Z-ring within three regions – two polar zones and a midcell zone – while the Min system prevents Z-ring assembly at the polar zone. The Min system consists of the MinC, MinD, and MinE expressed from the *minB* operon (de Boer et al. 1989) which restricts separation to the desired potential division site at the midcell through the oscillatory cycle from pole to pole (reviewed in Rothfield et al. 2005). *In vivo*, MinC co-localizes and co-oscillates with MinD (Hu & Lutkenhaus 1999; Raskin & de Boer 1999a) which acts together as a negative regulator of Z-ring assembly, and oscillatory dynamics depends on MinE (Hu & Lutkenhaus 1999; Raskin & de Boer 1999a,b). MinCD complex prevents the correct interaction of FtsA with the FtsZ ring *in vivo* (Justice et al. 2000), and MinC has been shown to inhibit FtsZ polymerization *in vitro* (Hu & Lutkenhaus 1999).

With regards to Min protein dynamics both *in vitro* and *in silico*, a considerable number of experiments have been done. Computationally, several studies have been carried out with different reaction-diffusion

* Co-first authors
** Corresponding author

Springer